Radiation effects on relativistic electrons in strong external fields

Khalid Iqbal

München 2012

Radiation effects on relativistic electrons in strong external fields

Khalid Iqbal

Dissertation

an der Fakultät für Physik

der Ludwig-Maximilians-Universität

München

vorgelegt von

Khalid Iqbal

aus Sargodha

München, den 07 December 2012

Statutory Declaration

Herewith I affirm that the presented dissertation was made autonomous without illegal help.

München: 07 December, 2012. Signature

Erstgutachter: Prof. Dr. Hartmut Ruhl

Zweitgutachter: Prof. Dr. Harald Lesch

Tag der mündlichen Prüfung: 08 May, 2013

Contents

Abstract **ix**

Zusammenfassung **xi**

1. Introduction and motivation **1**

1.1. Structure of the thesis 1

1.2. Introduction 2

1.3. Acceleration in plasma 2

1.3.1. Ponderomotive force 4

1.3.2. Linear wakefield 6

1.3.3. Nonlinear plasma wave 8

1.3.4. Bubble regime 9

1.3.5. Electron acceleration limits and dephasing 13

1.4. Electron acceleration by a focused laser beam 14

1.5. Radiation reaction 16

1.5.1. The electron as a point particle 17

1.5.2. The charged sphere 19

1.5.3. The Caldirola equation 19

2. The effects of betatron radiation on an electron beam in a laser wakefield 25

2.1. Introduction 25

2.2. The laser wakefield 27

2.2.1. The motion of a single charged particle 28

2.2.2. Electron beam dynamics 31

2.3. Emittance growth via betatron radiation 32

2.3.1. The critical energy 33

2.3.2. Emittance growth 34

2.3.3. Impact of density on emittance growth 39

2.4. Schematic representation of accelerating and decelerating phase . . 41

2.5. Summary of the chapter 42

3. Retardation and self radiation effects on electrons in a laser pulse 45

3.1. Introduction 45

3.2. The radiation fields 46

3.2.1. Electrons-radiation interaction model 47

3.2.2. Linear polarization 49

3.2.3. Circular polarization 49

3.3. The analytical solution of the Landau-Lifshitz equation 50

3.3.1. Linearly polarized plane wave 51

3.3.2. Circularly polarized plane wave 55

3.3.3. Examples 57

3.4. Summary of the chapter 65

4. TeV scale electron beam from multistage low density laser-plasma accelerators 67

4.1. Introduction 67

4.2. Accelerating field 68

4.3. Energy gain, stage length and total LPA length 69

4.4. Driver laser pulse and electron beam parameters 70
4.5. Single particle motion 71
4.5.1. The solution 73
4.5.2. Electron beam dynamics 74
4.6. Summary of the chapter 77

5. Retardation effects on electron beams in laser wakefields 79
5.1. Single particle motion 80
5.1.1. Electron beam dynamics 81
5.2. Summary of the chapter 84

6. Numerical solutions of the self force equations 85
6.1. Introduction 85
6.2. Numerical schemes 86
6.2.1. Equations of motion 87
6.2.2. Numerical scheme for the LL equation 88
6.2.3. Numerical scheme for the Caldirola equation 94
6.2.4. Numerical scheme for the LAD equation 97
6.3. Numerical Examples 98
6.4. Summary of the chapter 100

7. Radiation reaction in a tightly focused laser beam 103
7.1. Introduction 103
7.2. Governing equations 104
7.3. Summary of the chapter 112

8. Conclusions 115
8.1. 1 TeV energy linear wakefield electron accelerator 116
8.2. Retardation and radiation effects in strong external fields 116
8.3. Numerical simulation of self force equations 118

Appendix **118**

A. Linearly polarized plane wave **119**

B. Circularly polarized plane wave **121**

Bibliography **123**

Acknowledgements **135**

Abstract

The effects of radiation of high energy electron beams are a major issue in almost all types of charged particle accelerators. The objective of this thesis is both the analytical and numerical study of radiation effects. Due to its many applications the study of the self force has become a very active and productive field of research.

The main part of this thesis is devoted to the study of radiation effects in laser-based plasma accelerators. Analytical models predict the existence of radiation effects. The investigation of radiation reaction show that in laser-based plasma accelerators, the self force effects lower the energy gain and emittance for moderate energies electron beams and increase the relative energy spread. However, for relatively high energy electron beams, the self radiation and retardation (radiation effects of one electron on the other electron of the system) effects increase the transverse emittance of the beam. The energy gain decreases to even lower value and relative energy spread increases to even higher value due to high radiation losses.

The second part of this thesis investigates with radiation reaction in focused laser beams. Radiation effects are very weak even for high energy electrons. The radiation-free acceleration and the simple practical setup make direct acceleration in a focused laser beam very attractive.

The results presented in this thesis can be helpful for the optimization of future electron acceleration experiments, in particular in the case of laser-plasma accelerators.

Zusammenfassung

Die Strahlungseffekte von hochenergetischen Elektronen sind von grosser Bedeutung in fast allen Arten von Teilchenbeschleunigern. Das Ziel dieser Arbeit ist die analytische und numerische Untersuchung dieser Effekte. Die Untersuchung der Selbstkraft ist, dank ihrer vielen Anwendungsgebiete, zu einem sehr aktiven und produktiven Bereich der Forschung geworden.

Der Hauptteil dieser Arbeit widmet sich der Untersuchung von Strahlungseffekten in Laser-Plasma-Beschleunigern. Analytische Modelle sagen die Existenz von Strahlungseffekten voraus. Unsere Untersuchungen der Strahlungsrückwirkung zeigen, dass die Selbstkraft den Energiegewinn sowie die Emittanz von Elektronenstrahlen mittlerer Energie verringert und deren relative Energieverteilung verbreitert. Für hochenergetische Elektronenstrahlen jedoch bewirken die Strahlungseffekte (Strahlungsrückwirkung sowie retardierende Effekte) eine Erhöhung der transversalen Emittanz und, aufgrund von Strahlungsverlusten, eine Verringerung des Energiegewinns.

Der zweite Teil dieser Arbeit beschäftigt sich mit der Strahlungsrückwirkung in fokussierten Lasern. Die Strahlungseffekte auf die Teilchenbeschleunigung sind in diesem Fall nur sehr schwach ausgeprägt. Dies gilt auch für hochenergetische Elektronen. Der strahlungsarme und relativ einfache Versuchsaufbau lassen diesen Ansatz zur Elektronenbeschleunigung herausragen. Wir hoffen, dass unsere Ergebnisse bei der Optimierung von zukünftigen Experimenten im Bereich der Elektronenbeschleunigung von grossem Nutzen sind. Insbesondere gilt dies für Versuche mit Laser-Plasma-Beschleunigern.

CHAPTER 1

Introduction and motivation

1.1. Structure of the thesis

The thesis is structured as this

- Chapter 1 gives a general introduction into the subject and the motivation for the investigations.
- Chapter 2 deals with the theoretical and numerical investigation of self-radiation effects of high energy electron beams in a low density plasma channel. The growth and reduction of transverse emittance of the electron beam in the plasma channel are shown.
- In Chapter 3 retardation and self-radiation effects are studied. A simple theoretical model for two interacting electrons is presented, which analyses the-self radiation and retarded field effects of a bunch of electrons. This chapter investigates the basic effects of retarded potentials.
- Chapter 4 is devoted to design parameters of a 1 TeV electron accelerator. Five different density regimes are discussed. Almost all the basic parameters for linear laser wakefield accelerators are given with their optimum values.

- Chapter 5 investigates the retardation effects of a bunch of electrons in a laser wakefield in low density plasma.

- Chapter 6 presents the numerical solutions of the equations of radiating charged particles. Numerical schemes for equations of the point particles, i.e., the Landau-Lifshitz and the Lorentz-Abraham-Dirac equation, and equation of a radiating charged sphere, i.e., the Caldirola equation, are discussed.

- Chapter 7 is devoted to the study of radiation effects in a focused laser beam. A novel numerical approach is discussed to solve the Lorentz-Abraham-Dirac equation.

1.2. Introduction

With the recent development of laser technology it is possible to obtain ultra intense laser pulses. Laser pulses with normalized laser intensities $a_o = 8.5 \times 10^{-10}\lambda_L(\mu m)\sqrt{I_o(W/cm^2)} \gg 1$ are considered to be ultra relativistic intensities as they can accelerate electrons to much higher energies than their rest mass energy $(m_e c^2)$ [1, 2], where λ_L and I_o are the wavelength and intensity of the laser pulse. The Chirped-Pulse-Amplification (CPA) technique makes it possible to generate relativistically strong laser pulses with durations less than 100 fs [3]. Electron acceleration by conventional accelerators is complex and expensive. Therefore, electron acceleration via lasers has been of great interest.

1.3. Acceleration in plasma

In 1979 Tajima and Dawson proposed the idea of acceleration of electrons by plasma waves [4]. Because relativistic intensities ($a_o \gg 1$) are much higher than intensities needed for target ionization the interaction of light with matter can be assumed to be the interaction with fully ionized plasma. Electrons under the effect

of such intense pulses oscillate and accelerate to high velocities in the transverse and longitudinal directions [5, 6]. In a Laser-Wakefield-Accelerator (LWFA) an intense laser beam with a duration τ_L approximately equal to the plasma oscillation period $2\pi/\omega_p$ creates a large amplitude plasma wave with a phase velocity approximately equal to the speed of light [7, 8, 9, 10, 11, 12]. The electrons with appropriate initial conditions are trapped and accelerated to high energies depending on the density and type of the laser wakefield. For example, bubble regime has high accelerating gradient as compared to the linear wakefield for same plasma density.

The wakefield created by a laser pulse has two important advantages over a conventional acceleration field; (i) the longitudinal electric field gradient is 2-3 orders of magnitude higher without breakdown limitation as is the case in conventional accelerators and (ii) the acceleration length in the laser wakefield is much smaller [13, 14]. In a plasma-based accelerator compact and high energy electron beams can be produced over a much shorter distance than in conventional accelerators (for a review see [15, 16]). This promises compact accelerator designs and applications such as compact X-ray FELs (free electron lasers), high energy frontier accelerators, radiolysis [17, 18], electron diffraction and interactive radiotherapy [19] to name a few. Early experiments on laser wakefield were not able to produce the electrons beam of desired standard. Until the end of the last decade electron bunches from LWFAs with long exponentially small tails were obtained while most of the electrons have energies < 10 MeV and the bunch charge is $\sim$ nC [20]. In 2004 the quality of the LWFA beams improved as reported by [21, 22, 23]. The obtained electron bunches have charge ≥ 100 pC and a mean energy of ~ 100 MeV. In addition, the energy spread and transverse emittance were also small. These high quality electron beams were obtained by better control of the laser and plasma parameters. In particular, matching the acceleration length to the dephasing length. A high quality electron beam of 1 GeV was obtained using a plasma channel guided laser [24].

The accelerating gradients in conventional rf-linear accelerators are usually smaller than ~ 100 MV/m due to the breakdown limit. However, electron plasma waves can sustain an electric field $E_o = cm_e\omega_p/e$ greater than 100 GeV/m, or

$$E_o(V/)m = 96\sqrt{n_o cm^{-3}}, \tag{1.1}$$

where n_o is the background plasma density, $\omega_p = \sqrt{4\pi n_o e^2/m_e}$ is the frequency of the electron plasma wave, m_e and e are the mass and charge of the electron respectively and c is the speed of light. Equation (1.1) is the cold non-relativistic wave breaking field [25]. For a plasma density $n_o = 10^{19}$ cm^{-3} the plasma wave field is $E_o \simeq 960$ GeV/m, which is almost four orders of magnitude higher than what is found in linac. Plasma accelerators are also produce electron bunches with much smaller durations $\tau_b < \lambda_p/c$, where τ_b is the bunch duration and λ_p is the wavelength of the electron plasma wave.

The normalized laser intensity or laser strength parameter $a_o = eE_L/(m_e c\omega_L)$ is an important parameter to study the laser-plasma interaction, where E_L is the peak amplitude of the laser electric field and ω_L is the frequency of the laser pulse. The radiation pressure of the laser drives the wake in the plasma. Different aspects of propagation and transport of the driver beams will be discussed in the subsequent sections.

1.3.1. Ponderomotive force

Wakefields are created by the ponderomotive potential of the laser beam in LWFAs. The electric and magnetic fields of the laser can be written as $\vec{E} = -\partial\vec{A}/\partial(ct)$ and $\vec{B} = \vec{\nabla} \times \vec{E}$, where $\vec{A}$ is the vector potential of the laser and is polarized in the transverse direction i.e. $\vec{A} = A_o \cos(kz - \omega t)e_\perp$. For an intensity $a = e|A|/(m_e c^2) \ll 1$ the leading order electron motion is the quiver momentum $\vec{p} = m_e c\vec{a}$ given by the Lorentz force equation $d\vec{p}/dt = -e\vec{E}$. Let us suppose $\vec{p} = \vec{p} + \delta\vec{p}$ then the

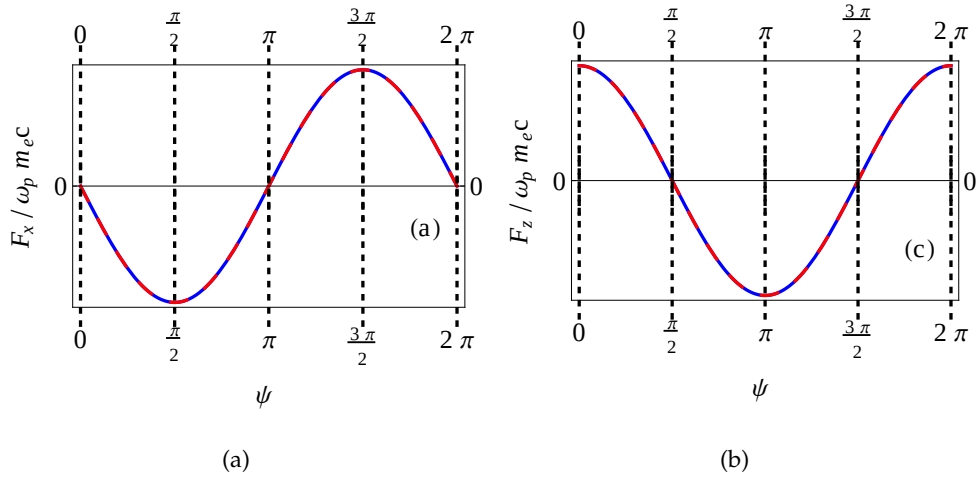

Figure 1.1.: Plasma wave phase representation. The normalized transverse force F_x and the longitudinal accelerating force F_z felt by an electron. The first quadrant $(0 - \pi/2)$ is appropriate for simultaneous focusing and acceleration.

second order momentum is given by

$$\frac{d\delta\vec{p}}{dt} = -(\vec{p}/m \cdot \vec{\nabla})\vec{p} - \vec{p} \times (c\vec{\nabla} \times \vec{a}), \tag{1.2}$$

$$\vec{F_p} = -m_e c^2 \nabla(a^2/2), \tag{1.3}$$

where F_p is the 3D ponderomotive force in the linear limit i.e. $(a_o^2 \ll 1)$. The ponderomotive force is also called radiation pressure (i.e. the gradient of the electromagnetic energy density). In the 1D nonlinear limit, $p_\perp = a_\perp$, which means in the 1D nonlinear limit, the ponderomotive force is $F_{pz} = -(m_e c^2/2\gamma)\partial a_\perp^2/\partial z$. In 3D nonlinear regime, the leading order transverse motion of the electron fluid is still the quiver motion, $\vec{u}_\perp \simeq \vec{a}_\perp$, for the situation that the laser is propagating in the under-dense plasma and the laser spot size $r_o \geq \lambda_p \simeq \lambda_L$. The second order momentum is given by

$$\frac{\partial\delta\vec{u}}{\partial ct} = \vec{\nabla}(\phi - \gamma), \tag{1.4}$$

where $\vec{\nabla}\phi$ is the space charge force and $\vec{\nabla}\gamma$ is the generalized nonlinear ponderomotive force $\vec{F}_{pn} = -m_e c^2 \vec{\nabla}\gamma$, see [26, 27, 28]. A LWFA can be operated in different regime depending on the intensity of the driver laser pulse. Non-relativistic laser pulses $(a_o \ll 1)$ create a linear plasma wave.

1.3.2. Linear wakefield

In the linear $(a_o \ll 1)$ 3D regime, wakefield generation can be studied using cold fluid equations, i.e., the Poisson equation, the continuity equation, and the momentum equation. A laser propagating in under-dense uniform plasma creates a plasma wave

$$(\frac{\partial^2}{\partial t^2} + \omega_p^2)\delta n/n_o = c^2\nabla^2 a^2/2, \tag{1.5}$$

$$(\frac{\partial^2}{\partial t^2} + \omega_p^2)\phi = \omega_p^2 a^2/2, \tag{1.6}$$

where δn is the density perturbation associated with the electrostatic wake ϕ in the linear intensity limit. The solutions to equations (1.5) and (1.6) are

$$\frac{\delta n}{n_o} = \frac{c^2}{\omega_p^2}\int_0^t dt' \sin(\omega_p(t-t'))\nabla^2 a^2(\vec{r},t')/2, \tag{1.7}$$

$$\frac{\vec{E}}{E_o} = -c\int_0^t dt' \sin(\omega_p(t-t'))\nabla^2 a^2(\vec{r},t')/2. \tag{1.8}$$

Equations (1.7) and (1.8) give the plasma wave of frequency ω_p in the linear regime ($a_o \ll 1$ or $E \ll E_o$) created by a laser pulse, where $E_o = m_e c\omega_p/e$ is the cold non-relativistic wave-breaking field. The solution of equation (1.8) shows that the maximum wakefield is generated when the envelope scale length of the incident laser pulse is of the order of the plasma wavelength λ_p. Usually the axial gradient of the wakefield is characterized by the length L of the pulse and the transverse width is determined by the spot size r_o of the laser.

1.3.2.1. Linear regime sine pulse

Let us consider a circularly polarized laser pulse with a normalized intensity $a^2 = a_o^2 \exp(-2r^2/r_o^2)\sin^2(\pi\xi/L)$ for $0 < \xi < L$, where $\xi = z - ct$ and $a_o^2 \ll 1$. The solution of equation (1.8) gives the wakefield created by the laser pulse and shows that it is maximum for $L \simeq \lambda_p$. The axial electric field and density perturbations of the wake behind the pulse are [29]

$$\frac{E_z}{E_o} = -\frac{\pi}{4} a_o^2 \exp\big(\frac{-2r^2}{r_o^2}\big)\cos(k_p\xi) \tag{1.9}$$

and

$$\frac{\delta n}{n_o} = -\frac{\pi}{4} a_o^2\Big[1 + \frac{8}{k_p^2 r_o^2}\big(1 - \frac{2r^2}{r_o^2}\big)\Big]\exp\big(\frac{-2r^2}{r_o^2}\big)\sin(k_p\xi) \tag{1.10}$$

1.3.2.2. Linear regime Gaussian pulse

For a Gaussian pulse of circular polarization with profile $a^2 = a_o^2\exp(-2\xi^2/L^2)$, the amplitude of the wakefield behind the pulse is

$$\frac{E_{max}}{E_o} \simeq \frac{\pi a_o^2}{2} k_p L \exp\big(\frac{-k_p^2 L^2}{4}\big), \tag{1.11}$$

where E_{max} is the peak electric field of the wake. Equation (1.11) shows the dependence of the wake amplitude on the laser pulse length L. The wake amplitude is maximum when L = $\lambda_p/(\pi\sqrt{2})$.

The transverse wakefield E_r is related to the longitudinal wakefield E_z by the Panofsky-Wenzel theorem [30] given by $\partial E_z/\partial r = \partial(E_r - B_\theta)/\partial(z - ct)$, where B_θ is the azimuthal magnetic field. Hence in a wakefield an electron moving with relativistic velocity i.e. $v \simeq c$ feels a radial force which is proportional to $E_r - B_\theta$. It is clear from the Panofsky-Wenzel theorem that if the axial field is given by $E_z \sim \exp(-2r^2/r_o^2)\cos(k_p(z - ct))$ the transverse field is$E_r \sim (4r/k_p r_o^2)\exp(-2r^2/r_o^2)$ $\sin\big(k_p(z - ct)\big)$ and an electron moving on the axis feels no transverse force.

1.3.3. Nonlinear plasma wave

For a laser intensity $a_o \simeq 1$ the plasma wave is highly nonlinear. In such a regime $E \geq E_o$ holds. Wakefield generation in the 1D nonlinear regime can be examined by assuming that the driver beam is non-evolving, i.e. the driver beam is a function of only the coordinate $\xi = z - v_p t$, where $v_p \leq c$ is the phase velocity of the plasma wave. The plasma fluid quantities are also considered functions of the co-moving variable ξ for the quasi-static approximation [31, 32]. The 1D quasi-static fluid momentum and continuity equations provide us with the following set of equation [16]

$$\vec{u}_\perp - \vec{a}_\perp = 0, \tag{1.12}$$

$$\gamma - \beta_p u_z - \phi = 0, \tag{1.13}$$

$$n(\beta_p - \beta_z) = \beta_p n_o, \tag{1.14}$$

and the poisson equation $\partial^2\phi/\partial\xi^2 = k_p^2(n/n_o - 1)$ implies that

$$\frac{\partial^2\phi}{\partial\xi^2} = k_p^2\gamma_p^2\Big(\beta_p(1 - \frac{\gamma_\perp^2}{\gamma_p^2(1+\phi)^2})\Big), \tag{1.15}$$

where $\gamma_\perp = 1 + u_\perp^2 = 1 + a^2$, $\gamma_p = (1 - \beta_p^2)$, and $\beta_p = v_p/c$. The axial electric field of the wake is $E_z = -E_o\partial\phi/\partial\xi$.

In the limit $\gamma_p^2 \gg 1$ equation (1.15) is reduced to

$$\frac{\partial^2\phi}{\partial\xi^2} = k_p^2\frac{1+a^2}{2(1+\phi)^2} - \frac{1}{2}. \tag{1.16}$$

The analytical solution of equation (1.16) can be found in terms of elliptic integrals for square laser pulse profiles [33, 31, 32]. As the plasma wave amplitude becomes nonlinear, the plasma wave steepens, which lengthens its period. The nonlinear plasma wavelength in the limit $\gamma_p \gg 1$ for the ellitpical integral is given by

$$\lambda_{np} = \lambda_p\Big(1 + 3(E_{max}/E_o)^2/16\Big), \quad \text{if} \quad E_{max}/E_o \ll 1 \tag{1.17}$$

and

$$\lambda_{np} = \lambda_p\Big(2\pi(E_{max}/E_o + E_o/E_{max})\Big), \quad \text{if} \quad E_{max}/E_o \gg 1 \tag{1.18}$$

where E_{max} is the peak electric field of the plasma wave and $\lambda_p = 2\pi c/\omega_p$.

The analytical modeling of the wakefield in the high intensity limit ($a_o \simeq 1$) is possible in 1D. However, in the 3D high intensity limit, only numerical modeling is possible. For a bounded pulse in three dimensions the structure of the wakefield deviates significantly from the sinusoidal form with increasing laser intensity as described by linear theory. Along with the wave steepening and period lengthening, which occur in the 1D limit, the radial structure of the wake can give rise to nonlinearities. One of the basic effect is that the wave front of the plasma wave can be curved.

Laser pulses with intensities well above the relativistic limit, $a_o \gg 1$, create a highly nonlinear plasma wave and wave breaking occurs after the first plasma oscillation. It expels all electrons from the axis and immediately behind the laser pulse and leaves behind an electron free ion cavity, which travels through the plasma as a soliton-like structure. This is called the blow-out or bubble regime.

1.3.4. Bubble regime

In the blow-out regime a relatively high laser intensity is required to completely expel all plasma electrons from the vicinity of the axis [34, 35, 36]. In the bubble regime most of the plasma electrons are expelled, however, a fraction of the plasma electrons can be self-trapped in the cavity and are accelerated to high energies.

The bubble regime can be created by both, laser [37] and electron or ion beam drivers [38, 39]. For electron beam drivers Rosenweig [38] was the first to study the blow-out regime and some early nonlinear Plasma-Wakefield-Accelerator (PWFA) experiments have been done at the Stanford Linear Accelerator Center (SLAC) using 30-40 GeV electron beams to drive plasma waves [40, 41]. In the blow-out regime of the PWFA ($n_b/n_o > 1$, $k_p\sigma_z < 1$, and $k_p\sigma_r < 1$, where σ_z and σ_r are the axial and radial bunch lengths respectively) almost all the plasma electrons

are driven out from the vicinity of and immediately behind the driver. As is the case in the linear wakefield there exist two kinds of fields in the bubble regime. The longitudinal accelerating field, which is constant as function of the radius and varies linearly as a function of distance behind the driver and other one is the focusing field that is linear as a function of radius. Due to these properties the bubble regime can be beneficial, e.g., because the focusing force is linear, therefore, the normalized emittance of an accelerated electron bunch can be preserved. Experiments at SLAC show an energy gain of 40 GeV for a fraction of the electrons in the tail of the bunch in the blow-out regime [42].

Usually the focusing force of the bubble regime is very high, for example, the transverse field of a long ion channel is $E_r = E_o(k_p r/2)$ [38]. The focusing field in convenient units at the edge of an electron beam with radius σ_r

$$E_r(MV/m) \simeq 9.06 \times 10^{-15} n_o(cm^{-3})\sigma_r(\mu m). \tag{1.19}$$

This transverse focusing force will force a relativistic electron with $\gamma \gg 1$ to perform betatron oscillations about the axis with a betatron wavelength $\lambda_\beta = (2\gamma)^{1/2}\lambda_p$ [43]. The rms radius of a highly relativistic electron bunch is described by the equation

$$\frac{d^2\sigma_r}{dz^2} + k_\beta^2\sigma_r = \frac{\epsilon_n^2}{\gamma^2\sigma_r^3}, \tag{1.20}$$

where ϵ_n is the normalized beam emittance, the focusing force is taken to be linear and we have neglected the space charge of the beam, energy spread and acceleration. Moreover, $k_\beta^2 = eE_r/(\gamma m_e c^2 r)$ or $k_\beta = 2\pi/\lambda_\beta = k_p/(\sqrt{2\gamma})$ in the bubble regime. The matched condition (i.e., the beam propagates with a constant bunch radius) for an electron bunch in such a focusing channel is $\sigma_{rm} = \sqrt{\epsilon_n/(\gamma k_\beta)}$. For example, $n_o = 10^{17}$ cm^{-3}, $\gamma = 1000$, and $\epsilon_n = 1$ rad mm give $\lambda_\beta = 4.7$ mm, $\sigma_{rm} = 0.86$ μm, and $E_r = 780$ MV/m [16].

If we assume a spherical ion cavity of radius R, which is centered at r = 0 and $\xi = 0$ and is moving with relativistic velocity then the transverse focusing field

E_r, the longitudinal accelerating field E_z, and azimuthal magnetic field B_θ within the cavity are given by [36, 44]

$$E_r = \frac{E_o k_p \xi}{4}, \tag{1.21}$$

$$E_z = \frac{E_o k_p r}{2}, \tag{1.22}$$

$$B_\theta = -\frac{E_o k_p r}{4}, \tag{1.23}$$

where $\xi = z - ct$. The axial electric field will be maximum when $\xi = r_\beta$, where r_β is the amplitude of the betatron oscillation of an electron inside the ion cavity. The radial wakefield is electromagnetic and the transverse force felt by a highly relativistic electron inside the cavity is equal to $F_r = E_r - B_\theta$.

In the case of laser beam drivers, the bubble wakefield can be obtained for many regimes, for example for the long pulse self-modulated regime [34, 45, 46, 47] and for the short pulse LWFA regime [35, 36, 44, 48, 49, 50]. For a long laser pulse with slowly varying axial profile the plasma density profile can be calculated by balancing the radial ponderomotive force with the space charge force. The plasma density in the long pulse adiabatic limit is given by

$$\frac{n}{n_o} = 1 + \frac{\nabla_\perp^2 \sqrt{1+a^2}}{k_p^2} \tag{1.24}$$

assuming circular polarization. If we assume a Gaussian pulse profile of the form $a^2 = a_o^2 \exp(-2r^2/r_o^2)$ then the on axis density is

$$\frac{n(r=0)}{n_o} = 1 - \frac{4}{r_o^2 k_p^2} \frac{a_o^2}{\sqrt{1+a_o^2}}, \tag{1.25}$$

which suggests that a complete blowout of plasma electrons is possible if the intensity of the laser satisfies the relation

$$\frac{a_o^2}{\sqrt{1+a_o^2}} \geq \frac{k_p^2 r_o^2}{4}. \tag{1.26}$$

In the relativistic intensity limit, $a_o^2 \gg 1$, the condition $a_o \geq k_p^2 r_o^2/4$ is required or in terms of spot size $r_o \leq 2\sqrt{a_o}/k_p$ has to hold to create a bubble. Moreover, to cavitate the electrons from a larger radius requires higher intensity [16].

For the case of a short intense laser pulse with $L \leq \lambda_p$ and $a^2 \geq 1$, a large amplitude wake of highly nonlinear nature can be generated in a manner analogous to that of an electron beam driver in the PWFA. The bubble regime created by laser beams has been studied by Mora [34] for laser fields $a_o = 0.25 - 3$, spot sizes $k_p r_o = 4 - 16$, and pulses lengths $k_p L = 10$ using a time averaged particle code. They observed the self-steepening pulse compression to $k_p L \sim 2$, self-focused propagation up to 30 Z_r through a uniform plasma, where $Z_r = k r_o^2/2$ is the Rayleigh length of the laser.

The blowout or bubble regime using a short ultra-intense laser pulse has also been studied using PIC simulations and theoretical modeling by [35, 36, 48]. The authors used a similarity theory in which the wake is characterized by the similarity parameter $S = k_p^2/(a_o k^2)$, where k is the wave vector. They found that a maximum wake amplitude can be generated for laser spot radius of $k_p r_o \simeq \sqrt{a_o}$, a pulse length $L = c\tau \leq r_o$, and a power P(GW) $> 30(\tau(fs/\lambda(\mu m)))^2$. They also stated the acceleration length equal to $L_{acc} \simeq 0.7(L/\lambda)Z_R$ and predicted the formation of a quasi-monoenergetic electron bunch with energy $W \simeq 0.22(L/\lambda)\sqrt{P(GW)}m_e c^2$.

An analytical treatment is also developed by Lu Hung [36] for the generation of a wake in the blowout regime. In the high intensity limit, $a_o \geq 4$, they find an optimal wake generation for a laser spot radius of $k_p r_o \simeq 2a_o$. They also predict that in such a case the dimension of the bubble is approximately a sphere with a radius $r_\beta \simeq (2/k_p)\sqrt{a_o}$, which is similar to the result obtained from balancing the radial ponderomotive force with the space charge force.

Laser-plasma interaction is a fast growing area of research due to many interesting phenomenon and applications [37, 51, 52, 53]. However, there are some factors, which limit the energy gain of the electrons from plasma waves.

1.3.5. Electron acceleration limits and dephasing

There are many effects and process that can limit the energy gain of the trapped particles in a LWFA. For example, laser diffraction, pump depletion, electron dephasing and some other instabilities arise due to laser plasma interaction. In vacuum a laser beam undergoes Rayleigh diffraction, which means that the laser beam radius evolves according to $r_s = r_o\sqrt{(1 + z^2/Z_R^2)}$, where r_o is the beam waist at the focus point $z = 0$ and Z_R is the Rayleigh length. Without optical guiding the laser plasma interaction distance will be limited to a few Z_R [16]. A laser driver that excites a plasma wave loses energy, i.e., depletes [54, 55, 56, 57]. The pump depletion length L_{pd} is estimated by equating the laser pulse energy to the energy left behind in the wakefield, which is given by the relation $E_z^2 L_{pd} \simeq E_L^2 L$, where E_L is the laser field.

We know that as an electron is accelerated its velocity increases and approaches the speed of light, $\vec{v} \rightarrow c$. The phase velocity of the plasma wave is normally smaller than the speed of light. Therefore, the accelerating electron outruns the plasma wave and moves into a region of deceleration. This phenomenon limits the energy gain of electrons in a plasma wave and is commonly know as electron dephasing. The dephasing length L_d of an electron can be defined as the length an electron must travel before its phase slips by one-half of a period with respect to the plasma wave. For a highly relativistic electron, $\vec{v} \simeq c$ the linear dephasing length is given by

$$L_d \simeq \gamma_p^2 \lambda_p \tag{1.27}$$

assuming that $\gamma_p = \omega_L/\omega_p \gg 1$. The maximum energy gain after a dephasing length is roughly $W_{max} \simeq eE_{max}L_d \simeq 2\pi\gamma_p^2(E_{max}/E_o)m_e c^2$ assuming $E_{max} < E_o$ [4, 58].

In the 1D limit, we consider a linearly polarized square profile laser pulse with $L \simeq \lambda_{Np}$. The dephasing and pump depletion length are given by [59, 60]

$$L_d \simeq \frac{\lambda_p^3}{2\lambda_L^2} \begin{cases} 1, & \text{for } a_o^2 \ll 1 \quad (1.28) \\ \sqrt{2}a_o/(N_p\pi), & \text{for } a_o^2 \gg 1 \quad (1.29) \end{cases}$$

$$L_{pd} \simeq \frac{\lambda_p^3}{\lambda_L^2} \begin{cases} 2/a_o^2, & \text{for } a_o^2 \ll 1 \quad (1.30) \\ \sqrt{2}a_o/(\pi), & \text{for } a_o^2 \gg 1 \quad (1.31) \end{cases}$$

where N_p is the number of plasma periods behind the laser pulse. The factor $\lambda_p^3/(2\lambda_L^2)$ arises from the fact that a highly relativistic electron traveling in the wake has a phase slip of $\lambda_p/4$, as only one quadrant of a plasma wave is suitable for simultaneous focusing and acceleration.

In the linear regime ($a_o^2 \ll 1$) the electron dephasing length is smaller than the pump depletion length, i.e. $L_d \ll L_{pd}$. Therefore, the energy gain of accelerating electrons is usually limited by dephasing not by pump depletion in the linear regime. However, in the nonlinear regime ($a_o^2 > 1$), $L_d \sim L_{pd}$ and the energy gain is limited by pump depletion.

Rapid developments in laser technology have made the direct electron acceleration a competitor to wakefield acceleration. Electron acceleration by focused laser beams and acceleration by laser produced plasma waves are of same order. However, for ultra short intense laser pulses direct electron acceleration by a laser pulse dominates.

1.4. Electron acceleration by a focused laser beam

With the development of the chirped-pulse-amplification technique table-top high-peak power lasers have been successfully developed with light intensities as high as $I_o \simeq 10^{21}$ W/cm^2, where I_o is the laser intensity. Use of intense lasers to accelerate electrons is also a very active field. The vacuum far-field acceleration has the advantage of a simple experimental setup. Malka et al., [61] have shown a 0.9 MeV electron beam for a normalized laser intensity of $a_o = 3$ and a few GeV energy electron beams have been obtained by focused laser beam acceleration in

vacuum as well [62, 63, 64]. However, electron acceleration by electromagnetic fields in vacuum is not very efficient even if ultra-intense lasers are used. To accelerate an electron up to GeV energies by far fields in vacuum we need to capture the electron by the laser field instead of reflecting or transmitting it, which mainly depends on the initial parameters of the incident electron.

It is a well-know fact that an accelerating electron radiates and that the emitted radiation reacts back on the electrons, which affects its energy gain, trajectory, and other energy dependent properties. For both, laser wakefield and laser acceleration in vacuum the accelerating electrons oscillate due to transverse electric field components (in a laser wakefield off-axis electrons exhibit betatron oscillations). The oscillating electrons emit radiation and this radiation reacts back on them. For low energy electron beams radiation effects are small, however, for high energy electron beams the effects of emitted radiation become severe. For example, in LWFA the transverse focusing field, in general, is of the order of the longitudinal accelerating field. Trapped electrons exhibit betatron oscillations due to the strong focusing force. The oscillating electrons in laser wakefields radiate in a similar fashion as the electrons in an undulator field [65]. The power radiated by a single electron in an undulator field scales as $P_u = \gamma^2 k_u^2 a_u^2$, where γ is the relativistic factor of the electron, $\lambda_u = 2\pi/k_u$ is the undulator wavelength and $a_u = eB_u/(k_u m_e c^2)$ is the undulator strength parameter, where B_u is the amplitude of the undulator magnetic field with e, m_e representing the charge and mass of the electron and c is the speed of light [65]. The amount of energy radiated by an electron can be substantial. It may have significant effects on the evolution of an electron beam. The basic effect of the betatron radiation is the decrease in energy gain of the electron beam which in turn affects the energy dependent properties of it [19, 66, 67, 68].

The effects of radiation reaction in laser pulses [69, 70, 71] and in laser wakefields [19, 66, 67] have been studied. Currently relativistic electron bunches with charge ≥ 100 pC are produced in laser wakefields [21, 22, 23], which implies $> 10^9$

electrons per bunch. It is apparent that if the radiation of a single electron inside the beam affects its own motion [19, 66, 67, 69] it should also affect the motion of the other electrons of the beam for certain parameters. A numerical study of retardation effects (radiation effects of one electron on the other electron of the system) is carried out in [72, 73]. Due its complex structure the self fields and retardation effects have been studied separately. However, the realistic system requires the investigation of accumulated effects (self-field effects plus the radiation effects from other electrons of the system) of radiation. Moreover, there is very limited literature available concerning the retardation effects. Therefore, there is a need to investigate the accumulated effects of radiation on the electron motion. In this thesis we study the effects of betatron radiation from a single particle and multiple particles. Different cases of the electron motion will be studied, for example, the case of a counter-propagating electron in the plane and circularly polarized electromagnetic wave, the motion of an electron beam in a plasma focusing channel and in a focused laser beam.

1.5. Radiation reaction

The motion of an electron in external electromagnetic fields is studied with the help of the Lorentz force equation $m\dot{u^\alpha} = -(e/c)F^{\alpha\beta}u_\beta$, where $F^{\alpha\beta}$ is the electromagnetic tensor, m, e are the mass and charge of the electron respectively, c is the speed of light and u_β is the four velocity of the electron. The Maxwell theory together with the Lorentz equation give the amount of the electromagnetic radiation that an accelerating charged particle radiates

$$\frac{dE}{dt} = \frac{e^2}{6\pi\epsilon_o c^3}\dot{u}^\alpha \dot{u}_\alpha, \tag{1.32}$$

where E is the energy and ϵ_o is the permittivity of free space. It is called the Larmour formula. The reaction of energy-momentum loss given by equation (1.32) is not included in the Lorentz equation. Thus, the Lorentz equation is limited to the

case when the emitted radiation is small. Recently [69] has shown that a relativistic electron with initial energy $\gamma_o = 1000$ interacting head-on with a laser pulse of normalized intensity $a_o = 100$, back reaction of the emitted radiation cannot be neglected. Lorentz himself provided another equation for the radiating electron, which is given by [74]

$$\frac{d\vec{p}}{dt} = e(\vec{E} + \vec{v} \times \vec{B}) + \frac{e^2}{6\pi\epsilon_o c^3}\ddot{v}. \tag{1.33}$$

1.5.1. The electron as a point particle

Later on Abraham developed a highly successful theory of the moving electron [75, 76] before Einstein's papers [77, 78] on special relativity, which appeared in 1905. He had derived the following equation of motion for a rigid sphere of charge e and radius a in the approximation of small a

$$\begin{aligned} m\frac{d(\gamma\vec{v})}{dt} &= \vec{F}_L - m_{ed}\frac{d(\gamma\vec{v})}{dt} + \frac{e^2\gamma^2}{6\pi\epsilon_o c^3}\Bigg[\ddot{\vec{v}} + 3\gamma^2\vec{v}\cdot\dot{\vec{v}}\dot{\vec{v}} \\ &\quad + \gamma^2[\vec{v}\cdot\ddot{\vec{v}} + 3\gamma^2(\vec{v}\cdot\dot{\vec{v}})^2]v\Bigg], \end{aligned} \tag{1.34}$$

where $m_{ed} = \frac{e^2}{6\pi\epsilon_o ac}$ is the electrodynamic mass of the charged sphere, F_L is the Lorentz force and the dot denotes the derivative with respect to time t. The second term on the R.H.S of equation (1.34) can be combined with L.H.S to get the observed rest mass of the sphere i.e. $m_o = m + m_{ed}$. This is called mass renormalization. Von Laue recognized the term in the square bracket of equation (1.34) as the relativistic generalization of the last term in the Lorentz equation (1.33) and represented it as $\Gamma^\mu = \frac{e^2}{6\pi\epsilon_o c^3}(\ddot{v}^\mu - \dot{v}^\alpha\dot{v}^\alpha v^\mu/c^2)$ [74]. Abraham also derived an equation for the energy change of a charged sphere, which is given by

$$m\frac{d\gamma}{dt} = \vec{F}_L\cdot\vec{v} - m_{ed}\frac{d}{dt}\left(\gamma - \frac{1}{4\gamma}\right) + \frac{e^2\gamma^4}{6\pi\epsilon_o c^3}\left[\vec{v}\cdot\ddot{\vec{v}} + 3\gamma^2(\vec{v}\cdot\dot{\vec{v}})^2\right]. \tag{1.35}$$

However, if we take the dot product of equation (1.34) with $\vec{v}$ then we see that it does not yield equation (1.35). This is know as $3/4$ problem and was solved by

Poincare leading to the following equation of motion [74]

$$m\dot{v}^{\mu} = F_L^{\mu} - m_{es}\dot{v}^{\mu} + \Gamma^{\mu}, \tag{1.36}$$

where $m_{es} = e^2/(8\pi\epsilon_o ac^2)$. In 1939 after the development of quantum mechanics, Dirac derived a classical equation for a point charge using Maxwell's equations, the conservation laws, and neglecting higher order terms. His equation is given by [74]

$$m\dot{v}^{\mu} = F_L^{\mu} + \Gamma^{\mu}. \tag{1.37}$$

Dirac's derivation is manifestly covariant, however, he did it for a point charge therefore, the m_{es} term is infinite in his derivation. Equation (1.37) is known as the Lorentz-Abraham-Dirac (LAD) equation.

The LAD equation (1.37) is considered as one of the adequate equations to describe the motion of a radiating electron but it and its non-relativistic form (i.e., equation 1.33) have unphysical solutions. For example, there is force-free acceleration, which means that a charged particle accelerates indefinitely (it is called the runaway solution) and the pre-acceleration, i.e., the charged particle accelerates before the arrival of the force.

The unphysical solutions can be avoided by including all power of a in the derivation of the equation. However, it can also be avoided without including higher order size dependent terms. For runaway solution we can apply the asymptotic condition that the acceleration in the distant future vanishes. The pre- acceleration problem has been solved by removing its origin by Yaghjian [79].

He emphasized that the function used in the derivation of the LAD equation must be analytical as one integrates over the retarded time. This analyticity is violated when the force changes too quickly (when the time is short compared to time it takes a light ray to cross the charged sphere). He introduced a smooth function $\eta(\tau)$, which vanishes for $\tau < 0$. He wrote equation (1.37) in a new form

$$m\dot{v}^{\mu} = F_L^{\mu} + \eta\Gamma^{\mu}, \tag{1.38}$$

equation (1.38) does not have pre-acceleration solution.

Many models have been developed to avoid these unphysical solutions by Landau and Lifshitz [5], Eliezer [80], Mo and Papas [81], Caldirola [82], Yaghjian [79] and Sokolov [83, 84]. However, the Landau-Lifshitz (LL) equation provides a good first order approximation of the LAD equation. It can be obtained by the perturbative expansion of the LAD equation by assuming that the radiation part is smaller than the applied Lorentz term

$$m\dot{u^{\alpha}} \;=\; -\frac{e}{c}F^{\alpha\beta}u_{\beta} - \frac{e}{c}\tau_o\Big[\frac{\partial F^{\alpha\beta}}{\partial x^{\gamma}}u^{\gamma}u_{\beta} - \frac{e}{mc}\Big(F^{\alpha\beta}F_{\beta\gamma}u^{\gamma} - F^{\beta\gamma}F_{\gamma l}u^{l}u_{\beta}u^{\alpha}\Big)\Big], \quad (1.39)$$

where $\tau_o = e^2/(6\pi\epsilon_o m_e c^3)$. The perturbative expansion is valid as long as radiation reaction is smaller than the applied Lorentz force.

1.5.2. The charged sphere

The problem of infinite self-energy of the electron in the LAD equation can be handled by considering a charged particle of finite size (i.e., a charged sphere). It includes the work of Abraham and many others, for a review see [74]. We mention the excellent work of Sommerfeld [85]. He showed that a sphere with uniform surface charge can be described by the following delay differential equation in the non-relativistic limit

$$m\dot{\vec{v}} \;=\; \vec{F}_L + m_{ed}\frac{1}{2a}\Big(\vec{v}(t-2a/c) - \vec{v}(t)\Big), \quad (1.40)$$

where $m_{ed} = e^2/(6\pi\epsilon_o ac)$ is the electrodynamic mass, v is the velocity, and a is the radius of the charged sphere. Equation (1.40) is a delay differential equation and it describes the motion of any charged sphere of finite dimension.

1.5.3. The Caldirola equation

The Sommerfeld equation describes the motion of a charged sphere in the non-relativistic limit. The relativistic generalization to the Sommerfeld equation was

provided by Caldirola [82]

$$m\dot{v}^{\mu} = F_L^{\mu} + m_{ed}\frac{1}{2a}\big[v^{\mu}(\tau - 2a/c) + v^{\mu}(\tau)v^{\alpha}(\tau)v_{\alpha}(\tau - 2a/c)/c^2\big]. \quad (1.41)$$

The Caldirola equation can be reduced to the LAD equation for a point particle, $i.e., a \to 0$. In the limit $a \to 0$ the delay terms can be expanded using a Taylor series expansion, which gives

$$\lim_{a\to 0} v^{\mu}(\tau - 2a/c) = v^{\mu}(\tau) - \frac{2a}{c}\dot{v}^{\mu}(\tau) + \frac{4a^2}{c^2 2!}\ddot{v}^{\mu} + \ldots \quad (1.42)$$

$$\lim_{a\to 0} v_{\alpha}(\tau - 2a/c) = v_{\alpha}(\tau) - \frac{2a}{c}\dot{v}_{\alpha}(\tau) + \frac{4a^2}{c^2 2!}\ddot{v}_{\alpha} + \ldots. \quad (1.43)$$

With the information $v^{\alpha}(\tau)v_{\alpha}(\tau) = -c^2$ and $v^{\alpha}(\tau)\dot{v}_{\alpha}(\tau) = 0$ equation (1.41) can be written as

$$m\dot{v}^{\mu} = F_L^{\mu} + m_{ed}\frac{1}{2a}\big[-\frac{2a}{c}\dot{v}^{\mu} + \frac{2a^2}{c^2}\ddot{v}^{\mu}(\tau) + \frac{2a^2}{c^2}v^{\mu}(\tau)v^{\alpha}(\tau)\ddot{v}_{\alpha}(\tau)/c^2\big], \quad (1.44)$$

where we have neglected the higher order terms as they are much smaller. We have $v^{\alpha}(\tau)\ddot{v}_{\alpha}(\tau) = -\dot{v}^{\alpha}(\tau)\dot{v}_{\alpha}(\tau)$ [74] and the first term in the square brackets will be combined with the term on the left hand side to yield the empirical rest mass. This is called mass renormalization and equation (1.44) will take the shape of the LAD equation

$$m\dot{v}^{\mu} = F_L^{\mu} + m_e\tau_o\big[\ddot{v}^{\mu}(\tau) - v^{\mu}(\tau)\dot{v}^{\alpha}(\tau)\dot{v}_{\alpha}(\tau)/c^2\big]. \quad (1.45)$$

The Caldirola equation, which describes the motion of a radiating charged sphere, has reduced to the LAD equation. Therefore, the Caldirola equation is equally valid as the LAD equation.

Let us now derive the Caldirola equation from a simple assumption. To drive the Caldirola equation we assume that an accelerating charge element de' at position $r'(t')$ produces an electric field $d\vec{E}(r,t)$ and is given by

$$d\vec{E}(r,t) = \frac{dq'}{4\pi\epsilon_0[1 - \hat{R}'\cdot u/c]^3}\Big\{\frac{\hat{R}'}{R'c^2}\times\Big[(\hat{R}' - \frac{u(r',t')}{c})\times\dot{u}(r',t')\Big] + \frac{1}{R'^2}\big[1 - \frac{u^2(r',t')}{c^2}\big]\big[\hat{R}' - \frac{u(r',t')}{c}\big]\Big\}, \quad (1.46)$$

where $u(r',t') = dr'(t')/dt'$ and $\dot{u}(r',t') = d^2r'(t')/dt'^2$ are the velocity and acceleration of the charge element at the retarded time $t' = t - |R'(t')|/c$ respectively. The factor $\vec{R}'(t') = \vec{r} - \vec{r}'(t')$ is the distance between the observation position of the observer and retarded position of the charge element de' and $\hat{R}' = \vec{R}'(t')/|\vec{R}'(t')|$ is a unit vector along the observation direction. Its expansion in a power series about t gives

$$\begin{aligned}\hat{R}' &= \hat{R} - \frac{R}{2c}\Big(\frac{\vec{r}'\cdot\dot{u}}{c^2} - 1\Big)((\hat{R}\cdot\dot{u})\hat{R} - \dot{u}) - R^2\hat{R}\left(\frac{(\hat{R}\cdot\dot{u})^2}{8c^4} + \frac{|\dot{u}|^2}{8c^4} + \frac{\hat{R}\cdot\ddot{u}}{6c^3}\right) \\ &\quad + R^2\left(\frac{(\hat{R}\cdot\dot{u})\dot{u}}{4c^4} + \frac{\ddot{u}}{6c^3}\right) + O(R^3). \qquad (1.47)\end{aligned}$$

In the proper frame of reference ($\vec{u}(r,t) = 0$) equation (1.46) can be written as

$$d\vec{E}(r,t) = \frac{dq'}{4\pi\epsilon_0[1 - \hat{R}\cdot u/c]^3}\left[\frac{\hat{R}\times(\hat{R}\times\dot{u}(t'))}{Rc^2} + \frac{\hat{R}' - \frac{u(r',t')}{c}}{R'^2}\right]. \qquad (1.48)$$

We use the expansion

$$\left(1 - \frac{\hat{R}\cdot\vec{u}(t')}{c}\right)^{-3} = 1 + \frac{3\hat{R}\cdot\vec{u}(t')}{c} + \text{nl terms} \qquad (1.49)$$

and (1.48) can be written as

$$d\vec{E}(r,t) = \frac{dq'}{4\pi\epsilon_0}\Big[\frac{\hat{R}(\hat{R}\cdot\dot{u}(t')) - \dot{u}(t')}{Rc^2} - \frac{u(t')}{R^2c} + \frac{3\hat{R}(\hat{R}\cdot u(t'))}{R^2c} + \frac{\hat{R}'(t')}{R'^2}\Big] \qquad (1.50)$$

and now

$$\vec{R}'(t') = \vec{R}(t) + \frac{\vec{u}(t)}{2}\Big(\frac{R}{c}\Big)^2 - \frac{\vec{\dot{u}}(t)}{6}\Big(\frac{R}{c}\Big)^3 + \cdots + \text{nl terms} \qquad (1.51)$$

or we can write

$$\vec{R}'(t') = \vec{u}(t - R/c) + \text{nonlinear terms}, \qquad (1.52)$$

similarly

$$\vec{u}(t') = \vec{u}(t - R/c) + \text{nonlinear terms}, \qquad (1.53)$$

$$\vec{\dot{u}}(t') = \vec{\dot{u}}(t - R/c) + \text{nonlinear terms}, \qquad (1.54)$$

$$R(t') = R(t - R/c) + \text{nonlinear terms}, \qquad (1.55)$$

$$R'(t') \;=\; R - \dot{R}\frac{R}{c} + \frac{\ddot{R}}{2}\big(\frac{R}{c}\big)^2 + \cdots + \text{nl terms.} \tag{1.56}$$

The quantities on the R. H. S in equation (1.56) are function of the observation time t. We can write

$$\begin{aligned}\frac{\vec{R}'(t')}{R'^3(t')} &= \frac{\vec{R}}{R^3}\Big[1 - \frac{3}{R}\big(\frac{\widehat{R}\cdot\dot{u}}{2}(\frac{R}{c})^2 - \frac{\widehat{R}\cdot\ddot{u}}{6}(\frac{R}{c})^3 + \dots\big)\Big] \\ &\quad + \frac{1}{R^3}\Big[\frac{\dot{u}}{2}(\frac{R}{c})^2 - \frac{\ddot{u}}{6}(\frac{R}{c})^3 + \dots\Big] + \text{nl terms.}\end{aligned} \tag{1.57}$$

Inserting equations (1.53), (1.54), and (1.57) in equation (1.50) and integrating over $dq' = de'$ and $dq = de$ for the total self force F_s, we are left with the integral of the form

$$\iint\limits_{charge} R^m dq dq' \;=\; 3\iint\limits_{charge}\frac{x^2}{R^2}R^m dq dq' = \frac{2^{m+1}}{m+2}a^m e^2, \tag{1.58}$$

$$\vec{F}_s(t) \;=\; \iint\limits_{charge}\frac{\vec{\ddot{u}}(t')}{R}\cdot\Big[\widehat{R}\widehat{R} - \bar{I}\Big]dq'dq, \tag{1.59}$$

$$\vec{F}_s(t) \;=\; \frac{1}{4\pi\epsilon_0}\iint\limits_{charge}\frac{\vec{\ddot{u}}(t')}{R}\cdot\Big[\widehat{R}\widehat{R} - \bar{I}\Big]dq'dq, \tag{1.60}$$

$$\;=\; -\frac{1}{4\pi\epsilon_o}\frac{2}{3}\iint\limits_{charge}\frac{\dot{u}(t - R/c)}{R}dq'dq + \text{nl terms,} \tag{1.61}$$

$$\;=\; \frac{1}{12\pi\epsilon_0 a^2 c}\sum_{n=0}^{\infty}\frac{(\frac{-2a}{c})^{n+1}}{(n+1)!}\frac{\partial^{n+1}}{\partial t^{n+1}}\vec{u}(t) + \text{nl terms,} \tag{1.62}$$

$$\vec{F}_s(t) \;=\; m_{ed}\frac{1}{2a}\Big[\vec{u}(t - 2a/c)\Big]. \tag{1.63}$$

Hence, the relativistic equation of motion of a particle of bare mass m under the Lorentz force can be written as

$$m\dot{v^\mu} \;=\; F^\mu_{total}, \tag{1.64}$$

$$m\dot{v^\mu} \;=\; F^\mu_L + F^\mu_s, \tag{1.65}$$

$$F^{\mu\alpha}_s \;=\; m_{ed}\frac{1}{2a}P^{\mu\alpha}v_\alpha(\tau - 2a/c), \tag{1.66}$$

$$F_s^{\mu\alpha} = m_{ed}\frac{1}{2a}\Big[v^\mu(\tau - 2a/c) + v^\mu(\tau)v^\alpha(\tau)v_\alpha(\tau - 2a/c)/c^2\Big], \quad (1.67)$$

$$m\dot{v^\mu} = F_L^\mu + m_{ed}\frac{1}{2a}\Big[v^\mu(\tau - 2a/c) + v^\mu(\tau)v^\alpha(\tau)v_\alpha(\tau - 2a/c)/c^2\Big]. \quad (1.68)$$

This is called the Caldirola equation and it is the relativistic form of the Sommerfeld equation. Both are free from unphysical solutions.

CHAPTER 2

The effects of betatron radiation on an electron beam in a laser wakefield

2.1. Introduction

As stated earlier, in a laser wakefield accelerator (LWFA) trapped electrons exhibit betatron oscillations due to the strong focusing force and these oscillations give rise to betatron radiation. The basic effect of betatron radiation is the decrease in energy gain of the electron beam, which in turn affects energy dependent properties of it [66].

The dynamics of the electron beam in a plasma channel is different from that in an undulator field. In the undulator all the electrons of the beam feel almost the same periodic transverse force, which is only a very weak function of the radius. As a result they perform similar transverse oscillations independent of their initial positions. This is not, however, the case in a plasma channel, where the transverse focusing field is a strong function of the radius. Hence, the lateral motion of electrons inside the channel strongly depends on their initial radial position. Electrons propagating along the axis of the plasma channel will not be affected by

the transverse focusing field of the latter. However, electrons initially off axis will experience a strong transverse focusing force. Betatron radiation can be characterized by the betatron strength parameter $a_\beta = \gamma k_\beta r_\beta$, where $\lambda_\beta = 2\pi/k_\beta$ is the betatron period and r_β is the radial amplitude of the betatron oscillation. A large a_β implies large radiation loss. Thus, electrons initially very close to the axis will hardly loose any energy while those with large lateral positions will have large betatron amplitudes and hence loose significant amounts of energy.

High energy loss by betatron radiation can expels electrons from the accelerating phase of the wake to the decelerating phase in the wakefield. As a consequence the energy of the electrons decreases rapidly. This decrease in energy leads to the increase in the amplitude of betatron oscillation, which in turn increases the transverse emittance of the beam. The transverse emittance is the measure of the phase space area occupied by the particles of the beam in transverse direction. It is an important parameter along with others such as mean energy and energy spread. High mean energy, low emittance, and low energy spread of the electron beam represent a good quality particle accelerator.

In what follows ultra relativistic electron beams with relativistic initial energy moving in a laser wakefield with plasma density $n_o = 10^{15}$ cm^{-3} are studied. The main emphasis is put on the investigation of the evolution of the transverse emittance of the particle beam by radiation damping at high energy. Other beam properties, e.g. mean energy and energy spread will also be discussed in short. The low density regime has been selected because (i) in the low density LWFA the transverse focusing force is strong even in the quasilinear regime [66, 19] while it is severe in the bubble regime [35], (ii) radiation loss is mitigated until the electron energy becomes very high, (iii) the one stage energy gain of electrons is so high (TeV) that energy loss due to betatron radiation must be considered, (iv) a sufficiently large accelerating gradient can be maintained that can compensate for the enlarged betatron radiation effects.

A weak betatron radiation can act as a cooling agent (in addition to being

an energy damper) so that the emittance of some of the electrons can decrease [66, 19]. However, strong radiation effects have a different impact, which will be studied here. Therefore, as we shall see, particularly interesting radiation physics can occur at very high energies in the low density LWFA regime (at higher density it occurs at much smaller energies). The low density LWFA regime also gives us the opportunity to study the spectral signature of betatron radiation at very high energies (beyond 30 TeV) to see if it obeys the known dependence on γ (as discussed above) or deviates from it, as postulated in [86] as evidence of Lorentz invariance violation.

2.2. The laser wakefield

In this section we present a review of the wakefield produced by an intense laser pulse in a plasma and study the motion of a single test electron in the wakefield. The study of test electrons is essential to understand the properties of the electron beam inside the plasma channel.

An ultra intense laser pulse with a duration τ_L approximately equal to a plasma oscillation period $2\pi/\omega_p$ creates a large amplitude plasma wave with a phase velocity approximately equal to the speed of light [7, 8, 9, 10, 11, 12]. Let us consider the propagation of a Gaussian laser pulse with the group velocity v_g through a uniform plasma medium along the longitudinal, say, $\hat{z}$-direction. It can be shown that it generates the trailing ponderomotive potential

$$\phi = \phi_{max}\varepsilon \sin(k_p\xi), \tag{2.1}$$

where $\phi_{max} = \pi a_o^2 E_{bk}/(4k_p)$, a_o is the normalized laser intensity, $\varepsilon = \exp(-2r^2/r_o^2)$, r is the transverse radius, r_o is the laser spot size, $E_{bk} = k_p m_e c^2/e$ is known as the Tajima-Dawson field and $\lambda_p = 2\pi/k_p$ is the plasma wavelength. The plasma wave travels almost with the group velocity of the laser pulse i.e. $v_p \simeq v_g$. Representing the phase of the plasma wave by $\psi = k_p\xi$, where $\xi = z - v_g t$. The longitudinal and

transverse wakefields can be written as

$$E_z = -\frac{\partial \phi}{\partial z} = -E_{zo}\,\varepsilon\,\cos(\psi)\,, \tag{2.2}$$

$$E_x = -\frac{\partial \phi}{\partial x} = E_{xo}\,\varepsilon\,x\,\sin(\psi)\,, \tag{2.3}$$

where $E_{zo} = (\pi a_o^2/4)(k_p m_e c^2/e)$, $E_{xo} = (\pi a_o^2/r_o^2)(m_e c^2/e)$, and x is the transverse coordinate [87].

2.2.1. The motion of a single charged particle

Given the recent development of laser-driven plasma-based electron accelerators it is possible to obtain high energy (TeV) electron beams with large energy lasers and low density operation [19]. It seems possible that a (PeV) energy beam is obtainable in the future [88]. As stated earlier, a beam that undergoes a strong transverse focusing force in plasma waves exhibits betatron oscillations. These betatron oscillations give rise to the emission of intense betatron radiation. It is obvious that for a high energy electron beam the effect of betatron radiation becomes stronger because the betatron radiation is a function of the electron energy. The betatron radiation reduces the energy gain and affects the energy spread, emittance and other properties of the beam in the plasma wave via radiation reaction.

The motion of a radiating electron can be described by the Landau-Lifshitz (LL) equation. The LL equation (1.39) in three vector notation can be written as [5]

$$\frac{d\vec{u}}{\mathrm{d(ct)}} = -\frac{e}{m_e c^2}\left(\vec{E} + \vec{v}\times\vec{B}\right) - \frac{\tau_o e}{m_e c^2 \gamma}\frac{\mathrm{d}}{\mathrm{dt}}\left(\vec{E} + \vec{v}\times\vec{B}\right) + \frac{\tau_o e^2}{m_e^2 c^3}\Big[c(\vec{E}\times\vec{B}$$
$$+(\vec{v}\times\vec{B})\times\vec{B}) + (\vec{v}/c\cdot\vec{E})\vec{E} - \vec{v}\frac{\gamma^2}{c}\left((\vec{E} + \vec{v}\times\vec{B})^2 - (\vec{v}/c\cdot\vec{E})^2\right)\Big], \tag{2.4}$$

where $\vec{u} = \gamma\vec{v}/c$ is the three vector momentum of the electron and $\gamma = \sqrt{1+\vec{u}^2}$ is the relativistic Lorentz factor of the electron. In what follows we consider only

velocities v_x and v_z. Equation (2.4) then becomes

$$\frac{\mathrm{du_x}}{\mathrm{d(ct)}} = -\frac{e}{m_e c^2}E_x + \frac{\tau_o e^2}{m_e^2 c^3}\left(v_z E_x E_z\right) - \frac{\tau_o e^2}{m_e^2 c^3}v_x\gamma^2\left(E_x^2 - 2v_x v_z E_x E_z\right), \quad (2.5)$$

$$\frac{\mathrm{du_z}}{\mathrm{d(ct)}} = -\frac{e}{m_e c^2}E_z - \frac{\tau_o e^2}{m_e^2 c^3}\gamma^2\left(E_x^2 - 2v_x v_z^2 E_x E_z\right), \quad (2.6)$$

where E_x, E_z are the electric field components in the x and z directions respectively and $\dot{x} = cv_x$. To obtain equations (2.5) and (2.6) we have assumed that $v_x \ll v_z \Longrightarrow \gamma^2 = 1/(1-v_z^2)$. Inserting equations (2.2) and (2.3) in equations (2.5) and (2.6) provides us with the following equations

$$\frac{\mathrm{du_x}}{\mathrm{dt}} = -cK^2 x\varepsilon\sin(\psi) - c\tau_o\zeta K^2 x\varepsilon^2\left(v_z\cos(\psi)\sin(\psi)\right) - c\tau_o K^4 x^2\dot{x}\gamma^2\varepsilon^2\sin^2(\psi)$$
$$-2\tau_o\zeta K^2\varepsilon^2 x\dot{x}^2\gamma^2\sin(\psi)\cos(\psi)/c, \quad (2.7)$$

$$\frac{\mathrm{d}\gamma}{\mathrm{dt}} = \zeta\varepsilon\cos(\psi) - \tau_o c^2 K^4\gamma^2 x^2\varepsilon^2\sin^2(\psi) - 2\tau_o\zeta K^2\varepsilon^2 x\dot{x}\gamma^2\cos(\psi)\sin(\psi), \quad (2.8)$$

where $K^2 = eE_{xo}/(m_e c^2)$ and $\zeta = eE_{zo}/(m_e c)$. To obtain equations (2.7) and (2.8) we have assume that $\gamma \simeq u_z$. Since the transverse trajectory of an electron is given by $\dot{x} = cu_x/\gamma$ and $\dot{u}_x$, $\dot{\gamma}$ are given by equations (2.7) and (2.8), we can write

$$\ddot{x} = \frac{c\dot{u}_x}{\gamma} - \frac{cu_x\dot{\gamma}}{\gamma^2} = \frac{c\dot{u}_x}{\gamma} - \frac{\dot{x}\dot{\gamma}}{\gamma}, \quad (2.9)$$

which leads to

$$\ddot{x} = -c^2K^2 x\varepsilon\sin(\psi)/\gamma - \zeta\dot{x}\varepsilon\cos(\psi)/\gamma - c^2\tau_o\zeta K^2 x\varepsilon^2 v_z\cos(\psi)\sin(\psi)/\gamma, \quad (2.10)$$

where dot denotes the derivative with respect to time t. Since $v_z = \sqrt{1-1/\gamma^2}$ holds it follow from equation (2.10)

$$\ddot{x} = -c^2K^2 x\varepsilon\sin(\psi)/\gamma - \zeta\dot{x}\varepsilon\cos(\psi)/\gamma$$
$$-c^2\tau_o\zeta K^2 x\varepsilon^2\sqrt{1-1/\gamma^2}\cos(\psi)\sin(\psi)/\gamma. \quad (2.11)$$

We use the following normalized quantities $\tilde{t} = t\omega_p$, $\tilde{x} = x/r_o$, and $\tilde{\gamma} = \gamma/\gamma_o$. We drop the $(\sim)$ sign for simplicity and find

$$\ddot{x} = -\eta_y x\varepsilon\sin(\psi)/\gamma - \eta_B\dot{x}\varepsilon\cos(\psi)/\gamma$$
$$-\eta_{xz}x\varepsilon^2(\sqrt{\gamma_o^2 - 1/\gamma^2})\cos(\psi)\sin(\psi)/\gamma, \quad (2.12)$$

$$\dot{\gamma} = \eta_B\varepsilon\cos(\psi) - \eta_\gamma\gamma^2 x^2\varepsilon^2\sin^2(\psi) - \eta_R\varepsilon^2 x\dot{x}\gamma^2\cos(\psi)\sin(\psi), \quad (2.13)$$

where $\eta_y = c^2K^2/(\omega_p^2\gamma_o)$, $\eta_B = \zeta/(\omega_p\gamma_o)$, $\eta_{xz} = \tau_o c^2K^2\zeta/(\omega_p^2\gamma_o^2)$, $\eta_R = 2\tau_o K^2\zeta r_o^2\gamma_o$, and $\eta_\gamma = \tau_o c^2K^4 r_o^2\gamma_o/(\omega_p)$.

Equations (2.12) and (2.13) describe the lateral motion and energy along the z-axis of a single charged particle in a plasma wave. The first term on the R.H.S of equation (2.12) simply represents the betatron oscillation of the electron with frequency $\omega_\beta = cK/\sqrt{\gamma}$ due to the transverse focusing force while the second term describes the damping behavior of the particle. The damping term arises due to the accelerating field. The third term is small as compared to the first and second terms and it has a negligible effect. Overall equation (2.12) is the equation of a damped harmonic oscillator provided the energy of the electron has the tendency to increase or remain constant.

Equation (2.13) shows that the energy of the electrons increases due to the accelerating field of the plasma wave while the radiative damping term, i.e. the second term in equation (2.13), counteracts the energy increase. For low energy and small radius the effect of radiation damping on the electron motion is almost negligible. The radiative damping term, which is quadratic both in energy and radial distance, will have a strong effect on the electrons with large initial radial distance in the ultra relativistic energy electron beam. In such a case the electrons will radiate a large amount of betatron radiation and will soon be dephased. In the beginning the effect of radiation reaction is very small due to the $\sin(\psi)$ function in the radiation damping term even for the electrons with large initial radii while the accelerating term will be dominant due to the $\cos(\psi)$ function. Later, however, radiation reaction starts affecting the electron motion. This phase sensitivity of the radiation damping could be vital for the beam dynamics. In particular, it can affect the number of the trapped particles and consequently the beam charge.

2.2.2. Electron beam dynamics

The behavior of an electron beam can be studied by averaging different quantities of a single electron over the ensemble of the electrons in the beam. The mean energy, e.g., is given by $\langle\gamma\rangle = \sum_i \gamma_i/N$, where γ_i is the energy of the ith particle and N is the number of electrons in the beam traveling in the plasma wave. However, energy is not the only important parameter to consider. Some other parameters also play a crucial role to fully reveal the underlying physics. Therefore, the performance of a laser wakefield accelerators should be determined by considering all parameters such as emittance, mean energy, and energy spread etc. [89].

2.2.2.1. Emittance

The normalized transverse emittance is the rms value of the phase space area

$$\epsilon_x \;=\; \sqrt{(\sigma_u\sigma'_u)^2 - c^2_{uu'}} \tag{2.14}$$

where $\sigma_u = \sqrt{\langle u^2\rangle - \langle u\rangle^2}$, $\sigma_{u'} = \sqrt{\langle u'^2\rangle - \langle u'\rangle^2}$, and $c_{uu'} = \sqrt{\langle uu'\rangle - \langle u\rangle\langle u'\rangle}$ with $u = \sqrt{\gamma}\; x$ and $u' = \sqrt{\gamma}\; dx/dt$ [87]. All of our results for emittance will correspond to the transverse phase space area of the beam.

In an accelerator, the emittance is considered as the most crucial parameter of the beam. For example, in the case of a collider, high luminosity is required to meet the practical objectives. Since the decrease of the cross section is, in general, inversely proportional to the energy of the beam, high luminosity is required to detect new physics. To obtain high luminosity, we require an electron beam with very low emittance [90]. In plasma-based accelerators, the emittance usually increases or remains almost constant [66, 67, 87, 90]. For example, let us consider beam parameters relevant for experiments on laser wakefield presented in [19]. Where an electron beam with 1 GeV initial energy, ($\langle\gamma_o\rangle \simeq 2000$), and an initial emittance of $\epsilon_{xo} = 2068$ radμm in a plasma channel of density $n_o = 10^{15}$ cm^{-3} is considered. The beam emittance decreases only to $\epsilon_x = 2045$ μm for the

final energy 0.5 TeV $\langle\gamma\rangle = 1 \times 10^6$, of the beam which is almost constant [19]. Highly relativistic electron beams of this class can have a much lower initial emittance, e.g. $\epsilon_{xo} = 10$ μm, than has been assumed in the above example. However, matching such a beam into a plasma channel would require a very small beam radius, $\sim 10^{-7}$ μm. Injecting such a radially small beam into the plasma channel is difficult. If we inject a beam with the same emittance as mentioned above but relatively large radius, say, $\sigma_{xo} = 10$ μm, it would be highly mismatched and the beam emittance would grow towards the matched value [66]. However, the super-Gaussian wakefield reduces the betatron oscillations and make the electron orbit ballistic over a single stage, which helps to preserve the initial small emittance [67].

2.2.2.2. Energy Spread

The energy damping mechanism in a plasma focusing channel is very different from the beam cooling and radiation damping using Thomson scattering [91] or the one in a magnetic undulator [92]. The radiation damping strongly depends on the initial radial positions of the electrons in the plasma focusing channel. The electrons that are initially close to the axis of the plasma channel exhibit small betatron oscillations due to weak focusing force and hence loose a very small amount of energy through radiation as compared to the electrons which are far away from the axis, i.e. near the boundary of the wakefield. This will, in turn, increase the energy spread of the beam [66]. The relative energy spread is $\sigma/\langle\gamma\rangle$, where $\sigma_\gamma^2 = \langle\Delta\gamma^2\rangle = \langle\gamma^2\rangle - \langle\gamma\rangle^2$ and $\langle\rangle$ represents the average over the ensemble of particles.

2.3. Emittance growth via betatron radiation

In this section we study the effects of the critical energy of the electron beam corresponding to the given density of the laser wakefield on the emittance of the beam.

2.3.1. The critical energy

The accelerating gradient created by a laser in a plasma of certain density, say, n_o behaves as an accelerator for an electron beam of a given average transverse radius corresponding to a critical value of the initial energy. In equation (2.13), let us consider the particular average value of the energy $E_{crit} = \langle\gamma\rangle$ and average value of transverse radius $x_{crit} = \langle x\rangle$ for a given density of the plasma channel such that $d\gamma/dt \simeq 0$. Taking average of equation (2.13) over the dephasing phase $0 \geq \psi \leq \pi/4$ we have

$$0 \simeq \eta_B - \eta_\gamma \langle\gamma^2\rangle_{crit} \langle x^2\rangle_{crit}, \tag{2.15}$$

$$\langle\gamma^2\rangle_{crit} \simeq \frac{\eta_B}{\eta_\gamma \langle x^2\rangle_{crit}}, \tag{2.16}$$

where we have neglected the third term in equation (2.13) because it is three orders of magnitude smaller than the first and second terms and function ε has been expanded assuming it has small argument. Equation (2.16) in a simplified form for the electron beam can be written as

$$\langle\gamma^2\rangle_{crit} \simeq \frac{\Lambda(n_0)}{\langle x^2\rangle_{crit}}, \tag{2.17}$$

where $\Lambda(n_o) = \frac{\eta_B}{\eta_\gamma} = \frac{\zeta}{\tau_o c^2 K^4 r_o^2 \gamma_o^2}$ is a density dependent parameter because both ζ and K are density dependent as described in the last section. The equation (2.17) gives the critical energy of the electron beam as a function of both the density of the plasma wave and the average transverse radius of the beam.

Plots for the critical energy are shown in Figure 2.1 (a) versus the density of the plasma for transverse average radius $\sqrt{\langle x^2\rangle} = \mu$m. Note that the critical energy γ_{crit} decreases with increasing density of the plasma wave. It is due to the fact that if we increase the density of the plasma wave radiation reaction effect also increases, which in turn decreases the critical energy of the beam. Moreover the critical energy also decreases as we increase the average radius keeping the

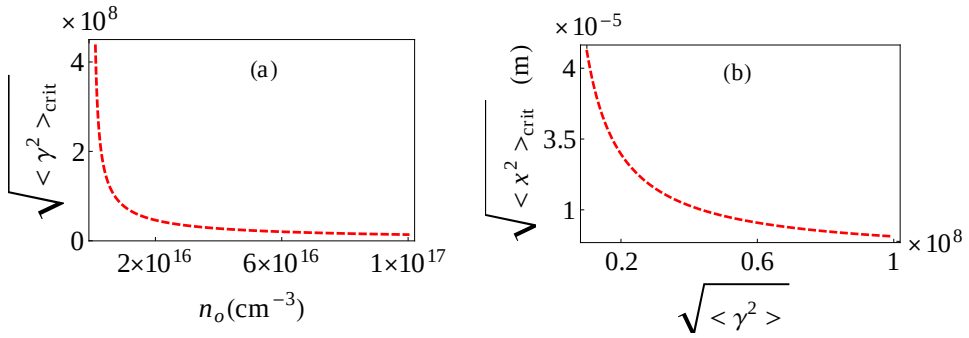

Figure 2.1.: (a) The critical energy $\sqrt{\langle\gamma^2\rangle_{crit}}$ of the electron beam versus density n_o of the plasma wave for average transverse radius $\sqrt{\langle x^2\rangle} = 10^{-6}$m. (b) The average transverse radius $\sqrt{\langle x^2\rangle_{crit}}$ of the electron beam versus the average beam energy $\sqrt{\langle\gamma^2\rangle}$ in a plasma channel of density $n_o = 1.0 \times 10^{15}\text{cm}^{-3}$.

density of the plasma constant. Equation (2.17) is rearranged in the form

$$\langle x^2\rangle_{crit} = \frac{\Lambda(n_0)}{\langle\gamma^2\rangle}, \tag{2.18}$$

Equation (2.18) provides us with average value of the transverse radius of the beam corresponding to the given energy and density of the plasma channel. Equation (2.18) has been plotted in Figure 2.1 (b). It gives the average value of radius as a function of the energy of the beam and consequently helps us in estimating the transverse emittance of the electron beam. It is clear from equation (2.18) that the transverse radius of oscillations of electron decrease as the energy of the electrons increase and vice versa.

2.3.2. Emittance growth

In a laser plasma-based accelerator, for an electron beam with initial energy well below the E_{crit} the emittance can decrease due to radiation reaction [19, 66]. However, it can increase as well for certain threshold values of parameters of the beam.

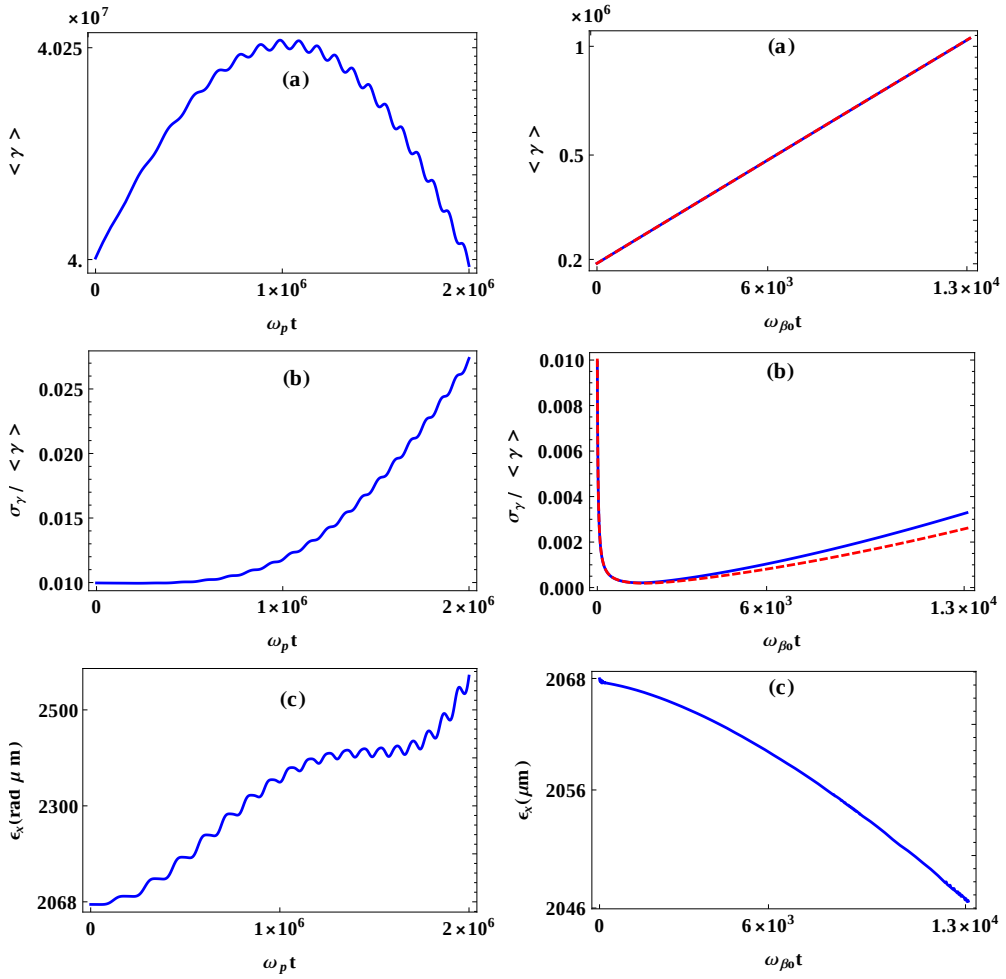

(a) ′ (b) ′

Figure 2.2.: The electron beam dynamics. (a) The mean energy $\langle\gamma\rangle$, (b) the relative energy spread $\sigma_\gamma/\langle\gamma\rangle$ and (c) the transverse normalized emittance ϵ_x versus $\omega_p t$ or $\omega_{\beta o} t$ of the accelerating electrons. The electron beam moves in plasma channel of density $n_o = 1.0 \times 10^{15}\text{cm}^{-3}$, initial emittance $\epsilon_o = 2068$ radμm and initial relative energy spread 1%. In (a)′ initial energy $\langle\gamma_o\rangle = 4 \times 10^7$ and in (b)′ $\langle\gamma_o\rangle \simeq 2000$. Initially there were 4000 electrons, 1624 have been dephased. Blue line represents the numerical solution of equations (2.12) and (2.13) and red dashed line represents the analytical expressions of corresponding quantities given in Chapter 4.

If the initial energy of the beam is nearly equal to the critical value, i.e. $E_{ini} \geq E_{crit}$, then the particles of the beam can be split into two major categories; the first one with large initial radius, they emit a large amount of radiation and some of the electrons move into a region of decelerating phase of the plasma wave (the detail is given in section 2.4). However, some radiating electrons can still remain inside the accelerating phase. These particles are accelerated for a very short time and then they cool down. The second one is those electrons that are very close to the axis of the plasma channel and do radiate a very small amount of energy. These particles are accelerated by the wakefield. The transverse betatron oscillation of the electrons depends linearly on the energy. The decrease in energy leads to the increase in the amplitude of oscillations. Therefore, the emittance of the beam increases.

To make our point clearer we consider an ultra relativistic electron beam of 20.46 TeV initial energy, ($\langle\gamma_o\rangle = 4 \times 10^7$), with relative energy spread $\sigma_{\gamma o}/\langle\gamma_o\rangle = 1\%$ and initial emittance of $\epsilon_{xo} = 2068$ radμm injected into a plasma channel of density $n_o = 10^{15}$ cm^{-3}. For the initially matched beam conditions the radius will be $\sigma_{xo} = 13$ μm. The propagation length for linear regime is almost 333m, which corresponds to $\omega_p t = 2 \times 10^6$ and $\omega_{\beta o} t = 13100$. The approximate final value of the transverse emittance is 2600 radμm after a propagation length of 333m. The relative energy spread increases by 2.7 $\%$. The results are shown in Figure 2.2 (a)′. However, if we inject the electron beam keeping all the initial parameters same except initial energy, which is now $\langle\gamma_o\rangle \simeq 2000$. The transverse emittance decreases to a final value of 2046 μm in this case. The relative energy spread decreases very quickly in the beginning, however, later on it increases due to increase in the radiation effects but it is still less than 0.3$\%$, which is less than the initial energy spread of 1%. The results are shown in Figure 2.2 (b)′. Red dashed line represents the analytical expressions of the corresponding quantities given in Chapter 4, (equations (4.28) and (4.30)), and solid blue line represents corresponding quantities for the numerical solution of equations (2.12) and (2.13). The analytical solution is in

good agreement with the numerical solution, which also testifies our numerical solution.

To examine the radiation effects in more detail, we need to study the behavior of electrons with large initial transverse radius and the one with small initial transverse radius from the axis of the plasma channel separately. As mentioned earlier that electron with large initial radius radiate more as compared to the electrons, which are near the axis. In the pervious example for high energy beam case ($\langle\gamma_o\rangle = 4 \times 10^7$), the emittance remains constant at the start when the radiation damping term is small due to $\sin(\psi)$ in equation (2.13), however, for later times the electrons with large initial radius radiate a large amount of energy and fall in the decelerating region of the plasma wave and its energy decreases. The radial amplitude of oscillations is given by $r_\beta = a_\beta/(k_\beta\gamma)$, where a_β is the betatron strength parameter and $\lambda_\beta = 2\pi/k_\beta$ is the betatron period. Consequently the transverse oscillation of such electrons increases, which increases the beam emittance. The emittance increasing rate is very high for almost half of the propagation length (165m) because of the high radiation effects. After half the propagation length the electrons with large initial radial distance from the center of the plasma channel are either move to decelerating phase or come much closer to the axis because of their damped trajectories. There exists a lower lateral oscillation amplitude of the trajectory for which transverse oscillations do not get damped any further. For a detailed understanding see [93]. It is found that the transverse emittance of accelerating electrons decreases while the total emittance increases. The results are shown in Figures 2.3 (a)′. The relative energy spread of the accelerated electrons decreases in the beginning but later on it increases due to relatively less increase in the energy and increase in the radiation reaction. The mean energy of accelerated electrons increase. The electrons which remain in accelerating phase of the plasma wave after traveling a distance of 333 m are once again injected into plasma channel with their pervious initial conditions, which were preserved. It is found that the mean energy of the electrons increases while transverse emittance decreases.

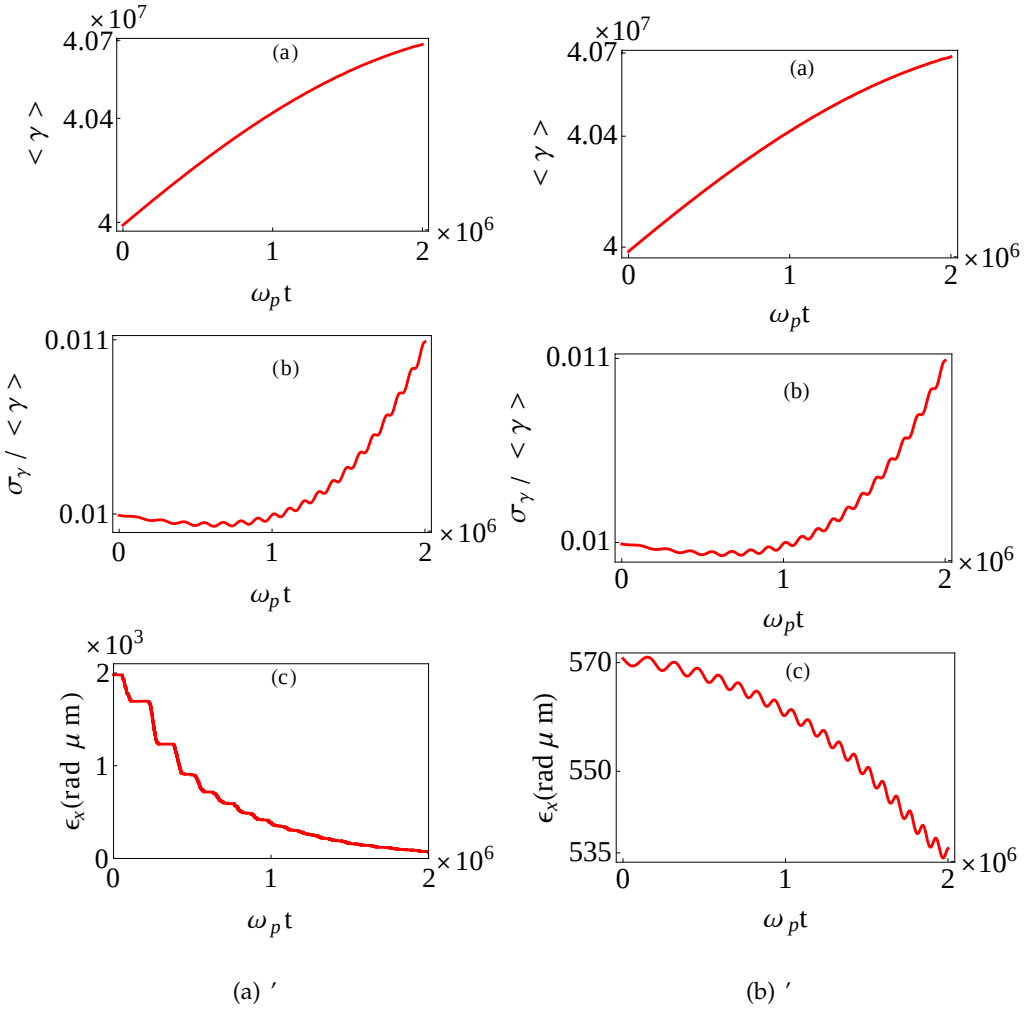

Figure 2.3.: The electron beam dynamics. (a) The mean energy $\langle\gamma\rangle$, (b) the relative energy spread $\sigma_\gamma/\langle\gamma\rangle$ and (c) the transverse normalized emittance ϵ_x versus $\omega_p t$ of the accelerating electrons. The initial conditions are the same as given in Figure 2.2. Initially there were 4000 electrons, 1624 have been dephased. (a)′ demonstrates the behavior of accelerating particles and (b)′ represents the rerun of accelerating particles. In the second run all particles remain trapped

The results are shown in Figure 2.3 (b)′.

If, however, we inject the beam with much lower initial emittance, say, $\epsilon_{xo} = 2$ radμm, with 20.46 TeV initial energy, ($\langle\gamma_o\rangle = 4 \times 10^7$), and relative energy spread $\sigma_{\gamma o}/\langle\gamma_o\rangle = 1\%$ into a plasma channel of density $n_o = 10^{15}$ cm^{-3} then there is a small increase in the transverse emittance because there is no radiation effects. Since the electrons of the beam have relatively small initial radial distance (for example the maximum transverse radius in this case is $\sigma_{xo} = 0.34$ μm) as compared to the last example, therefore, electrons do not radiate much and remain all in the accelerating phase. The beam gains 50 GeV more energy than for the high emittance, $\epsilon_{xo} = 2068$, radμm electron beam case. The relative energy spread $\sigma_\gamma/\langle\gamma\rangle$ decreases since there is only small radiation damping. The results are shown in the Figure 2.4 (a)′.

It is obvious from equation (2.13) that the magnitude of radiation reaction depends on the transverse distance of the electrons from the axis of the channel and their energy. In the last example we have seen that if we reduce the initial radius of the electrons the radiation effects are small and have no impact on the beam dynamics. As mentioned earlier that the weak radiation effects lead to the decrease in the transverse emittance of the beam [19, 66]. Thus, we conclude that weak radiation effects decrease the emittance while the strong radiation effects increase the emittance of the beam.

2.3.3. Impact of density on emittance growth

Both the transverse focusing and the longitudinal accelerating wakefields are functions of the density of the plasma. The accelerating field E_{zo} and focusing parameter K scale as $\sqrt{n_o}$. This means that the accelerating term (first term) in equation (2.13) will increase as $\sqrt{n_o}$. In the absence of radiation effects the energy gain of the electron beam increases with increasing density of the plasma. Hence, as long as $\omega_p < \omega_o$ holds high densities are beneficial in the absence of radiation reac-

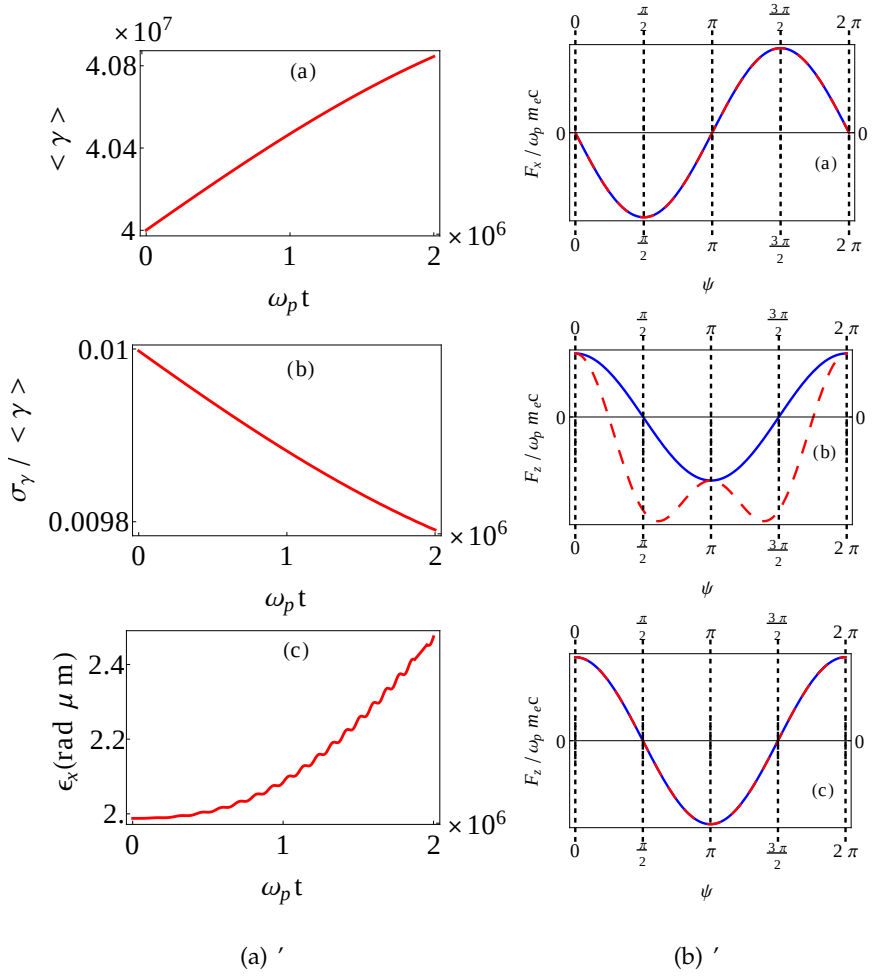

Figure 2.4.: In (a)′ (a) The mean energy $\langle\gamma\rangle$, (b) the relative energy spread $\sigma_\gamma/\langle\gamma\rangle$ and (c) the normalized transverse emittance ϵ_{xo} versus $\omega_p t$ of the electrons. The electron beam moves with an initial emittance $\epsilon_{xo} = 2$ radμm, the all other initial parameters are the same as given in the Figure 2.2. There are 10000 electrons. All remain in accelerating phase. In (b)′ the forces felt by an electron with radiation and with out radiation effects are represented by red-dashed and blue lines respectively. (a) and (b) an electron in the plasma wave with initial energy 20.4 TeV, transverse velocity $v_{xo} = 1068$ m/s and initial radius $x_o = 13.8$ μm. (c) initial radius $x_o = 0.138$ μm, all the others quantities are same. F_x and F_z represent the transverse and accelerating force respectively.

tion. However, we know that the electrons of the beam inside the plasma channel exhibit betatron oscillations with frequency $\omega_B = cK/\sqrt{\gamma}$ and that they emit betatron radiation. Their betatron frequency ω_B increases as $\sqrt{n_o}$ with increasing density of the plasma wave. This suggests that an electron radiates more with increasing density.

From equation (2.13) we see that radiation reaction force scales as n_o^2. This means that the radiation reaction force increases faster than the acceleration force with increasing plasma density. Therefore, plasma channels with higher plasma density will have higher radiation loss as compared to focusing channels at low density for a beam of same energy and average transverse radius. To avoid radiation effects we need to use low density plasma channels.

If the energy of the beam is near the critical energy electrons with large initial radius radiate a large amount of energy. Some of them lose so much energy that they move quickly into decelerating phase of the plasma wave and leads to an increase in the transverse oscillations and consequently there is an increase in the transverse emittance. This emittance increasing is due to radiation reaction. Therefore an increase in density can result in a further increase of the emittance. Since increasing density increases the number of radiating electrons and also the amount of radiated energy.

2.4. Schematic representation of accelerating and decelerating phase

In this section we will present a graphical illustration of the accelerating and decelerating processes of the charged particles due to radiation reaction in a plasma focusing channel. The plasma wave can be split into four sectors, each of them has different impact on the electrons traveling inside the plasma wave. There is one quarter-wave region that is most appropriate for good quality beam acceleration

since focusing and acceleration act simultaneously. This region is the first sector $(0 - \pi/2)$ in the Figure 2.4 (b)′. It is found that electrons with large initial radius perform betatron oscillations with large amplitudes, loose a large amount of energy through betatron emission and quickly move into a region of deceleration. In other words we can say that such electrons see accelerating or focusing region for a very short time while the electrons, which are initially on axis or have small initial radii, would not loose much energy and see a relatively long accelerating or focusing region. For example, consider an electron with 20.4 TeV initial energy, transverse initial velocity $v_{xo} = 1086$ m/s and initial radius 13.8 μm moving in a plasma channel of density $n_o = 10^{15}$ cm^{-3}. It feels almost the same transverse focusing force with and without radiation damping. However, it feels a different longitudinal accelerating force with and without radiation reaction. Since the radiation effects are taken into accounts, the electron radiates a large amount of energy and soon it goes into the region of deceleration. It is represented by red-dashed line in Figure 2.4 (b)′ (b). If we ignore the radiation effects then the electron will be accelerated over a full quarter-wave region (the blue line in Figure 2.4 (b)′ (b)). If, however, we inject the same electron closer to the channel axis, say $x_o = 0.138$ μm it will feel the same transverse and accelerating force with and without radiation reaction as shown in Figure 2.4 (b)′ (c).

2.5. Summary of the chapter

The effects of radiation reaction on the emittance of the electron beam in a plasma focusing channel are studied. We have examined the motion of test electrons to estimate the evolution of the electron beam through numerical simulation of the equation of motion of radiating electrons (the Landau-Lifshitz equation). The electrons that are traveling far away form the axis of the plasma channel feel a strong focusing force. These electrons start betatron oscillations in the transverse direction. The farther away an electron is from the axis of the plasma channel the larger

will be its betatron oscillation amplitude and the more it will radiate. The betatron radiation of electrons decreases the energy gain in the laser wakefield, which, in turn, expels the electrons with large initial transverse radius from the accelerating phase to the decelerating phase of the plasma wave. Consequently the amplitude of transverse oscillation increases and results in the increase of transverse emittance of the electron beam considerably.

A variety of cases are studied to testify our finding. For example, electron beams with large and small initial radii have been injected by keeping the other parameters the same. It is found that for weak radiation effects the transverse emittance of an electron beam decreases. However, it can increase for strong radiation effects. We have estimated the transverse emittance of the electrons in accelerating phase and total transverse emittance separately to testify our findings. The energy gain and energy spread of the beams are also studied. The radiation reaction reduces the energy gain but increases the relative energy spread of the electron beam. It is found that the effects of radiation reaction become very strong near the critical energy (the energy at which radiation reaction and accelerating force become equal) of the beam.

Moreover, the density dependence of the emittance is studied. The emittance can be increased with increasing plasma density because it enhances the effects of radiation.

In addition, we have noticed the phase sensitivity of the focusing and accelerating forces in the radiation reaction terms. It could be crucial for the self trapping and external injection of electron bunches. It could also limit the bunch length in a high energy regime.

CHAPTER 3

Retardation and self radiation effects on electrons in a laser pulse

3.1. Introduction

High energy charged particle beams are of fundamental importance and they are the basic instrument to explore and investigate the fundamental physics of matter. Beams of energetic electrons, however, are subjected to the interaction with radiation fields of co-propagating electrons and to their self fields.

In this chapter we will study the motion of an electron under the effects of self radiation force and retardation fields (radiation fields of other electrons of the system) in laser pulses of different polarization.

The effects of radiation reaction in a laser pulse [69, 70, 71] and in a laser wakefield [19, 66, 67] have been studied. The numerical study of retardation effects is carried out in [72, 73]. Due its complex structure the self fields and retardation effects have been studied separately. However, the realistic system demands the study of accumulated effects (self fields plus the effects of retarded fields) of radiation. Moreover, there is very limited literature available concerning the retardation

effects.

Currently relativistic electron bunches with charge ≥ 100 pC are being produced in laser wakefields, [21, 22, 23] which implies $> 10^9$ electrons per bunch. It is apparent that if the radiation of a single electron inside the beam affects its own motion [19, 66, 67, 69] it should also affect the motion of the other electrons of the beam for certain parameters. Therefore, there is a need to investigate the accumulated effects of radiation on the electron motion. In the following we will study the effects of betatron radiation from a single particle and multiple particles. We will consider a simple model of two electrons (one of which may be a macro-particle), which are interacting with each other through their retarded potentials, self fields, and with the external electromagnetic fields of the laser pulse.

3.2. The radiation fields

Radiation fields produced by a radiating electron are known as Lienard-Wiechert fields and are given by

$$\vec{E}_{LW}(\vec{r},t) = \frac{e}{4\pi\epsilon_o}\Big(\frac{\hat{n}-\vec{\beta}(t')}{\gamma^2(1-\hat{n}\cdot\vec{\beta}(t'))^3|\vec{R}^2(t')|} + \frac{1}{c}\frac{\hat{n}\times(\hat{n}-\vec{\beta}(t'))\times\dot{\vec{\beta}}(t')}{(1-\hat{n}\cdot\vec{\beta}(t'))^3|\vec{R}(t')|}\Big), \quad (3.1)$$

$$\vec{B}_{LW}(\vec{r},t) = \hat{n}\times\vec{E}_{LW}(\vec{r},t)/c, \quad (3.2)$$

where $\vec{\beta}(t') = \vec{v}(t')/c$ is the velocity of the electron at retarded time, $\vec{R}(t') = (\vec{z}(t) - \vec{y}(t'))$ is the distance between observation position and retarded position (when it emit radiation) of electron, $t' = t - |\vec{R}(t')|/c$ is the retarded time, and $\hat{n} = \vec{R}(t')/|\vec{R}(t')|$ is the unit vector along the observation position. $\mathrm{E}_{LW}(\vec{r},t)$ and $\mathrm{B}_{LW}(\vec{r},t)$ are the Lienard-Wiechert electric and magnetic fields. The first and second terms in equation (3.1) represent the Coulomb and radiation fields of an accelerating electron respectively. The Coulomb field is short-range and fall off as R^{-2} whereas radiation field is usually transverse to $\vec{R}(t')$ and fall of as R^{-1}. As the Coulomb field is short-range and is very small as compared to the radiation field. Therefore, we will study the effects of the latter.

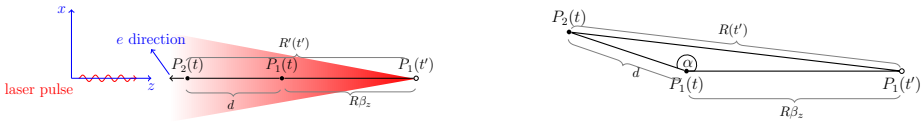

(a) (b)

Figure 3.1.: Two electrons counter-propagating to the laser pulse. The laser pulse is propagating in the $\hat{z}$-direction. (a) Electrons are located on a line parallel to the z-axis and are moving towards the laser. (b) $\vec{R}(t')$ is almost parallel to unit vector $\hat{n}$ and is very greater than the mutual distance d of electrons. $P_1(t')$ and $P_1(t)$ represent the retarded and observation positions of the electron P_1 respectively.

3.2.1. Electrons-radiation interaction model

To study radiation effects we consider an arrangement of electrons as shown in Figure 3.1 (a). We assume that two electrons are counter-propagating in a laser pulse with almost the same longitudinal velocity v_z located at a line which is parallel to the $\hat{z}$-axis. The laser pulse is moving along the $\hat{z}$-axis while electrons are moving to the $(-\hat{z})$-direction. Particle P_2 is ahead of particle P_1 and both are separated by a small distance d, which is of the order of one laser wavelength. One laser wavelength separation will make both electrons oscillate with same phase. Let $P_i(t')$ and $P_i(t)$ represent the retarded and observation positions of the electrons respectively, where $i = 1, 2$. For electrons moving relativistically, radiation is emitted purely in the initial direction of motion (here $-\hat{z}$ direction) within an angle of $1/\gamma$ [65]. Therefore, we assume that radiation emitted by P_1 in Figure 3.1 (a) at retarded time t' at retarded position $P_1(t')$ will catch the electron P_2 at observation position $P_2(t)$ at time t, which is also taken as the observation time, where $t > t'$. However, radiation emitted by particle P_2 will have very weak effects on particle P_1 [72] as radiation is emitted in $(-\hat{z})$-direction and unit vector

$\hat{n}$ and the velocity of the electron will be in the opposite direction and the term with $1/(1+\hat{n}\cdot\vec{\beta})^3$ is very small as compared to the term with $1/(1-\hat{n}\cdot\vec{\beta})^3$. As mentioned earlier that self radiation effects of an electron counter-propagating in a laser pulse with relativistic velocity affect its motion considerably [69, 70, 71]. Therefore, we assume that both particles are affected by their own radiation as well. Overall we can say that particle P_2 is affected by its self force and by the retarded potential of particle P_1 (which may be a macro-particle) whereas P_1 is affected by its own radiation. However, both are affected by the electromagnetic fields of the laser pulse. A bunch of N electrons located so close to each other that they oscillate almost with the same phase under the impact of the external field can be approximated as a single particle at distant position. This approximation is good if the bunch size is very much smaller than the wavelength of the laser pulse or external field.

The retarded quantities $\vec{\beta}(t'), \dot{\vec{\beta}}(t')$, etc., in equation (3.1) can be expanded about the observation time t for electrons with small mutual separation [79]

$$\vec{\beta}(t') = \vec{\beta}(t-|\vec{R}(t')|/c), \tag{3.3}$$

$$\vec{\beta}(t') = \vec{\beta}(t) - \dot{\vec{\beta}}(t)\frac{|\vec{R}(t')|}{c} + \frac{\ddot{\vec{\beta}}(t)}{2}\Big(\frac{|\vec{R}(t')|}{c}\Big)^2 + \ldots. \tag{3.4}$$

Similarly other retarded quantities can be expanded around the observation time. We will restrict ourself to the first order terms for $R(t')/c \ll t$ and higher order terms will be very small.

The distance $\vec{R}(t')$ for the orientation given in Figure 3.1 can be represented in terms of the current mutual distance of two particles. It is given by the relation [72]

$$|\vec{R}(t')| = |\vec{R}(t')|\beta_z(t) + d, \quad \Rightarrow |\vec{R}(t')| = \frac{d}{1-\beta_z}. \tag{3.5}$$

If both electrons oscillate with same phase and they have same initial longitudinal and transverse velocities then for weak retardation effects their mutual distance d and unit vector $\hat{n}$ are almost undisturbed and the above relation remains valid.

Moreover, as $R(t')$ is much greater than d, therefore, a small change in their velocities and mutual distance will not cause much effect.

3.2.2. Linear polarization

In general, the retarded fields are complex in structure and it is difficult to study their effects analytically. From equation (3.1) it is clear that the components of radiation fields depend upon the polarization of the external laser pulse. For example, if external laser pulse is polarized in the $\hat{x}$-direction and is propagating to the $\hat{z}$-direction then the electron will have its velocities in $\hat{x}$ and $\hat{z}$-directions. For the unit vector $\hat{n}$ along the $(-\hat{z})$-direction we will have only x component of the retarded electric field.

Using expansion of the retarded quantities of the form given by equation (3.4) in equations (3.1) and (3.2), we can write the retarded field components in a simple form for different polarization. For linearly polarized laser pulse the retarded field can be written as

$$E^x_{LW} = \frac{e}{4\pi\epsilon_o c}\left[\left(\frac{-\beta_x\dot{\beta}_z}{(1-\beta_z)^3|\vec{R}(t')|}\right)+\left(\frac{-\dot{\beta}_x}{(1-\beta_z)^2|\vec{R}(t')|}\right)\right], \tag{3.6}$$

$$B^y_{LW} = \hat{y}E^x_{LW}, \tag{3.7}$$

3.2.3. Circular polarization

Making use of the retarded quantities of the form given by equation (3.4) in equations (3.1) and (3.2), we can write the retarded field for circularly polarized laser pulse as follows

$$E^x_{LW} = \frac{e}{4\pi\epsilon_o c}\left[\left(\frac{-\beta_x\dot{\beta}_z}{(1-\beta_z)^3|\vec{R}(t')|}\right)+\left(\frac{-\dot{\beta}_x}{(1-\beta_z)^2|\vec{R}(t')|}\right)\right], \tag{3.8}$$

$$E^y_{LW} = \frac{e}{4\pi\epsilon_o c}\left[\left(\frac{-\beta_y\dot{\beta}_z}{(1-\beta_z)^3|\vec{R}(t')|}\right)+\left(\frac{-\dot{\beta}_y}{(1-\beta_z)^2|\vec{R}(t')|}\right)\right], \tag{3.9}$$

$$B^x_{LW} = -\hat{x}E^y_{LW}, \tag{3.10}$$

$$B^y_{LW} = \hat{y}E^x_{LW}. \tag{3.11}$$

It should be noted that in equations (3.6)-(3.11) the first terms on R.H.S are smaller. Therefore, only second terms will be used in our model. Moreover, to remember that for relativistic electrons counter-propagating in a laser pulse the Coulomb field is 5-6 order of magnitude smaller than the radiation fields.

3.3. The analytical solution of the Landau-Lifshitz equation

In this section we will give an analytical solution of the LL equation by including retarded fields. Arrangement of electrons considered in Fig 3.1 will help us to understand the effects of emitted radiation of the electrons at different locations inside the electron beam. The radiation effects of an electron (or bunch of electrons) on the other electron is implemented through the Lienard-Wiechert fields. The Landau-Lifshitz equation for such a system of particles under radiation effects of other particles in three vector notation can be written as

$$\frac{d\vec{p}}{dt} = -e\Big(\vec{E} + \vec{E}^{(other)}_{rad} + \vec{v} \times (\vec{B} + \vec{B}^{(other)}_{rad})\Big) - \tau_o e\gamma \frac{d}{dt}(\vec{E} + \vec{v} \times \vec{B})$$
$$+\frac{\tau_o e^2}{mc}\Big[c(\vec{E} \times \vec{B} + (\vec{v} \times B) \times \vec{B}) + (\frac{\vec{v}}{c} \cdot \vec{E})\vec{E} - \frac{\vec{v}\gamma^2}{c}\Big((\vec{E} + \vec{v} \times \vec{B})^2 - (\frac{\vec{v}}{c} \cdot \vec{E})^2\Big)\Big], \quad (3.12)$$
$$\frac{d\vec{p}}{dt} = \vec{F}_{Lo} + \vec{F}^{other}_{rad} + \vec{F}_{self}, \quad (3.13)$$

where F_{Lo}, F_{rad} and F_{self} are the Lorentz force, the force due to the retarded fields and self force respectively. The subscript "rad" in equation (3.12) stands for retarded fields. It is convenient to use normalized quantities, i.e $\tilde{t} = \omega_L t$, $\tilde{\vec{v}} = \vec{v}/c$, and $\tilde{\vec{p}} = \vec{p}/mc$, we drop ($\sim$) sign for simplicity. Equation (3.12) for P_1 and P_2 can be written as

$$\frac{d\vec{p}^{(2)}}{dt} = -\kappa(\vec{E} + \vec{v}^{(2)} \times \vec{B}) - \kappa(\vec{E}^{(1)}_{rad} + \vec{v}^{(1)} \times \vec{B}^{(1)}_{rad}) - \tau_o \kappa\gamma \frac{d}{dt}(\vec{E} + \vec{v}^{(2)} \times \vec{B})$$
$$+\tau_o\kappa^2\Big[c(\vec{E} \times \vec{B} + c(\vec{v}^{(2)} \times \vec{B}) \times \vec{B}) + (\vec{v}^{(2)} \cdot \vec{E})\vec{E}$$
$$-\vec{v}^{(2)}\gamma^2\Big((\vec{E} + \vec{v}^{(2)} \times \vec{B})^2 - (\vec{v}^{(2)} \cdot \vec{E})^2\Big)\Big], \quad (3.14)$$

$$\frac{d\vec{p}^{(1)}}{dt} = -\kappa(\vec{E} + \vec{v}^{(1)} \times \vec{B}) - \tau_o \kappa \gamma \frac{d}{dt}\Big(\vec{E} + \vec{v}^{(1)} \times \vec{B}\Big) + \tau_o \kappa^2 \Big[c\vec{E} \times \vec{B} + c^2(\vec{v}^{(1)} \times \vec{B}) \times \vec{B} + (\vec{v}^{(1)} \cdot \vec{E})\vec{E} - \vec{v}\gamma^2\Big((\vec{E} + \vec{v}^{(1)} \times \vec{B})^2 - (\vec{v}^{(1)} \cdot \vec{E})^2\Big)\Big], \tag{3.15}$$

where $\kappa = e/(m_e \omega_L c)$, superscript labels (1), (2) represent the corresponding particles in Figure 3.1 (a) and ω_L is the laser frequency.

3.3.1. Linearly polarized plane wave

Let us consider a linearly polarized laser pulse propagating in the $\hat{z}$-direction and polarized in the $\hat{x}$-direction. The electric and magnetic field components of such a pulse can be written as

$$E_x = E_L \cos(t - z),\ E_y = E_z = 0, \tag{3.16}$$

$$B_y = \frac{E_L}{c} \cos(t - z),\ B_x = B_z = 0. \tag{3.17}$$

Using equations (3.6), (3.7), (3.16) and (3.17) in equations (3.14) and (3.15), we have

$$\frac{dp_x^{(2)}}{dt} = -a_o(1 - v_z)\cos(\tau) - a_o \tau_r \gamma (1 - v_z)^2 \frac{d}{d\tau}\cos(\tau) - a_o^2 \tau_r \Big[p_x \gamma (1 - v_z)^2 \cos^2(\tau)\Big] - \frac{\sigma}{\gamma - u_z}\frac{dp_x^{(1)}}{dt}, \tag{3.18}$$

$$\frac{dp_x^{(1)}}{dt} = -a_o(1 - v_z)\cos(\tau) - a_o \tau_r \gamma (1 - v_z)^2 \frac{d}{d\tau}\cos(\tau) - a_o^2 \tau_r \Big[p_x^{(1)} \gamma (1 - v_z)^2 \cos^2(\tau)\Big], \tag{3.19}$$

$$\frac{d(\gamma - p_z)^{(1,2)}}{dt} = -a_o^2 \tau_r \gamma (\gamma - p_z)\Big[(1 - v_z)^2 \cos^2(\tau)\Big], \tag{3.20}$$

where $a_o = eE_L/(m_e \omega_L c)$ is the normalized laser intensity, $\sigma = Ze^2/(4\pi\epsilon_o m_e c^2 d)$, Z is the number of electron in the marco-particle, $\tau = t - z$ and $\tau_r = \tau_o \omega_L$. We have also assumed that for an electron moving in the $(-\hat{z})$-direction with large

initial energy, $v_x \ll v_z$ holds. The terms with higher power in v_x are neglected because they are very small as compared to the other terms. As we have $\tau = t - z$, therefore, we can substitute $d/dt = (1 - v_z)d/d\tau$

$$\frac{dp_x^{(2)}}{d\tau} = -a_o \cos(\tau) + a_o \tau_r K \sin(\tau) - \frac{\sigma}{K}\frac{dp_x^{(1)}}{d\tau} - a_o^2 \tau_r p_x^{(2)} K \cos^2(\tau), \quad (3.21)$$

$$\frac{dp_x^{(1)}}{d\tau} = -a_o \cos(\tau) + a_o \tau_r K \sin(\tau) - a_o^2 \tau_r p_x^{(1)} K \cos^2(\tau), \quad (3.22)$$

$$\frac{dK}{d\tau} = -a_o^2 \tau_r K^2 \cos^2(\tau), \quad (3.23)$$

where $\gamma - p_z = K$. The parameter K is almost same for both particles and therefore, we drop the label for K. We can easily integrate the coupled equations (3.21) - (3.23). Equation (3.23) $\Rightarrow$

$$K = \frac{K_o}{1 + a_o^2 \tau_r K_o (2\tau + \sin(2\tau))/4}, \quad (3.24)$$

using equation (3.24) in equation (3.22) and integrating

$$p_x^{(1)}(\tau) = \frac{1}{6\big(1 + \eta(2\tau + \sin(2\tau))\big)}\Big(a_o\eta + 6\zeta - (9a_o\eta + 6\zeta)$$
$$\cos(\tau) + a_o\eta\cos(3\tau) - 6a_o(1 + 2\tau\eta)\sin(\tau)\Big). \quad (3.25)$$

Using the values of K and $p_x^{(1)}$ in equation (3.21) and integrating, we have

$$p_x^{(2)}(\tau) = \frac{1}{180(1 + 2\tau\eta + \eta\sin(2\tau))}\Big(60(4a_o\eta(1 + \Lambda(3 - 2\tau\eta)) + 3(1 + \Lambda$$
$$-2\tau\eta\Lambda)\zeta) - 90(a_o\eta(3 + 8\Lambda + 16\tau\eta\Lambda) + 2(1 + \Lambda + 2\tau\eta\Lambda)\zeta)\cos(\tau)$$
$$+30a_o\eta\cos(3\tau) - 30(a_o(6(1 + \Lambda) + \eta(12\tau + 24\tau\Lambda - 71\eta\Lambda + 24\tau^2\eta\Lambda))$$
$$-33\eta\Lambda\zeta)\sin(\tau) - 60\eta\Lambda(4a_o\eta + 3\zeta)\sin(2\tau) + 5\eta\Lambda(17a_o\eta + 6\zeta)\sin(3\tau)$$
$$+3a_o\eta^2\Lambda\sin(5\tau)\Big), \quad (3.26)$$

where $\zeta = a_o\tau_r K$, $\eta = a_o^2\tau_r K_o/4$ and $\Lambda = -\sigma/K_o$. We know that $\gamma^2 = 1 + p_x^2 + p_z^2$ and $p_z = \gamma - K$

$$\gamma = \frac{1 + p_x^2}{2K} + \frac{K}{2}, \quad (3.27)$$

$$p_z = \frac{1 + p_x^2}{2K} - \frac{K}{2}. \quad (3.28)$$

Making use of equations (3.27) and (3.28) we obtain

$$\gamma^{(2)}(\tau) = \frac{1}{2K_o\big(1+\eta(2\tau+\sin(2\tau))\big)}\Bigg(K_o^2 + 32400(1+\eta(2\tau+\sin(2\tau)))\times$$
$$\Big(60(4a_o\eta(1+\Lambda(3-2\tau\eta))+3(1+\Lambda-2\tau\eta\Lambda)\zeta)-90(a_o\eta(3+8\Lambda+16\tau\eta\Lambda)$$
$$+2(1+\Lambda+2\tau\eta\Lambda)\zeta)\cos(\tau)+30a_o\eta\cos(3\tau)-30(a_o(6(1+\Lambda)+\eta(12\tau+24\tau\Lambda$$
$$-71\eta\Lambda+24\tau^2\eta\Lambda))-33\eta\Lambda\zeta)\sin(\tau)-60\eta\Lambda(4a_o\eta+3\zeta)\sin(2\tau)+5\eta\Lambda$$
$$(17a_o\eta+6\zeta)\sin(3\tau)+3a_o\eta^2\Lambda\sin(5\tau)\Big)^2\Bigg), \tag{3.29}$$

$$p_z^{(2)}(\tau) = \frac{1}{2K_o\big(1+\eta(2\tau+\sin(2\tau))\big)}\Bigg(-K_o^2 + 32400(1+\eta(2\tau+\sin(2\tau)))\times$$
$$\Big(60(4a_o\eta(1+\Lambda(3-2\tau\eta))+3(1+\Lambda-2\tau\eta\Lambda)\zeta)-90(a_o\eta(3+8\Lambda+16\tau\eta\Lambda)$$
$$+2(1+\Lambda+2\tau\eta\Lambda)\zeta)\cos(\tau)+30a_o\eta\cos(3\tau)-30(a_o(6(1+\Lambda)+\eta(12\tau+24\tau\Lambda$$
$$-71\eta\Lambda+24\tau^2\eta\Lambda))-33\eta\Lambda\zeta)\sin(\tau)-60\eta\Lambda(4a_o\eta+3\zeta)\sin(2\tau)+5\eta\Lambda$$
$$(17a_o\eta+6\zeta)\sin(3\tau)+3a_o\eta^2\Lambda\sin(5\tau)\Big)^2\Bigg). \tag{3.30}$$

The trajectories and the time t of the electrons are given by

$$\frac{d\vec{r}}{d\tau} = \frac{\vec{u}}{K}, \quad \Rightarrow \vec{r}(\tau) = \int_0^\tau \frac{\vec{u}}{K}d\tau, \tag{3.31}$$
$$t(\tau) = \tau + z(\tau). \tag{3.32}$$

Equations (3.26), (3.29) and (3.30) together with equation (3.32) give the transverse, longitudinal momenta and the Lorentz factor γ of the particle P_2 as a function of laboratory time t respectively. The expression of trajectories and time are long and are given in Appendix A. For the limits τ_o and $\sigma \to 0$, which corresponds to self and retarded effects equal to zero, equation (3.12) reduces to the Lorentz force equation, therefore, the solution of equation (3.12) reduces to the solution of the Lorentz equation for the same conditions.

For self force effects, we know that the LL equation is derived from the LAD equation (i.e., equation 1.37) using perturbative expansion and assuming that the

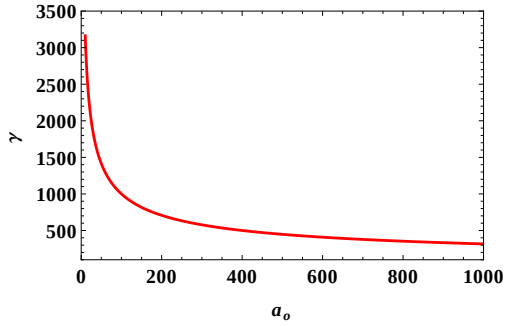

Figure 3.2.: The validity limit of the LL equation in the (a_o, γ)-plane. The LL equation is applicable to all a_o, γ below the red line.

radiation reaction is smaller than the Lorentz force. The coefficient of leading order term in the LL equation and the Lorentz force give

$$\frac{e^2}{m_e c} F^{\beta\gamma} F_{\gamma l} u^l u_\beta u^\alpha \sim \tau_o m_e \omega_L^2 a_o^2 \gamma^3, \tag{3.33}$$

$$eF^{\alpha\beta} u_\beta \sim m_e \omega_o a_o \gamma, \tag{3.34}$$

$$m_e \omega_L a_o \gamma \gg \tau_o m_e \omega_L^2 a_o^2 \gamma^3, \quad \text{or } \gamma \ll \frac{10^4}{\sqrt{a_o}}. \tag{3.35}$$

Condition (3.35) gives the validity limit of the LL equation. For the normalized laser intensity $a_o = 100$, the use of the LL equation is valid if γ is less than 1000. With the increase in the laser intensity, the LL equation violate the validity limit at lower energy of the electron as shown in Figure 3.2. The solution of the LL equation contains terms in power of normalized laser intensity up to a_o^6 while the solution of the Lorentz equation contains power up to a_o^2. Therefore, increasing the intensity of the applied laser leads to RR dominated electron motion. At this point the Lorentz force will not be able to predict the motion of charged particles to a good approximation [69]. It becomes essential to use the LL or LAD equation for such a regime.

The retarded effects become essential when the correction supplied by the

retarded fields to the acceleration of the electron is comparable to the acceleration given by the Lorentz force (3.12)

$$m_e\omega_L a_o \simeq \Lambda m_e\omega_L a_o, \tag{3.36}$$

or in other words $\Lambda \simeq 1$, where $\Lambda \propto Ze/d$, i.e it depends upon the total charge and the mutual distance of the two particles.

The retarded quantities are expanded around the observation time assuming $|\vec{R}(t')|/c < t \simeq \Delta t = t - t' < t$, which implies that t' should be a positive definite quantity. The $|\vec{R}(t')|$ in terms of mutual distance d among the particles for Figure 3.1 (a) is given by

$$|\vec{R}(t')| \;=\; \frac{d}{(1-\beta_z)}, \tag{3.37}$$

for a relativistic particle moving to the $-\hat{z}$-direction, $\beta_z \simeq 1$, and

$$|\vec{R}(t')| \;\simeq\; 0.5d. \tag{3.38}$$

The RR force and retarded fields arise from the emitted radiation and emission of radiation depends on the acceleration of the charged particles, see equation (1.32). Therefore, acceleration of electrons plays a vital role to study the radiation effects. It is well known that the magnitude of acceleration obtained by hitting an electron at rest with a laser pulse is usually small, however, for a head on collision the electron feels a boosted force and higher acceleration can be obtained. Hence in this chapter we are mainly going to study the motion of the electron counter-propagating to the laser pulse.

3.3.2. Circularly polarized plane wave

Now we solve the LL equation including retarded effects for a circularly polarized electromagnetic wave. Let us consider a circularly polarized laser pulse propagat-

ing in positive $\hat{z}$-direction. The field components are given by

$$E_x = B_y = E_o \sin(t-z), \quad E_z = 0, \tag{3.39}$$

$$E_y = -B_x = E_o \cos(t-z), \quad B_z = 0. \tag{3.40}$$

Equation (3.12) for such a polarization can be written as

$$\frac{dp_x^{(2)}}{d\tau} = -a_o \sin(\tau) - a_o \tau_r K(\cos(\tau) + a_o p_x^{(2)}) - \frac{\sigma}{K}\frac{dp_x^{(1)}}{d\tau}, \tag{3.41}$$

$$\frac{dp_y^{(2)}}{d\tau} = -a_o \cos(\tau) + a_o \tau_r K(\sin(\tau) - a_o p_y^{(2)}) - \frac{\sigma}{K}\frac{dp_y^{(1)}}{d\tau}, \tag{3.42}$$

$$\frac{dp_x^{(1)}}{d\tau} = -a_o \sin(\tau) - a_o \tau_r K \cos(\tau) - a_o^2 \tau_r K p_x^{(1)}, \tag{3.43}$$

$$\frac{dp_y^{(1)}}{d\tau} = -a_o \cos(\tau) + a_o \tau_r K \sin(\tau) - a_o^2 \tau_r K p_y^{(1)}, \tag{3.44}$$

$$\frac{dK}{d\tau} = -a_o^2 \tau_r K^2. \tag{3.45}$$

Integration of equation (3.45) is straight forward

$$K = \frac{K_o}{1 + a_o^2 \tau_r K_o \tau}. \tag{3.46}$$

Inserting the value of K in equations (3.43) and (3.44) and integrating, we get

$$p_x^{(1)}(\tau) = a_o \frac{1 - \cos(\tau) - \eta_o\Big(\tau\cos(\tau) + \sin(\tau)\Big)}{1 + \eta_o \tau} \tag{3.47}$$

$$p_y^{(1)}(\tau) = \frac{\eta_o(\cos(\tau) - 1)}{1 + \eta_o \tau} + a_o \sin(\tau), \tag{3.48}$$

where $\eta_o = a_o^2 \tau_r K_o$. Using the solutions of P_1 and the value of K in equations (3.41) and (3.42) and integrating we obtain

$$\begin{aligned} p_x^{(2)}(\tau) = \frac{1}{1+\eta_o\tau}\Big(&a_o(-1 + (-1 + \eta_o(\tau + 4\eta_o))\Lambda) + 2\eta_o\Lambda\zeta + (a_o(1 + \Lambda \\ &+\eta_o(\tau + 2\Lambda\tau - 4\eta_o\Lambda + \eta_o\Lambda\tau^2)) - 2\eta_o\Lambda\zeta)\cos(\tau) \\ &-(a_o\eta_o(1 + 3\Lambda + 3\eta_o\Lambda\tau) + (1 + \Lambda + \eta_o\Lambda)\zeta)\sin(\tau))\Big), \end{aligned} \tag{3.49}$$

$$\begin{aligned} p_y^{(2)}(\tau) = \frac{1}{(1+\eta_o\tau)}&(a_o\eta_o(1 + (3 - \tau\eta_o)\Lambda) + (1 + \Lambda - \tau\eta_o\Lambda)\zeta \\ &-(a_o\eta_o(1 + 3\Lambda + 3\tau\eta_o\Lambda) + (1 + \Lambda + \tau\eta_o\Lambda)\zeta)\cos(\tau) \\ &-(a_o(1 + \Lambda + \eta_o(\tau + 2\tau\Lambda - 4\eta_o\Lambda + \tau^2\eta_o\Lambda)) - 2\eta_o\Lambda\zeta)\sin(\tau)). \end{aligned} \tag{3.50}$$

To obtain the value of p_z and γ, we use the definition of $\gamma^2 = 1 + p_x^2 + p_y^2 + p_z^2$

$$\gamma = \frac{1 + p_x^2 + p_y^2}{2K} + \frac{K}{2}, \tag{3.51}$$

$$p_z = \frac{1 + p_x^2 + p_y^2}{2K} - \frac{K}{2}, \tag{3.52}$$

$$\begin{aligned}\gamma^{(2)}(\tau) = \frac{1}{2K_o(1+\eta_o\tau)}\Bigg(& K_o^2 + \Big((1+\eta_o\tau)^2\big(a_o\eta_o(-1-3\Lambda+\eta_o\Lambda\tau) \\ & +(-1-\Lambda+\eta_o\Lambda)\zeta + (a_o\eta_o(1+3\Lambda+3\eta_o\Lambda\tau)+(1+\Lambda+\eta_o\Lambda\tau)\zeta)\cos(\tau) \\ & +(a_o(1+\Lambda+\eta_o(\tau+2\Lambda\tau-4\eta_o\Lambda+\eta_o\Lambda\tau^2))-2\eta_o\zeta\Lambda)\sin(\tau)\big)^2 \\ & +\Big(a_o(-1+(-1+\eta_o(\tau+4\eta_o))\Lambda)+2\eta_o\zeta\Lambda \\ & +(a_o(1+\Lambda+\eta_o(\tau+2\Lambda\tau-4\eta_o\Lambda+\eta_o\Lambda\tau^2))-2\eta_o\zeta\Lambda)\cos(\tau) \\ & -(a_o\eta(1+3\Lambda+3\eta_o\Lambda\tau)+(1+\Lambda+\eta_o\Lambda\tau)\zeta)\sin(\tau)\Big)^2\Bigg),\end{aligned} \tag{3.53}$$

$$\begin{aligned}p_z^{(2)}(\tau) = \frac{1}{2K_o(1+\eta_o\tau)}\Bigg(& -K_o^2 + \Big((1+\eta_o\tau)^2\big(a_o\eta_o(-1-3\Lambda+\eta_o\Lambda\tau) \\ & +(-1-\Lambda+\eta_o\Lambda)\zeta + (a_o\eta_o(1+3\Lambda+3\eta_o\Lambda\tau)+(1+\Lambda+\eta_o\Lambda\tau)\zeta)\cos(\tau) \\ & +(a_o(1+\Lambda+\eta_o(\tau+2\Lambda\tau-4\eta_o\Lambda+\eta_o\Lambda\tau^2))-2\eta_o\zeta\Lambda)\sin(\tau)\big)^2 \\ & +\Big(a_o(-1+(-1+\eta_o(\tau+4\eta_o))\Lambda)+2\eta_o\zeta\Lambda \\ & +(a_o(1+\Lambda+\eta_o(\tau+2\Lambda\tau-4\eta_o\Lambda+\eta_o\Lambda\tau^2))-2\eta_o\zeta\Lambda)\cos(\tau) \\ & -(a_o\eta(1+3\Lambda+3\eta_o\Lambda\tau)+(1+\Lambda+\eta_o\Lambda\tau)\zeta)\sin(\tau)\Big)^2\Bigg).\end{aligned} \tag{3.54}$$

The trajectories and time t are given by equations (3.31) and (3.32). The analytical expression for trajectories and time t for circular polarized pulse are given in Appendix B. Equation (3.49) - (3.54) along with equation (3.32) give the transverse and longitudinal momenta of P_2 as a function of laboratory time t.

3.3.3. Examples

Now we discuss examples of motion of P_2 in the linear and circular polarized plane waves. We consider that the electrons P_1 and P_2 are initially moving towards the laser pulse for head on collision with initial $\gamma_o = 1000$. The laser pulse

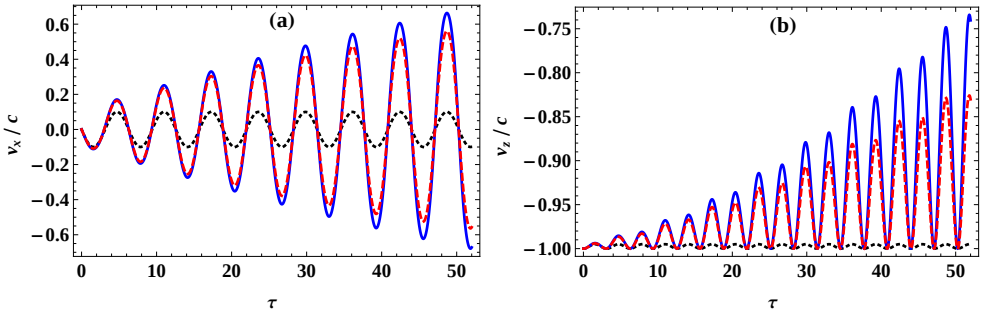

Figure 3.3.: The dynamics of counter-propagating electron P_2 with $\gamma_o = 1000$ in a linearly polarized plane wave with $a_o = 100$. (a) The transverse velocity v_x/c and (b) the longitudinal velocity v_z/c versus τ. The bunch charge is 1.122 nC and mutual distance d between P_1 and P_2 is = 0.8 μm. The red dashed line represents the motion of $P - 2$ with the LL equation plus retarded effects, solid blue line stands for the LL equation and dotted black line shows motion by the Lorentz equation.

has a normalized intensity $a_o = 100$ and wavelength $\lambda_L = 0.8\,\mu$m. Both, P_1 and P_2 are affected by their own radiation, however, P_2 is also affected by the radiation of P_1.

The solution of the Lorentz equation is well know and it gives transverse and longitudinal momentum oscillations with the amplitude depending on the amplitude of the incident laser field and shows a figure eight trajectory in the rest frame of the electron. The solid black line in Figure 3.3 shows the transverse and longitudinal momenta of P_2 obtained by the Lorentz equation (without including the retarded and self-force effects) counter-propagating to the linearly polarized laser pulse. However, the LL equation predicts a transfer of the energy of a counter-propagating electron in a laser pulse. As we can see in Figure 3.4 that the energy of the electron in the transverse direction increases and it decreases in the longitudinal direction. Along with this shift of energy the electron also loses its energy

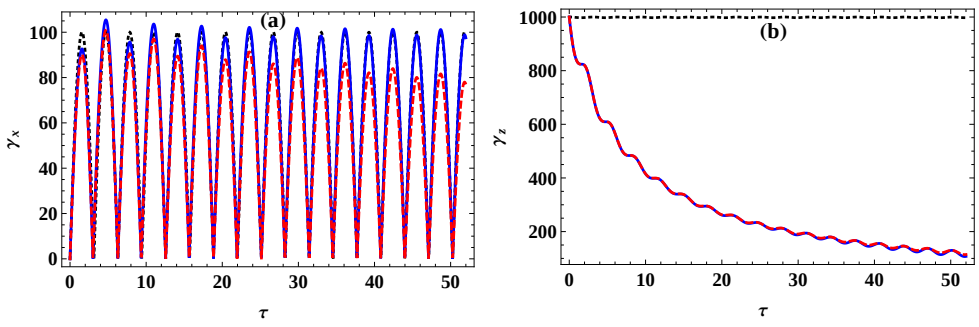

(a) (b)

Figure 3.4.: The initial parameters and color scheme as mentioned in Figure 3.3. (a) The transverse energy γ_x and (b) the longitudinal energy γ_z versus τ of particle P_2 in a linearly polarized plane wave.

i.e., the total energy of a radiating electron is not conserve in a plane electromagnetic wave as predicted by [69]. In other words, the self force in a laser pulse has the ability to stop the counter-propagating electron. The solid blue line in Figures 3.3 and 3.4 represents the self radiation effects of P_2.

Currently femtosecond electron bunches with the charge of few pC are being produced in laser wakefield accelerators [22, 23]. For such kind of electron bunches the average distance d between any two electrons in the bunch is less than 10^{-7} m. As an example, consider the retarded effects of 1.122 nC electron bunch (P_1 in Figure 3.1) on an electron (P_2 in Figure 3.1) with initial $\gamma_o = 1000$ counter-propagating to a linearly polarized laser pulse with $a_o = 100$. The electron bunch is considered as a single macro particle located at a distance $d = 0.8\ \mu$m from the electron under observation P_2. The effects of retarded fields are shown in Figures 3.3 and 3.4 by the red dashed line. We see that the retarded effects reduce the self force effects both in transverse and longitudinal direction. The momentum has lower amplitude and now it lies between the Lorentz and LL equations. The transverse energy γ_x is decreasing and the longitudinal energy increasing to-

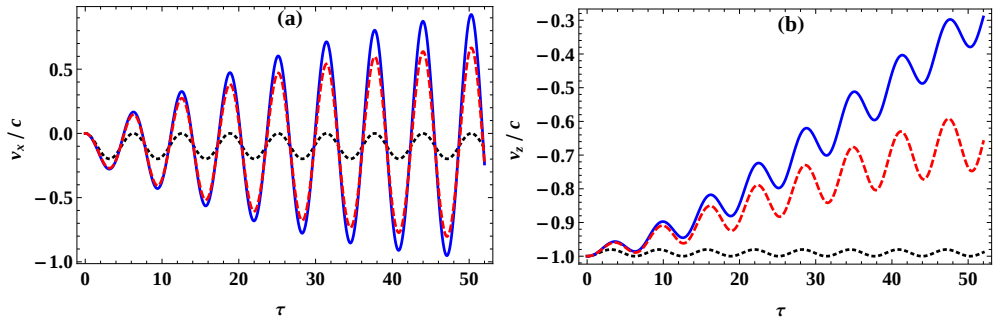

(a) (b)

Figure 3.5.: For a circularly polarized wave (a) the transverse velocity v_x/c and (b) the longitudinal velocity v_z/c as a function τ of particle P_2. The color scheme and numerical parameters as mentioned in Figure 3.3.

wards the end due to retardation effects, see Figure 3.4. The retarded field is weak in the beginning because the transverse momentum of P_1 is small in the beginning and retarded field depends linearly on derivative of transverse momentum. Hence, the momenta of P_2 is same with and with out retarded effects of P_1 in the beginning. However, as the transverse momentum of P_1 increases the retardation effects also increase and momenta of P_2 differ with and with out retarded effects.

The same kind of effects are observed for the circularly polarized laser pulse of same intensity as we have seen for laser pulse with linear polarization. For the LL equation, however, we see a drift for the longitudinal momentum.

The retarded effects of a 1.122 nC electron bunch on an electron with initial $\gamma_o = 1000$ counter-propagating in a circularly polarized laser pulse with $a_o = 100$ for the same mutual distance mentioned above are shown in Figures 3.5 and 3.6 by the red dashed line. The solid blue and black lines represent the LL and Lorentz equations respectively. Again the retarded fields mitigate the self-force effects for the momentum and energy of the electron as can be seen in Figures 3.5 and 3.6. The solid blue line shows the energy gain in the transverse direction and energy

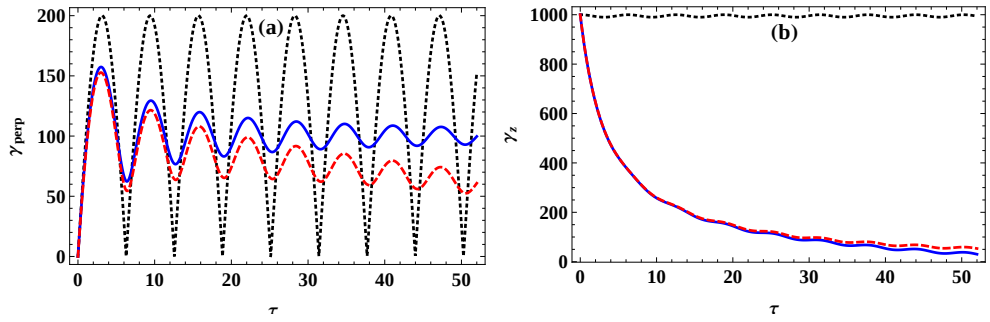

(a) (b)

Figure 3.6.: The numerical parameters and color scheme as mentioned in Figure 3.3. (a) The transverse energy γ_x and (b) the longitudinal energy γ_z versus τ of particle P_2 in a circularly polarized plane wave.

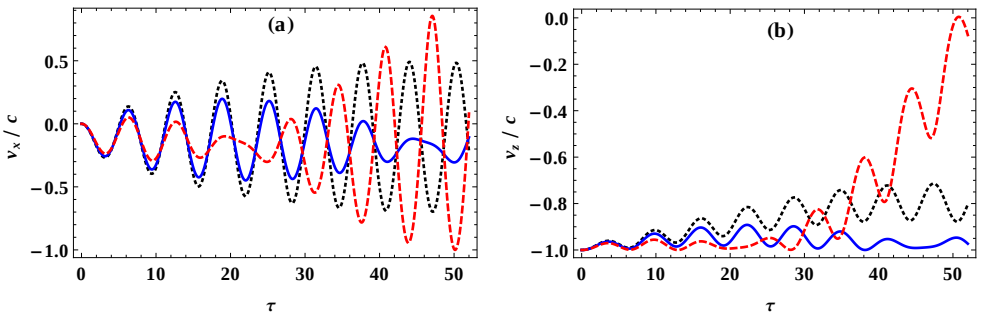

(a) (b)

Figure 3.7.: For a circularly polarized wave of $a_o = 100$ (a) the transverse velocity v_x/c and the longitudinal velocity v_z/c versus τ of particle P_2 with $\gamma_o = 1000$. The dotted black, solid blue and red dashed lines represent macro bunch with charge (80.1, 160.2 and 320)pC respectively.

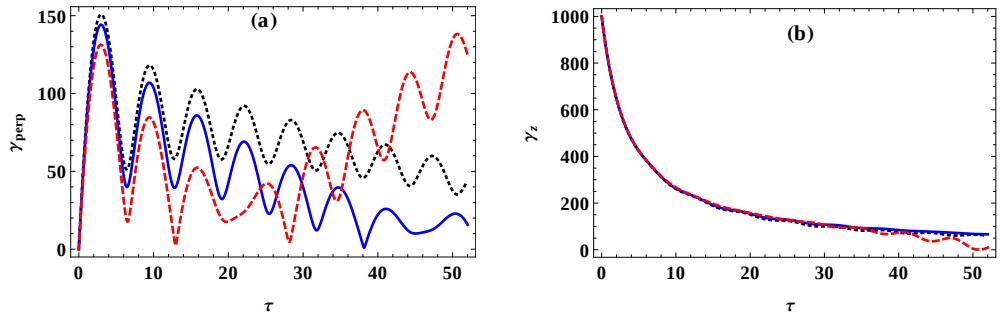

(a) (b)

Figure 3.8.: The color scheme and other parameters as mentioned in Figure 3.7. (a) The transverse energy γ_x and (b) the longitudinal energy γ_z as a function τ of particle P_2.

loss in the longitudinal direction of the electron due to radiation reaction while red dashed line shows the counter action of retarded fields of a 1.122 nC electron bunch P_1 on the self fields of electron P_2. Clearly electron gains more energy in the transverse direction for circular polarization. We can also notice that even though the bunch have same total charge for both linearly polarized and circularly polarized pulses, however, self-force and retarded fields are more effective for circularly polarized laser pulse.

It should be noted that the normalized laser intensity a_o and constant K_o play key roles to determine the strength of radiation and retarded effects. High intensity laser pulse makes the electron radiates more energy because of high acceleration and as a consequence the retarded and self-field effects are severe. The retarded effects increase linearly with total bunch charge and inversely to the mutual distance between the particles. For an electron bunch of small duration and high total charge the retarded effects are stronger. If we increase the charge of the bunch the retardation effects also increase as expected, see Figures 3.7 and 3.8. The transverse energy gain of P_2 due to self fields reduces under the retarded effects

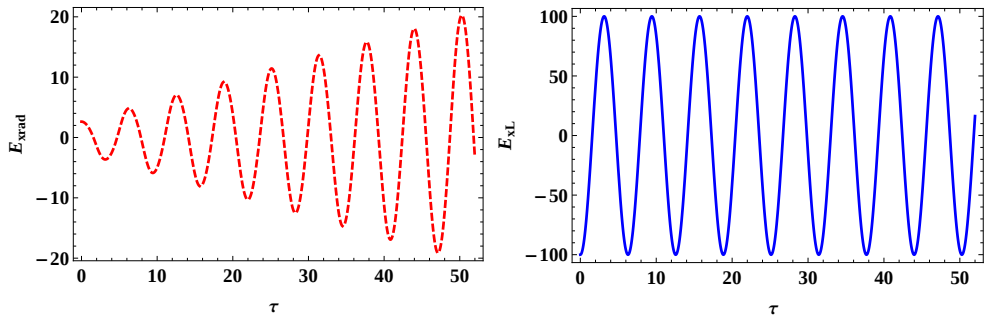

(a) (b)

Figure 3.9.: For linearly polarized plane wave. (a) Normalized retarded electric field component E_{xrad} and (b) the transverse electric field E_x of laser pulse felt by electron P_2 versus τ. Numerical parameters as mentioned in Figure 3.3.

of electron bunch of higher charge. The dotted black, solid blue and red dashed lines in Figures 3.7 and 3.8 represent the retarded effects on electron P_2 of bunches with charge (80.1, 160.2 and 320)pC respectively.

In fact, the nature of the emitted betatron radiation is the same as the one by a free-electron-laser in an undulator magnet [65]. In the examples considered above, the electrons are moving relativistically, therefore, the radiation is emitted purely in the initial direction of motion ($-z$ direction) [65]. The polarization of the emitted betatron radiation is always opposite to the polarization of applied external laser pulse. Therefore, it always reduces the effects of applied laser pulse no matter if electrons are initially co-propagating or counter-propagating as shown in Figures 3.9 and 3.10. For the model considered in Figure 3.1, the betatron radiation mitigates the fields of applied laser pulse and hence the total fields felt by the electron become less, which makes self radiation effects small. The retarded field is weak in the beginning because the transverse momentum of P_1 is small in the beginning and retarded field depends linearly on derivative of transverse

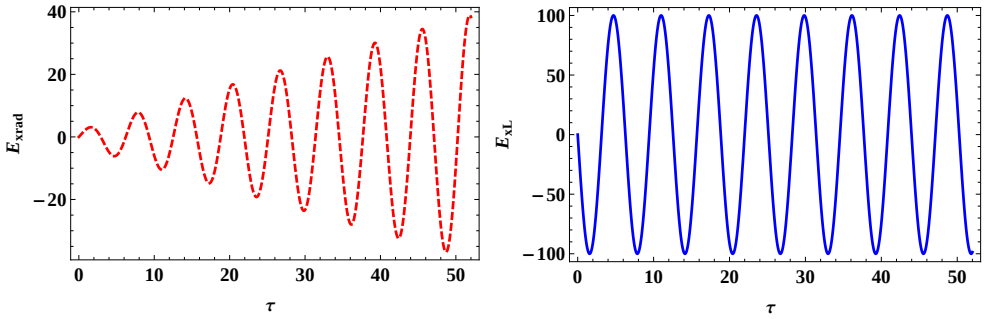

(a) (b)

Figure 3.10.: Numerical parameters and color scheme as mentioned in Figure 3.3. (a) Normalized retarded electric field component E_{xrad} and (b) the transverse electric field E_x of laser pulse felt by electron P_2 versus τ in a circularly polarized plane wave.

momentum. Hence, the retarded field of P_1 felt by P_2 is also small. However, for later time as the transverse momentum of P_1 increases the retarded field also increases. The total field $E_L + E_{rad}$ felt by P_2 become less for later time because both have opposite polarization, where E_{rad} are the retarded field of P_1 felt by P_2. The results are shown in Figures 3.9 3.10.

The retarded effects are not usually beneficiary contrary to the eye meet in the above mentioned results. In the laser wakefield it can reduce the effects of transverse focusing force, which increases the transverse oscillation of the electrons. The increase in amplitude of the transverse oscillation can cause an increase in the transverse emittance of the electron beam in a plasma focusing channel as we will see in Chapter 5.

Let us study the retarded effects of a single particle on the other electron separated by a small distance such that the retarded fields of one electron affect the motion of the other electron. We assume that P_1 in Figure 3.1 consists of a single electron. Both particles (P_1 and P_2) are traveling opposite to the laser pulse with

initial $\gamma_o = 1000$. The laser intensity is the same as the one we have considered in the pervious examples. It is interesting to mention that the retarded effects are effective if both charges are separated by a distance, which is smaller than the classical electron radius i.e. $d \ll 10^{-15}$ m.

3.4. Summary of the chapter

The retardation and radiation reaction effects on the motion of an electron in laser pulses of different polarization are studied by using the Landau-Lifshitz (LL) equation and the Lienard-Wiechert fields. The analytical solutions are presented for the corresponding polarization.

We found that radiation reaction transfers the longitudinal energy of a relativistic electron counter-propagating in a laser pulse of high intensity to the transverse energy. The total energy of the electron does not remain conserve in a plane electromagnetic wave due to radiation reaction. It is found that the retardation effects of an electron bunch of high density (i.e., high charge) mitigate the radiation reaction effects for both momentum and energy. The retarded fields are always polarized in opposite direction to the polarization of the applied laser pulse. Moreover, retardation effects increase with increasing bunch charge or with decreasing mutual distance between two interacting particles. Both, self force and retarded fields are more effective for circularly polarized laser pulse as compared to the linearly polarized laser pulse of same intensity. The retarded fields of a single electron is considerable if it is located at a distance, which is smaller than the classical electron radius from the other electron i.e $d \ll r_e$.

CHAPTER 4

TeV scale electron beam from multistage low density laser-plasma accelerators

4.1. Introduction

As stated earlier the acceleration length of a single stage Laser-Plasma-Accelerator (LPA) is limited by the dephasing of the accelerating particles or by the energy depletion of a driver pulse. Therefore, to obtain a high energy charged particle beam, which exceeds the energy gain of a single stage LPA, a multistage arrangement is required. The total length of a large scale LPA consisting of periodic structures of a coupling and a plasma accelerator can be determined by the single stage energy gain for a given beam energy and the coupling distance between two stages. The coupling section that installs both laser and beam focusing systems could be of several meter in length. The application of multistage LPA for the high energy physics experiments requires a high quality beam with small energy spread and transverse emittance along with sufficient charge. These requirements reduce the optimum operating plasma density below 10^{16} cm^{-3}. Moreover, the coupling of different stages in LPA is complex and it leads to the degradation of the emit-

tance. Therefore, low density LPAs are recommended. The advantage of working with low density plasma accelerators is that the single stage energy gain increases, while the accelerating gradient reduces and the pump depletion length L_{pd} increases. Usually the degradation of the transverse emittance and energy spread is induced by dephasing and betatron oscillations of accelerated particles of the beam that undergo strong accelerating and focusing in the multistage LPAs. Compromising between the linac length and the beam quality requirements allows us to find the proper operating plasma density [19].

In this chapter we consider the design of the multistage LPAs operating in the quasilinear regime i.e. $a_o \sim 1$. The expressions for the single stage are presented as a function of the operating plasma density. The total LPA length for a beam energy of 1 TeV is calculated for operating plasma densities of 10^{15} to 10^{18} cm^{-3}.

4.2. Accelerating field

As mentioned earlier in under-dense plasma an ultra-intense laser pulse creates plasma waves with accelerating electric fields of the order of $E_o = m_e c\omega_p/e$, where ω_p is the frequency of the plasma wave. The ponderomotive force of the laser expels plasma electrons out of the laser pulse and the space charge force of immovable plasma ions can accelerate the electrons. In the linear wakefield regime $(a_o \simeq 1)$ the maximum accelerating wakefield driven by a Gaussian laser pulse is given by

$$E_M = \frac{\sqrt{\pi}}{4} a_o^2 E_o k_p \sigma_z \exp\Big(-\frac{k_p^2\sigma_z^2}{4}\Big), \tag{4.1}$$

where $\lambda_p = 2\pi/k_p$ is the plasma wavelength and σ_z is the length of the laser pulse. The maximum field $E_M \simeq 0.33 a_o^2 E_o$ for the resonant condition $k_p\sigma_z = 2$ for a given plasma density. The optimum conditions can be determined by changing the plasma density and pulse duration, which is $k_p\sigma_z = 1$ and the maximum

wakefield is given by

$$E_M[GV/m] \simeq 10.6 a_o^2 \Big(\frac{n_o}{10^{17}[cm^{-3}]}\Big)^{1/2}. \tag{4.2}$$

For a beam of total charge $Q_b = eN_b$, where N_b is the number of particle in the beam, the net accelerating field is determined by the beam loading that means the energy absorbed per unit length

$$Q_b E_z \;\; = \;\; \frac{m_e c^2}{8 r_e} \frac{E_M^2}{E_o^2} k_p^2 r_b^2 \Big(1 - \frac{E_z^2}{E_M^2}\Big), \tag{4.3}$$

where $1 - E_z^2/E_M^2 = \eta_l$ is the beam loading efficiency that is the fraction of the plasma wave energy absorbed by particles of the beam with radius r_b and $r_e = e^2/(4\pi\epsilon_o m_e c^2)$ is the classical electron radius. With the help of (4.2) equation (4.3) can be recast as

$$Q_b \;\; \simeq \;\; 3.9 \frac{m_e c^2}{r_e} \frac{\eta_l}{1-\eta_l} k_p^2 r_b^2 \frac{E_z}{E_o} \Big(\frac{n_c}{n_o}\Big)^{1/2}, \tag{4.4}$$

where $E_z/E_o = 0.35 a_o^2 \sqrt{1-\eta_l}$ for $k_p \sigma_z = 1$ and n_c is the critical plasma density.

4.3. Energy gain, stage length and total LPA length

Total length of the LPA for a beam energy E_b is given by

$$L_{tot} \;\; = \;\; (L_{stage} + L_{coupl}) E_b / W_{stage}, \tag{4.5}$$

where L_{coupl} is the required coupling distance for injecting a new drive laser pulse and a charged particle beam into the next stage of the LPA, W_{stage} is the energy gain in a single stage, and L_{stage} is the single stage length of LPA. Usually the stage length is determined by the pump depletion length L_{pd} over which the total field energy is equal to the half of the initial energy of the laser. For a laser pulse of length $k_p \sigma_z = 1$ of Gaussian shape the pump depletion length is given by the relation

$$k_p L_{pd} \simeq \frac{8\omega_L^2}{\omega_p^2 \sqrt{\pi a_o^2 k_p \sigma_z}} \exp\Big(\frac{k_p^2 \sigma_z^2}{4}\Big) \sim 7.4 \frac{n_c}{a_o^2 n_o}, \tag{4.6}$$

where ω_L is the frequency of the laser pulse. The pump depletion length is almost $8(n_c/n_o)$ for $a_o = 1$ and $3.4(n_c/n_o)$ for $a_o = 1.4$. The dephasing length is approximately given by $L_{dp} = (\lambda_p/2)(n_c/n_o)$. In the quasi-linear regime $a_o \simeq 1$ the energy gain is usually limited by dephasing not by pump depletion. The approximate dephasing length in terms of pump depletion is given by $L_{dp} = 0.85 L_{pd}$ [16].

The energy spread starts increasing after half of the dephasing length at which it decreases to its minimum value due to the phase rotation of the bunch [66]. Recently it has been shown that the energy spread of an externally injected electron beam rapidly increases after half of the dephasing length in a weakly nonlinear blowout regime [94]. Therefore, to minimize the energy spread, the stage length should be set to half of the dephasing length, which means

$$L_{stage} \simeq \frac{\lambda_p}{4}\frac{n_c}{n_o} = \frac{\lambda_L}{4}\big(n_c/n_o\big)^{3/2}, \tag{4.7}$$

where λ_L is the laser wavelength and $\lambda_p = \lambda_L\big(n_c/n_o\big)^{1/2}$. The energy gain per stage is equal to $W_{stage} \simeq eE_z L_{stage}$

$$W_{stage} \simeq \frac{\pi m_e c^2}{2}\frac{E_z}{E_o}\frac{n_c}{n_o}, \tag{4.8}$$

and total number of stages

$$N_{stage} \;=\; \frac{E_b}{W_{stage}} \simeq \frac{2\gamma_f}{\pi}\Big(\frac{E_z}{E_o}\Big)^{-1}\Big(\frac{n_c}{n_o}\Big)^{-1}, \tag{4.9}$$

where $\gamma_f = E_b/(m_e c^2)$ is the relativistic Lorentz factor at the final beam energy. The coupling distance between two LPA stages can be estimated by the following relation $L_{coupl} = (\lambda_L/8)(n_c/n_o)^{3/2}$ [19] and the minimum LPA length is

$$\begin{aligned} L_{tot} \;&\simeq\; (L_{stage} + L_{coupl})E_b/W_{stage} \simeq \frac{3}{2}L_{stage}N_{stage}, \\ &\approx\; \frac{3\gamma_f\lambda_L}{4\pi}\Big(\frac{E_o}{E_z}\Big)\Big(\frac{n_c}{n_o}\Big)^{1/2}. \end{aligned} \tag{4.10}$$

4.4. Driver laser pulse and electron beam parameters

The self-focusing of the driver laser and self-injection of plasma electrons must be suppressed in a multi-staged LPA to improve the beam quality. In the quasi-linear

regime the laser spot size must be $k_p^2 r_o^2/4 > \frac{a_o^2}{\sqrt{1+a_o^2/2}}$ to avoid bubble formation, where r_o is the laser spot size. The strong self-focusing can be avoided by the condition $P_L/P_c = (k_p r_o a_o)^2/32 \leq 1$, where P_L and $P_c = 2(m_e^2 c^5/e^2)\omega_L^2/\omega_p^2$ are the peak and critical laser power respectively. With these conditions the laser spot size should have the value $1.8 \leq k_p r_o \leq 5.7$ for $a_o = 1$ and $1.8 \leq k_p r_o \leq 5.7$ for $a_o = \sqrt{2}$. The peak laser power can be obtained by the formula

$$P_L = \frac{(k_p r_o a_o)^2}{16} \frac{m_e^2 c^5}{e^2} \frac{n_c}{n_o}. \tag{4.11}$$

The FWHM pulse length is $c\tau_L = 2\sqrt{ln2}\sigma_z \simeq 0.265\lambda_p$ [16] and the laser energy per stage can be calculated by the relation $U_L = P_L \tau_L$.

The envelope equation of the rms beam radius σ_r is given by

$$\frac{d^2\sigma_r}{dz^2} + \frac{K^2}{\gamma}\sigma_r - \frac{\epsilon_n^2}{\gamma^2 \sigma_r^3} = 0, \tag{4.12}$$

where ϵ_n is the normalized emittance. The solution of equation (4.12) for an unmatched beam is well known and it gives the oscillations of the beam envelope with betatron period $\lambda_\beta = \sqrt{\gamma}/(2\pi K)$ [95]. If the electron beam is initially matched in the plasma channel and we assume that there are no betatron oscillations in the radial envelope of the electron beam then $\sigma_r^2 = \epsilon_n/(K\sqrt{\gamma})$ [66].

Table 4.1 shows different parameters for $a_o = \sqrt{2}$, beam loading efficiency $\eta_l = 1/2$, $k_p r_o = 3$, and $k_p \sigma_z = 1$ for a linear laser wakefield.

4.5. Single particle motion

Let us study the motion of an electron beam moving in a laser wakefield. As stated earlier a charged particle moving in a laser wakefield feels a transverse focusing force along with an axial accelerating force. In the quasilinear regime the focusing constant K is related to the accelerating field

$$K^2 = \frac{4}{r_o^2}\frac{E_z}{E_o}\langle \sin\psi \rangle, \tag{4.13}$$

Table 4.1.: Parameters for 1 TeV linear laser plasma accelerator

Beam final energy E_b (TeV)	1	1	1	1	1
Injection beam energy E_i (GeV)	1	1	1	1	1
Plasma density n_o (cm^{-3})	10^{15}	10^{16}	2.3×10^{16}	10^{17}	10^{18}
Plasma wavelength $\lambda_p(\mu)$m	1056	334	220	106	33
Acceleration field E_z (GV/m)	1.5	4.7	7.2	15	47
Energy gain per stage W_{stage} (GeV)	500	45	19	4.5	0.47
Number of stages N_{stage}	2	22	50	222	2125
Stage length L_{stage} (m)	333	9.7	2.8	0.3	0.01
Total linac length L_{total} (L_{coupl})m	1000(167)	321(4.9)	210(1.4)	100(0.15)	32(0.005)
Total linac length L_{total} (L_{coupl})m	686(10)	433(10)	640(10)	2287(10)	21271(10)
Total linac length L_{total} (L_{coupl})m	668(1)	235(1)	190(1)	289(1)	2146(1)
Particles per bunch N_b (10^9)	7.5	2.4	1.6	0.75	0.24
Initial emittance ε_{no} rad(μm)	2068	646	432	209	54
Initial beam radius σ_{xo} (μm)	168	53	35	17	5.3
Bunch length σ_{bz} (μm)	4.1	1.3	0.9	0.4	0.13
Normalized laser intensity a_o	1.4	1.4	1.4	1.4	1.4
Laser wavelength λ_o (μm)	1	1	1	1	1
Laser pulse duration τ_L (fs)	950	300	200	100	30
Laser spot radius r_o (μm)	504	160	105	51	16
Laser peak power P_L (TW)	10913	1091	474	109	11
Laser energy per stage U_L (J)	10367	327	95	11	0.33

where $\langle \sin\psi \rangle$ is set to be an average value over the dephasing phase $0 \leq \psi \geq \pi/4$. The LL equation (1.39) for a single electron moving in a laser wakefield can be written as

$$\frac{du_x}{dct} = -K^2 x - c\tau_o K^2 u_x (1 + K^2 \gamma x^2), \tag{4.14}$$

$$\frac{du_z}{dct} = \eta - c\tau_o K^4 \gamma^2 x^2, \tag{4.15}$$

where $\eta = eE_z/(m_e c^2)$, and $\vec{u} = \gamma\vec{v}/c$ is the electron three vector momentum. Moreover, we have used the fact that for an electron beam traveling along the

$\hat{z}$-direction with large initial γ_o, $v_x \ll v_z$. We assume $\gamma \simeq u_z$

$$\frac{du_x}{dt} = -cK^2x - c^2\tau_o K^2 u_x(1 + K^2\gamma x^2), \tag{4.16}$$

$$\frac{d\gamma}{dt} = \zeta - c^2\tau_o K^4\gamma^2 x^2, \tag{4.17}$$

where $\zeta = c\eta$ as we have $\dot{x} = cu_x/\gamma$, $\dot{u_x}$ and $\dot{\gamma}$ are given by equations (4.16) and (4.17). With this information we can write

$$\ddot{x} + \zeta\dot{x}/\gamma + c^2K^2x/\gamma = 0. \tag{4.18}$$

The transverse motion of the electron will be damped as is clear from the equation (4.18). The frequency of oscillation is given by $\omega_\beta = ck_\beta = cK/\sqrt{\gamma_o}$ [4]. For simplicity we introduce the normalized quantities $\tilde{\gamma} = \gamma/\gamma_o$, $\tilde{x} = x/x_m$ and $\tilde{t} = \omega_{\beta o}t$ in equations (4.17) and (4.18)

$$\ddot{\tilde{x}} + \xi_o\dot{\tilde{x}}/\tilde{\gamma} + \tilde{x}/\tilde{\gamma} = 0, \tag{4.19}$$

$$\dot{\tilde{\gamma}} = \xi_o - 2\delta\tilde{\gamma}^2\tilde{x}^2, \tag{4.20}$$

where $\xi_o = \zeta/(\omega_{\beta o}\gamma_o)$, $\delta = c^2\tau_o K^4 x_m^2\gamma_o/(2\omega_{\beta o})$ and $x_m^2 = x_o^2 + u_{xo}^2/(k_\beta^2\gamma_o^2)$ is the maximum transverse radius, x_o and u_{xo} are the initial transverse position and momentum of the particle respectively.

4.5.1. The solution

To solve the coupled equations (4.19) and (4.20), we use the separation of time scales as done in [66]. The time scale of fast betatron oscillations is of the order of ω_β^{-1} and the time scale of slow radiation damping oscillations is usually of the order of δ^{-1}, where $\delta \ll 1$. The expansion of the quantities in a series of δ gives $\tilde{x} = \tilde{x}^{(0)} + \delta\tilde{x}^{(1)}$ and $\tilde{\gamma} = \tilde{\gamma}^{(0)} + \delta\tilde{\gamma}^{(1)}$. The zeroth order equations are

$$\ddot{\tilde{x}}^{(0)} + \xi_o\dot{\tilde{x}}^{(0)}/\tilde{\gamma}^{(0)} + \tilde{x}^{(0)}/\tilde{\gamma}^{(0)} = 0, \tag{4.21}$$

$$\dot{\tilde{\gamma}}^{(0)} = \xi_o. \tag{4.22}$$

The solution of equation (4.22) is $\tilde{\gamma}^{(0)} = 1 + \xi_o \tilde{t}$ and of equation (4.21)

$$\tilde{x}^{(0)} = \frac{\cos(\psi)}{\tilde{\gamma}^{(0)1/4}}, \tag{4.23}$$

the first order equation in δ for $\tilde{\gamma}$ is

$$\dot{\tilde{\gamma}}^{(1)} = -2(\tilde{x}^{(0)}\tilde{\gamma}^{(0)})^2 = -2(\tilde{\gamma}^{(0)})^{3/2}\cos^2(\psi). \tag{4.24}$$

We perform the time average over the fast oscillations which yields

$$\dot{\tilde{\gamma}}^{(1)} = -(\tilde{\gamma}^{(0)})^{3/2}, \tag{4.25}$$

$$\tilde{\gamma}^{(1)} = \frac{2}{5\xi_o}\big(1 - (\tilde{\gamma}^{(0)})^{5/2}\big), \tag{4.26}$$

as we have $\tilde{\gamma} = \tilde{\gamma}^{(0)} + \delta\tilde{\gamma}^{(1)}$, which implies that

$$\gamma = \gamma_o + \zeta t + \frac{2\nu_\alpha \gamma_o^2}{5\zeta}\left[1 - \left(1 + \frac{\zeta}{\gamma_o}t\right)^{5/2}\right]. \tag{4.27}$$

4.5.2. Electron beam dynamics

The behavior of the electron beam can be studied by averaging different quantities for the motion of a single electron over an ensemble of electrons. Single particle quantities will be expanded about the ensemble averaged value of that quantity plus small perturbation. For example, the initial energy $\gamma_o = \langle\gamma_o\rangle + \delta\gamma_o$, where $\langle\rangle$ represents the average over the ensemble of particles. Suppose that there are N electrons in the beam and we want to estimate (for example) the mean energy of the beam. The mean energy $\langle\gamma\rangle = \sum_i \gamma_i/N$, where γ_i is the energy of the ith particle. Equation (4.27) for the mean energy to the lowest order for a beam injected on axis can be written as

$$\langle\gamma\rangle = \langle\gamma_o\rangle + \zeta t + \frac{2\bar{\nu}_\alpha \langle\gamma\rangle_o^2}{5\zeta}\Big[1 - \Big(1 + \frac{\zeta}{\langle\gamma_o\rangle}t\Big)^{5/2}\Big]. \tag{4.28}$$

The relative energy spread of the electron beam is $\sigma_\gamma/\langle\gamma\rangle$, where σ_γ^2 is given by

$$\sigma_\gamma^2 = \langle\delta\gamma^2\rangle = \langle\gamma^2\rangle - \langle\gamma\rangle^2, \tag{4.29}$$

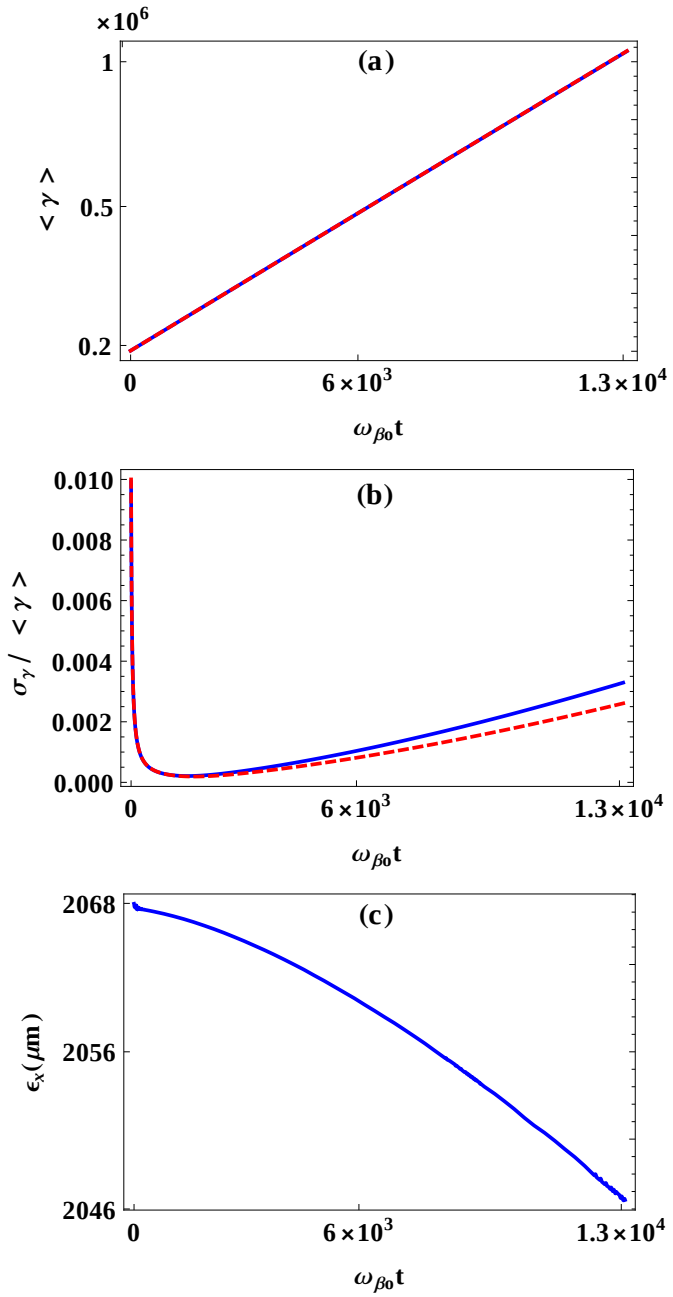

Figure 4.1.: The electron beam dynamics: (a) the mean energy $\langle\gamma\rangle$, (b) the relative energy spread $\sigma_\gamma/\langle\gamma\rangle$, and (c) the normalized transverse emittance ε_{nx}. The electron beam moves with an initial energy of 1 GeV, an initial energy spread 1% and with an initial transverse emittance $\epsilon_{nxo} = 2068$ μm in a plasma channel of density of 10^{15} cm^{-3}.

$$\frac{\sigma_\gamma^2}{\langle\gamma\rangle^2} = \frac{\left[\sigma_{\gamma o}^2 + \frac{4\bar{\nu}_\alpha^2\langle\gamma\rangle_o^4}{25\zeta^2}\left\{1-\left(1+\frac{\zeta}{\langle\gamma_o\rangle}t\right)^{5/2}\right\}^2\left(\langle\gamma\rangle_0^2\sigma_{xo}^4+\frac{\sigma_{uxo}^4}{K^4}\right)\right]}{(\langle\gamma_o\rangle+\zeta t)^2}. \quad (4.30)$$

The particle trajectories and transverse momenta are obtained from the numerical solution of the coupled equations (4.19) and (4.20). Using the numerical results for the ensemble of test particles the different quantities such as energy spread and transverse emittance of the electron beam can be obtained as well. We have calculated the solution for 10^4 particles in plasma channels of density 10^{15} cm^{-3}, the column 1 case of Table 4.1. We have mainly focused on the first stage of acceleration. For multistage accelerators there are other effects that need to be considered such as injection jitters and beam focusing error between two subsequent stages, etc. The numerical solutions together with the analytical estimates for the mean energy $\langle\gamma\rangle$ (equation 4.28) and relative energy spread $\sigma_\gamma/\langle\gamma\rangle$ (equation 4.30) are shown in Figure 4.1. As can be seen in Figure 4.1 the numerical estimates are in good agreement with the analytical solutions. The relative energy spread in the beginning decreses approximately linearly in time due to the linear increase in the mean energy of the beam. However, for $t^2 > \sigma_{\gamma o}^2/(\langle\gamma\rangle_o^2\bar{\nu}_\alpha^2)$, it increases due to radiative effects.

If the beam is matched initially then the normalized transverse emittance decreases (with out acceleration fields) as $\varepsilon_{nx} = \varepsilon_{no}(1-3\bar{\nu}t/2)$ [66]. For a mismatched beam with small initial energy spread the transverse emittance increases in the beginning for very short time due to the fact that the different particles undergo betatron oscillations with different frequencies, which leads to the decoherence that is the slippage of the particles with respect to each other. Once the emittance reaches the matched value it remains almost constant.

As we have used a low density plasma channel the radiative damping is small and hence the emittance decreases linearly with time. Roughly speaking the transverse emittance remains almost constant in one stage in low density plasma.

4.6. Summary of the chapter

In this chapter we have considered design issues for high energy laser-based plasma accelerators working in the quasilinear regime operating at plasma densities 10^{15}, 10^{16}, 2.3×10^{16}, 10^{17} and 10^{18} cm^{-3}. The accelerating field is 1.5, 4.7, 7.2, 15, and 47 GeV for fixed laser intensity $a_o = 1.4$ and the beam loading efficiency $\eta_l \sim 50\%$. If we take the stage length equal to the effective dephasing length $L_d \simeq (\lambda_p/4)(n_c/n_o)$ the energy gain per stage is 500, 45, 19, 4.5 and 0.47 GeV for each case respectively. The total LPAs length can be minimized if we choose the coupling length equal to half of the effective dephasing length $L_{coupl} = (\lambda_p/8)(n_c/n_o)$, which gives a total stage length equal to 1.5 L_{stage}. Higher operating density gives smaller LPAs length, however, the mm coupling length is not practical to install with both laser and beam focusing. If we increase the coupling distance to a meter range or above the total length of the LPA increases even for the high density case. Moreover, the total number of stages increases with a increasing density, which makes it complex and leads to degradation of the beam parameters. On the other hand, at lower operating density the total number of stages reduce with low accelerating gradient to a small total LPA length. Moreover, the total energy gain per stage increases for low density LPA. In particular, the less number of stages helps to get a beam with the desired parameters.

CHAPTER 5

Retardation effects on electron beams in laser wakefields

As discussed earlier radiation emitted by a relativistic electron bunch of charge $\geq$ 100 pC affects the subsequent motion of the electrons of the beam [19, 66, 67, 68]. In Chapter 3 we have studied the electron motion in a laser pulse under the retarded effects of an electron bunch and saw that the retarded effects become essential for a high charge electron bunch with smaller size. Now we will investigate the accumulated effects (self radiation and retardation effects) of radiation on the evolution of the properties of an electron beam in a laser wakefield.

In this chapter we will study the motion of an electron bunch in a plasma focusing channel. We suppose that every particle of the bunch is affected by the laser wakefield, self radiation field, and also by the retarded potentials of other electrons in the bunch. Let us assume that there are N electrons in the bunch and that the ith particle (which is the particle under observation) is under the effect of retarded potentials of a, say, bunch of particles (the remaining N-1 electrons). Similarly, next we take the jth$= (i + 1)$th particle and so on. In other words, each electron of the beam is under the retarded effects of all the other electrons

of the beam and it is also affected by its own radiation (self force effects). In our model, the self force effects of emitted radiation is included through LL equation and retarded effects are implemented through Lienard-Wiechert fields.

We study the motion of test electrons which are traveling in a laser wakefield and estimate the beam properties in the latter. Electron beam properties will be estimated by averaging different quantities of single electron over an ensemble of particles as done in Chapter 4.

5.1. Single particle motion

Let us consider an electron beam moving along the $\hat{z}$-axis in a plasma focusing channel of axially uniform but varying transverse potential as discussed in [66]. To study the retarded effects in a laser wakefield we will use the same approach as discussed in the Chapter 3. We notice that for our formulation the retarded effects mainly acts in the transverse direction for linearly and circularly polarized laser pulses. Moreover, the retarded effects on an electron can be implemented through the momentum of the radiating electron. Equations (4.14) and (4.15) for P_2 including retarded effects of P_1 can be written as

$$\frac{du_x}{dct} = -K^2 x - c\tau_o K^2 u_x(1 + K^2\gamma x^2) - \sigma_o(1 - v_z)^{-1}\frac{dv_{x1}}{dct}, \tag{5.1}$$

$$\frac{du_z}{dct} = \zeta_z - c\tau_o K^4 \gamma^2 x^2. \tag{5.2}$$

For particle P_1 it takes the form

$$\frac{du_{x1}}{dct} = -K^2 x_1 - c\tau_o K^2 u_{x1}(1 + K^2\gamma_1 x_1^2), \tag{5.3}$$

$$\frac{du_{z1}}{dct} = \zeta_z - c\tau_o K^4 \gamma_1^2 x_1^2, \tag{5.4}$$

where $K^2 = \frac{4}{r_o^2}\frac{E_z}{E_o}\langle \sin\psi \rangle$, $\zeta_z = eE_z/(m_e c^2)$ as discussed in Chapter 4, $\vec{u} = \gamma\vec{v}/c$ is three vector momentum of the electron, and $\sigma_o = Ze^2/(4\pi\epsilon_o d m_e c^2)$. The different quantities in this section correspond to particle P_2 in Figure 3.1 (a) if not labeled. We have assumed that for an electron beam traveling in the $\hat{z}$-direction with large

initial γ_o, $v_x \ll v_z$. From equations (5.1) - (5.4) it is clear that both particles have the same expressions for energy and there is one extra term for the trajectory of particle P_2. Therefore, from now on we will write the expressions only for electron P_2. The corresponding expressions for electron P_1 can be obtain by taking the limit $\sigma_o \to 0$. From equations (5.1) and (5.2) we obtain

$$\frac{du_x}{dt} = \dot{u}_x = -cK^2x - c^2\tau_o K^2 u_x(1 + K^2\gamma x^2) - \sigma_o \dot{v}_{x1}, \tag{5.5}$$

$$\frac{d\gamma}{dt} = \dot{\gamma} = c\zeta_z - c^2\tau_o K^4\gamma^2 x^2, \tag{5.6}$$

where the $(1 - v_z)$ term in equation (5.1) can be expanded using a power series as $v_z < 1$ and we have assumed that $\gamma \simeq u_z$. For simplicity we introduce the normalized quantities $\tilde{\gamma} = \gamma/\gamma_o$, $\tilde{x} = x/x_m$, $\tau_1 = \omega_{\beta o}t$, and $x_m^2 = x_o^2 + u_{xo}^2/(k_{\beta o}^2\gamma_o^2)$. With the trajectory $\dot{x} = cu_x/\gamma$ equations (5.5) and (5.6) can be written as

$$\ddot{\tilde{x}} = -\xi\dot{\tilde{x}}/\tilde{\gamma} - \tilde{x}/\tilde{\gamma} - \chi\ddot{x}_1/\tilde{\gamma}, \tag{5.7}$$

$$\dot{\tilde{\gamma}} = \xi - 2\epsilon\tilde{\gamma}^2\tilde{x}^2, \tag{5.8}$$

where $\xi = c\zeta_z/(\omega_{\beta o}\gamma_o)$, $\epsilon = c^2\tau_o K^4 x_m^2\gamma_o/(2\omega_{\beta o})$, $\chi = \sigma_o/\gamma_o$, and $\ddot{\tilde{x}}_1$ is the acceleration of particle P_1 and is given by

$$\ddot{\tilde{x}}_1 = -\xi\dot{\tilde{x}}_1/\tilde{\gamma}_1 - \tilde{x}_1/\tilde{\gamma}_1. \tag{5.9}$$

To solve the coupled equations (5.7) and (5.8) without retarded effects we use the separation of time scales as has been done in [66] and has been discussed in detail in Chapter 4. Thus, we write here only analytical expression for mean energy and relative energy spread of the electron beam.

5.1.1. Electron beam dynamics

The behavior of the electron beam can be studied by averaging the different quantities for the motion of a single electron over an ensemble of the electrons of the beam. Single particle quantities will be expanded about the ensemble averaged

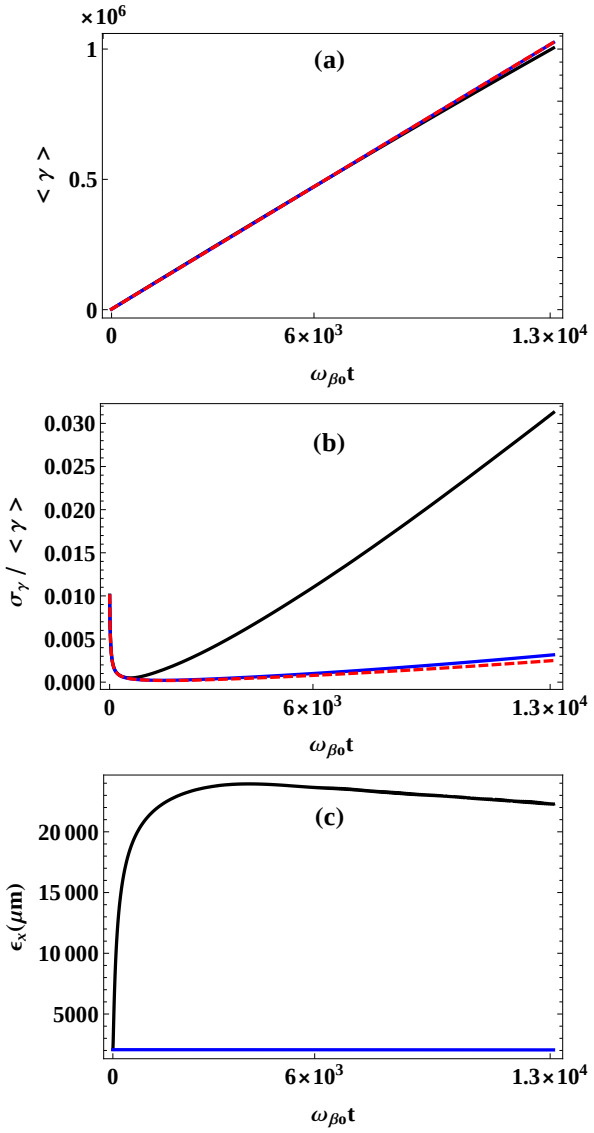

Figure 5.1.: Electron beam dynamics. (a) The mean energy $\langle\gamma\rangle$, (b) the relative energy spread $\sigma/\langle\gamma\rangle$, and (c) the transverse emittance ϵ_x of an electron beam with initial energy $\langle\gamma_o\rangle = 2000$, relative energy spread of 1%, and initial transverse emittance $\epsilon_{ox} = 2068$ radμm propagating in a plasma channel of density $n_o = 10^{15}$ cm^{-3}. The solid black and blue lines represent the corresponding quantities with retarded and without retarded effects, respectively, obtained numerically. The red dashed line represents the corresponding analytical expressions.

value of that quantity plus small perturbation. For example, the initial energy is $\gamma_o = \langle\gamma_o\rangle + \delta\gamma_o$, where $\langle\rangle$ represents the average over the ensemble of particles. Suppose that there are N electrons in the beam. Then, for example, the mean energy $\langle\gamma\rangle = \sum_i \gamma_i/N$, where γ_i is the energy of the ith particle. The equation for the mean energy to the lowest order for a beam injected on axis can be written as

$$\langle\gamma\rangle \quad = \quad \langle\gamma_o\rangle + \zeta t + \frac{2\bar{\nu}_\alpha\langle\gamma\rangle_o^2}{5\zeta}\big[1 - \big(1 + \frac{\zeta}{\langle\gamma_o\rangle}t\big)^{5/2}\big]. \tag{5.10}$$

The relative energy spread of the electron beam is $\sigma_\gamma/\langle\gamma\rangle$, where σ_γ^2 is equal to $\sigma_\gamma^2 = \langle\delta\gamma^2\rangle = \langle\gamma^2\rangle - \langle\gamma\rangle^2$

$$\frac{\sigma_\gamma^2}{\langle\gamma\rangle^2} = (\langle\gamma_o\rangle + \zeta t)^{-2}\big[\sigma_{\gamma o}^2 + \frac{4\bar{\nu}_\alpha^2\langle\gamma\rangle_o^4}{25\zeta^2}\big(1 - \big(1 + \frac{\zeta}{\langle\gamma_o\rangle}t\big)^{5/2}\big)^2\big(\langle\gamma\rangle_0^2\sigma_{xo}^4 + \frac{\sigma_{uxo}^4}{K^4}\big)\big]. \tag{5.11}$$

The transverse emittance of the beam will be obtained by the numerical solution of equations (5.7) and (5.8) with and without retarded effects.

Consider the case of a femtosecond electron bunch of 0.801 nC charge (5.0×10^9 electrons), with 1.02 GeV ($\langle\gamma_o\rangle \simeq 2000$) initial energy moving in a plasma channel of density $n_o = 10^{15}$ cm^{-3}. The initial transverse emittance is $\epsilon_{xo} = 2068$ radμm, which is the matched beam emittance for a low density plasma channel [19]. The mutual distance d between any two electrons is taken to be 0.01 μm, which is still large. Electrons in an electron bunch can have much smaller mutual distances than what we have taken. The transverse emittance ϵ_x increases to a final value of 22000 radμm, which is almost 1.5 times greater than the initial emittance. The relative energy spread also increases to a final value of 3 $\%$. There is also a small decrease in the mean energy of the electron beam due to retardation effects. The results are shown in Figure 5.1. The solid black line represents the corresponding quantities with retardation effects while the solid blue line represents the quantities with out retardation effects and the red dashed line represents the analytical expressions of the corresponding quantities given by equations (5.10) and (5.11). The analytical expressions are in good agreement with the numerical solutions without retarded effects, which eliminates any possibility of error in the

numerical approach. If we decrease the total bunch charge or decrease the transverse bunch size the retardation and self radiation effects become less.

As discussed in Chapter 2 the electrons of the beam with large initial radius feel a strong focusing force in the laser wakefield. This transverse force gives rise to betatron oscillations and the electrons emit radiation. The frequency of oscillations is $\omega_\beta = cK/\sqrt{\gamma}$ and depends on the plasma density and the energy of the electrons. Electrons with large initial radius radiate more as compared to electrons, which are close to or on the axis of the channel.

We know that the retarded field has its component in the transverse direction. In a laser wakefield this transverse component of the retarded potential will increase the amplitude of oscillation of the electrons. The electrons that are initially close to the axis do not radiate but are under the effect of strong radiation of those electrons, which are initially far away from the axis and radiate. This will cause an increase in the amplitude of oscillation of the near axis electrons of the beam. As a consequence the transverse emittance and energy spread of the beam can increase as is seen in Figure 5.1. Since the electron beam is relativistic the emitted radiation will be purely in the $\hat{z}$-direction, therefore, the electrona at the front of the beam will be affected more as compared to the ones that are in the tail of the bunch.

5.2. Summary of the chapter

The retarded and radiation reaction effects on the motion of an electron beam in a laser wakefield have been studied by using the Landau-Lifshitz (LL) equation and the Lienard-Wiechert fields.

It is found that for an electron bunch of sufficiently high charge (of the order of a few pC) with very small duration (of the order of a femtosecond) the retarded fields are strong and affect the properties of the electron beam. It reduces the energy gain, increases the energy spread and transverse emittance of the electron beam with large initial radius.

CHAPTER 6

Numerical solutions of the self force equations

6.1. Introduction

The numerical solution of the self-force equations, e.g., the Lorentz-Abraham-Dirac (LAD) equation, the Landau-Lifshitz (LL) equation and the Caldirola equation is difficult due to their complex structures. For example, the LAD equation contains a second derivate of velocity and its analytical solution shows unphysical behavior. The LL equation is highly nonlinear in external fields and velocity and thus maintaining accuracy and stability is a challenge. The Caldirola equation is a delay differential equation and there is no well developed and trust worthy numerical technique to solve it. On the other hand to study the effects of radiation in laser-plasma interaction and the motion of high energy electron beams in laser-based plasma wakefield accelerators it becomes essential to implement numerical solvers for the self-radiation forces.

In this chapter we will develop numerical recipes to solve different radiation reaction forces. We will mainly use the Boris-Yee scheme for Particle-In-Cell (PIC) simulations. PIC is being used in numerical plasma physics for several decades. The radiation reaction force with the best numerical results will be implemented

in the Plasma Simulation Code (PSC) originally developed by H. Ruhl [96]. The code already includes many features of plasma simulations, however, it does not include radiation reaction. The present work is to extend the PSC for the study of motion of high energy electrons beams where radiation reaction considerably affects the motion of the electrons.

The PSC solves the Vlasov-Boltzmann equations, which are kinetic equations for the one particle probability distributions of electrons, ions and neutral atoms. The PSC method makes the assumption that the distribution functions can be approximated by a finite number of quasi-particles, for which classical equations of motion in the presence of external electromagnetic fields are derived. The electromagnetic fields are calculated from the Maxwell equations and momentum of the particles is updated by the Lorentz force equation in the absence of radiation reaction. To include the effects of self radiation the momentum of the particles will be updated by any of the self-force equations. The kinetic description of plasma gives the most detailed account of the collision-less interaction of the plasma electrons with waves. We will give here a short summary of the PSC code. The details about the PSC code can be found in a number of articles and books (e.g. [96, 97]).

6.2. Numerical schemes

The idea of the PIC method is to combine the continuous variables of particles in configuration and momentum space with the grid representation of fields, potentials and densities. The freely moving particles are represented on the grid. An approximate distribution function f_k of particles of sort k using a finite number of quasi-particles is defined as

$$f(\vec{x},\vec{p},t) \quad = \quad \frac{n_o}{N_c}\sum_i \phi(\vec{x},\vec{x}_i(t))\frac{\xi(\vec{p},\vec{p}_i(t))}{\prod_{j=1}^{3}\Delta p_j}, \tag{6.1}$$

where n_o is the background plasma density. The summation over i is performed over all particles of a particular type. The term n_o/N_c is the density of quasi-

particles, where N_c is the mean number of quasi-particles in one cell. ϕ and ξ are form factors of the particles, which are used to integrate them for a representation on the grid

$$\phi(\vec{x},\vec{x}_i) = \prod_{j=1}^{3} S_j(x_j, x_{ij}(t)), \tag{6.2}$$

$$\xi(\vec{p},\vec{p}_i) = \prod_{j=1}^{3} S_j(p_j, p_{ij}(t)), \tag{6.3}$$

where

$$S_j(x_j, x_{ij}(t)) = \begin{cases} 1 - |\dfrac{x_j - x_{ij}}{\Delta x_j}|, & \text{for } x_{ij} - \Delta x_j \leq x_j \leq x_{ij} + \Delta x_j \quad (6.4) \\ 0, & \text{else} \quad (6.5) \end{cases}$$

and similarly for $S_j(p_j, p_{ij}(t))$.

As we need only represent the position of the particles on the grid, the distribution function uses finite size form factors in configuration space and δ-functions in momentum space. Thus $\Delta p_j \to 0$, which produces the following form of the distribution function

$$f(\vec{x},\vec{p},t) = \frac{n_o}{N_c} \sum_i \phi(\vec{x} - \vec{x}_i(t)) \delta^3(\vec{p} - \vec{p}_i(t)), \tag{6.6}$$

which is used to get the charge and current densities.

6.2.1. Equations of motion

The equations of motion of the quasi-particles can be obtained by using the Vlasov equation

$$\Big(\frac{\partial}{\partial t} + \vec{v} \cdot \frac{\partial}{\partial \vec{x}} + \vec{F} \cdot \frac{\partial}{\partial \vec{p}}\Big) f = 0, \tag{6.7}$$

where $\vec{F}$ is the electromagnetic force on the quasi-particles. We multiply equation (6.7) by the momentum $\vec{p}$ and integrate it over momentum space

$$\frac{\partial}{\partial t} \int d^3p\, \vec{p}\, f + \frac{\partial}{\partial x_l} \int d^3p\, v_l\, \vec{p}\, f - \int d^3p \frac{\partial}{\partial p_l} (\vec{F}_l\, \vec{p}) f = 0. \tag{6.8}$$

Inserting the discrete representation of the distribution function (6.1) in equation (6.8) and integrating yields

$$\sum_j \big(\dot{\vec{x}}_j \frac{\partial\phi(\vec{x},\vec{x}_j)}{\partial\vec{x}_j} + \dot{\vec{x}}\frac{\partial\phi(\vec{x},\vec{x}_j)}{\partial\vec{x}}\big)\vec{p}_j + \sum_j \big(\dot{\vec{p}}_j - \vec{F}\big)\phi(\vec{x},\vec{x}_j) = 0, \tag{6.9}$$

where the momenta $\vec{p}_j$ result from the δ-function in the distribution function. Since the form factor ϕ is symmetric the two derivatives in the first sum annihilate. To validate the equality of the remaining two sums the equality must hold for every single j. Integrating over the volume V of one cell we get

$$\frac{d\vec{x}_j}{dt} = \vec{v}_j, \tag{6.10}$$

$$\frac{d\vec{p}_j}{dt} = \frac{1}{\prod_{l=1}^{3}\Delta x_l}\Big(\int_V d^3x\phi(\vec{x},\vec{x}_j)\vec{F}\Big). \tag{6.11}$$

The product in the denominator on the right hand equation arises from the integration over the volume in equation (6.9). As $\dot{\vec{p}}$ is independent of x the integration can be performed and gives the volume of one cell. The motion of the quasi-particle j is described by equations (6.10) and (6.11), which have the same form as usual Newtonian equations under the approximations made [97].

As mentioned earlier we are interested to incorporate the radiation reaction in the PSC code. Therefore, instead of the Lorentz force equation in equation (6.11) we will solve the self force equation.

6.2.2. Numerical scheme for the LL equation

To get an accuracy up to second order in the integration the PSC uses staggered steps in both, space and time. One basic advantage of this concept over taking half the step sizes is a reduction of computational effort and an increase of stability [97]. We describe the scheme in some detail for one complete time step to show in which order the different variables are updated. We assume that all quantities except the current density $\vec{j}$ are known at the time step n and before. The time step is denoted by a superscript n. The Euler method for half time steps, if n represents

the starting time step, gives

$$\dot{\vec{x}} = \vec{v}, \tag{6.12}$$

$$\frac{\vec{x}^{n+\frac{1}{2}} - \vec{x}^{n}}{\frac{\Delta t}{2}} = \vec{v}^{n}, \tag{6.13}$$

$$\vec{x}^{n+\frac{1}{2}} = \vec{x}^{n} + \frac{\Delta t}{2}\vec{v}^{n}. \tag{6.14}$$

As the velocity $\vec{v}$ and the momentum $\vec{p}$ have the same direction, therefore, the velocity-momentum relation gives

$$\vec{v} = \frac{\vec{p}}{\sqrt{1+|p|^2}}. \tag{6.15}$$

Instead of the velocity $\vec{v}^{n}$ we use the momentum $\vec{p}^{n}$ to obtain

$$\vec{x}^{n+\frac{1}{2}} = \vec{x}^{n} + \frac{\Delta t}{2}\frac{\vec{p}^{n}}{\sqrt{1+|\vec{p}^{n}|^2}} \tag{6.16}$$

The numerical recipe for the LL equation is as follows: With the use of the electric and magnetic fields at half integer time steps the normalized LL equation (3.12) in three vector notation for one particle can be written as

$$\begin{aligned} p^{n+1}_{x,y,z} &= p^{n}_{x,y,z} + \eta\Delta t\Big[E^{n+\frac{1}{2}}_{x,y,z} + \Big(\vec{v}^{n+\frac{1}{2}} \times \vec{B}^{n+\frac{1}{2}}\Big)_{x,y,z}\Big] \\ &+\eta'\Delta t\Big[\Big(\vec{E}^{n+\frac{1}{2}} \times \vec{B}^{n+\frac{1}{2}}\Big)_{x,y,z} + (\vec{v}^{n+\frac{1}{2}} \cdot \vec{B}^{n+\frac{1}{2}})B^{n+\frac{1}{2}}_{x,y,z} - \vec{B}^{2(n+\frac{1}{2})}v^{n+\frac{1}{2}}_{x,y,z} \\ &+(\vec{E}^{n+\frac{1}{2}} \cdot \vec{v}^{n+\frac{1}{2}})E^{n+\frac{1}{2}}_{x,y,z} - v^{n+\frac{1}{2}}_{x,y,z}\Big((\vec{E}^{n+\frac{1}{2}} + \vec{v}^{n+\frac{1}{2}} \times \vec{B}^{n+\frac{1}{2}})^2 - (\vec{E}^{n+\frac{1}{2}} \cdot \vec{v}^{n+\frac{1}{2}})^2\Big)\Big], \end{aligned} \tag{6.17}$$

where $\eta = eE_o/(m_e c\omega_L)$, ω_L is the laser frequency, c is the speed of light, e and m_e are the charge and mass of the electron and $\eta' = a_o^2\tau_o\omega_L$. Subscripts x, y and z represent the corresponding components of the different quantities. We have also neglected the derivative term of the LL equation as it is much smaller than the other terms of the LL equation. Equation (6.17) in component form can be written as

$$\begin{aligned} p^{n+1}_{x} &= p^{n}_{x} + \eta\Delta t\Big[E^{n+\frac{1}{2}}_{x} + \Big(v^{n+\frac{1}{2}}_{y}B^{n+\frac{1}{2}}_{z} - v^{n+\frac{1}{2}}_{z}B^{n+\frac{1}{2}}_{y}\Big)\Big] \\ &+\eta'\Delta t\Big[\Big(E^{n+\frac{1}{2}}_{y}B^{n+\frac{1}{2}}_{z} - E^{n+\frac{1}{2}}_{z}B^{n+\frac{1}{2}}_{y}\Big) + (\vec{v}^{n+\frac{1}{2}} \cdot \vec{B}^{n+\frac{1}{2}})B^{n+\frac{1}{2}}_{x} - \beta^{2(n+\frac{1}{2})}v^{n+\frac{1}{2}}_{x} \\ &+(\vec{E}^{n+\frac{1}{2}} \cdot \vec{v}^{n+\frac{1}{2}})E^{n+\frac{1}{2}}_{x} - v^{n+\frac{1}{2}}_{x}\Upsilon^{n}\Big], \end{aligned} \tag{6.18}$$

$$p_y^{n+1} = p_y^n + \eta\Delta t\Big[E_y^{n+\frac{1}{2}} + \big(v_z^{n+\frac{1}{2}}B_x^{n+\frac{1}{2}} - v_x^{n+\frac{1}{2}}B_z^{n+\frac{1}{2}}\big)\Big]$$
$$+\eta'\Delta t\Bigg[\big(E_z^{n+\frac{1}{2}}B_x^{n+\frac{1}{2}} - E_x^{n+\frac{1}{2}}B_z^{n+\frac{1}{2}}\big) + (\vec{v}^{n+\frac{1}{2}}\cdot\vec{B}^{n+\frac{1}{2}})B_y^{n+\frac{1}{2}} - \beta^{2(n+\frac{1}{2})}v_y^{n+\frac{1}{2}}$$
$$+(\vec{E}^{n+\frac{1}{2}}\cdot\vec{v}^{n+\frac{1}{2}})E_y^{n+\frac{1}{2}} - v_y^{n+\frac{1}{2}}\Upsilon^n\Big], \tag{6.19}$$

$$p_z^{n+1} = p_z^n + \eta\Delta t\Big[E_z^{n+\frac{1}{2}} + \big(v_x^{n+\frac{1}{2}}B_y^{n+\frac{1}{2}} - v_y^{n+\frac{1}{2}}B_x^{n+\frac{1}{2}}\big)\Big]$$
$$+\eta'\Delta t\Bigg[\big(E_x^{n+\frac{1}{2}}B_y^{n+\frac{1}{2}} - E_y^{n+\frac{1}{2}}B_x^{n+\frac{1}{2}}\big) + (\vec{v}^{n+\frac{1}{2}}\cdot\vec{B}^{n+\frac{1}{2}})B_z^{n+\frac{1}{2}} - \beta^{2(n+\frac{1}{2})}v_z^{n+\frac{1}{2}}$$
$$+(\vec{E}^{n+\frac{1}{2}}\cdot\vec{v}^{n+\frac{1}{2}})E_z^{n+\frac{1}{2}} - v_z^{n+\frac{1}{2}}\Upsilon^n\Big], \tag{6.20}$$

where $\beta = \vec{B}^{n+\frac{1}{2}}\cdot\vec{B}^{n+\frac{1}{2}}$ and

$$\Upsilon^n = \Big((\vec{E}^{n+\frac{1}{2}} + \vec{v}^{n+\frac{1}{2}}\times\vec{B}^{n+\frac{1}{2}})^2 - (\vec{E}^{n+\frac{1}{2}}\cdot\vec{v}^{n+\frac{1}{2}})^2\Big) \tag{6.21}$$

To obtain velocity we introduce the new variables

$$p_x^{n+1} = p_x^+ + \frac{1}{2}\eta\Delta t E_x^{n+\frac{1}{2}} + \frac{1}{2}\eta'\Delta t\big(E_y^{n+\frac{1}{2}}B_z^{n+\frac{1}{2}} - E_z^{n+\frac{1}{2}}B_y^{n+\frac{1}{2}}\big) \tag{6.22}$$
$$p_y^{n+1} = p_y^+ + \frac{1}{2}\eta\Delta t E_y^{n+\frac{1}{2}} + \frac{1}{2}\eta'\Delta t\big(E_z^{n+\frac{1}{2}}B_x^{n+\frac{1}{2}} - E_x^{n+\frac{1}{2}}B_z^{n+\frac{1}{2}}\big), \tag{6.23}$$
$$p_z^{n+1} = p_z^+ + \frac{1}{2}\eta\Delta t E_z^{n+\frac{1}{2}} + \frac{1}{2}\eta'\Delta t\big(E_x^{n+\frac{1}{2}}B_y^{n+\frac{1}{2}} - E_y^{n+\frac{1}{2}}B_x^{n+\frac{1}{2}}\big), \tag{6.24}$$
$$p_x^n = p_x^- - \frac{1}{2}\eta\Delta t E_x^{n+\frac{1}{2}} - \frac{1}{2}\eta'\Delta t\big(E_y^{n+\frac{1}{2}}B_z^{n+\frac{1}{2}} - E_z^{n+\frac{1}{2}}B_y^{n+\frac{1}{2}}\big), \tag{6.25}$$
$$p_y^n = p_y^- - \frac{1}{2}\eta\Delta t E_y^{n+\frac{1}{2}} - \frac{1}{2}\eta'\Delta t\big(E_z^{n+\frac{1}{2}}B_x^{n+\frac{1}{2}} - E_x^{n+\frac{1}{2}}B_z^{n+\frac{1}{2}}\big), \tag{6.26}$$
$$p_z^n = p_z^- - \frac{1}{2}\eta\Delta t E_z^{n+\frac{1}{2}} - \frac{1}{2}\eta'\Delta t\big(E_x^{n+\frac{1}{2}}B_y^{n+\frac{1}{2}} - E_y^{n+\frac{1}{2}}B_x^{n+\frac{1}{2}}\big). \tag{6.27}$$

Inserting equations (6.22)-(6.27) in equations (6.18)-(6.20) we have

$$p_x^+ - p_x^- = \eta\Delta t\big(v_y^{n+\frac{1}{2}}B_z^{n+\frac{1}{2}} - v_z^{n+\frac{1}{2}}B_y^{n+\frac{1}{2}}\big) + \eta'\Delta t\Bigg[(\vec{v}^{n+\frac{1}{2}}\cdot\vec{B}^{n+\frac{1}{2}})B_x^{n+\frac{1}{2}}$$
$$-\beta^{2(n+\frac{1}{2})}v_x^{n+\frac{1}{2}} + (\vec{E}^{n+\frac{1}{2}}\cdot\vec{v}^{n+\frac{1}{2}})E_x^{n+\frac{1}{2}} - v_x^{n+\frac{1}{2}}\Upsilon^n\Big], \tag{6.28}$$

$$p_y^+ - p_y^- = \eta\Delta t\big(v_z^{n+\frac{1}{2}}B_x^{n+\frac{1}{2}} - v_x^{n+\frac{1}{2}}B_z^{n+\frac{1}{2}}\big) + \eta'\Delta t\Bigg[(\vec{v}^{n+\frac{1}{2}}\cdot\vec{B}^{n+\frac{1}{2}})B_y^{n+\frac{1}{2}}$$
$$-\beta^{2(n+\frac{1}{2})}v_y^{n+\frac{1}{2}} + (\vec{E}^{n+\frac{1}{2}}\cdot\vec{v}^{n+\frac{1}{2}})E_y^{n+\frac{1}{2}} - v_y^{n+\frac{1}{2}}\Upsilon^n\Big], \tag{6.29}$$

$$p_z^+ - p_z^- = \eta\Delta t\Big(v_x^{n+\frac{1}{2}}B_y^{n+\frac{1}{2}} - v_y^{n+\frac{1}{2}}B_x^{n+\frac{1}{2}}\Big) + \eta'\Delta t\Big[(\vec{v}^{n+\frac{1}{2}}\cdot\vec{B}^{n+\frac{1}{2}})B_z^{n+\frac{1}{2}}$$
$$-\beta^{2(n+\frac{1}{2})}v_z^{n+\frac{1}{2}} + (\vec{E}^{n+\frac{1}{2}}\cdot\vec{v}^{n+\frac{1}{2}})E_z^{n+\frac{1}{2}} - v_z^{n+\frac{1}{2}}\Upsilon^n\Big], \tag{6.30}$$

Equation (6.15) leads to

$$v_{x,y,z}^{n+\frac{1}{2}} = \frac{p_{x,y,z}^{n+\frac{1}{2}}}{\sqrt{1+(p_x^{n+\frac{1}{2}})^2+(p_y^{n+\frac{1}{2}})^2+(p_z^{n+\frac{1}{2}})^2}}, \tag{6.31}$$

where we have

$$p_{x,y,z}^+ + p_{x,y,z}^- = p_{x,y,z}^{n+1} + p_{x,y,z}^n \tag{6.32}$$

and

$$p_{x,y,z}^{n+\frac{1}{2}} = \frac{p_{x,y,z}^{n+1}+p_{x,y,z}^n}{2}, \tag{6.33}$$
$$p_{x,y,z}^{n+\frac{1}{2}} = \frac{p_{x,y,z}^+ + p_{x,y,z}^-}{2} \tag{6.34}$$

up to first order of accuracy and finally

$$v_{x,y,z}^{n+\frac{1}{2}} = \frac{p_{x,y,z}^+ + p_{x,y,z}^-}{2\sqrt{1+(\frac{p_x^+ + p_x^-}{2})^2+(\frac{p_y^+ + p_y^-}{2})^2+(\frac{p_z^+ + p_z^-}{2})^2}}. \tag{6.35}$$

Introducing new variables

$$\tau_{x,y,z} = \frac{\eta\Delta t B_{x,y,z}^{n+\frac{1}{2}}}{2\sqrt{1+(\frac{p_x^+ + p_x^-}{2})^2+(\frac{p_y^+ + p_y^-}{2})^2+(\frac{p_z^+ + p_z^-}{2})^2}}, \tag{6.36}$$
$$\sigma_1 = \frac{\eta'\Delta t(E_xE_y + B_xB_y)^{n+\frac{1}{2}}}{2\sqrt{1+(\frac{p_x^+ + p_x^-}{2})^2+(\frac{p_y^+ + p_y^-}{2})^2+(\frac{p_z^+ + p_z^-}{2})^2}}, \tag{6.37}$$
$$\sigma_2 = \frac{\eta'\Delta t(E_xE_z + B_xB_z)^{n+\frac{1}{2}}}{2\sqrt{1+(\frac{p_x^+ + p_x^-}{2})^2+(\frac{p_y^+ + p_y^-}{2})^2+(\frac{p_z^+ + p_z^-}{2})^2}}, \tag{6.38}$$
$$\sigma_3 = \frac{\eta'\Delta t(E_yE_z + B_yB_z)^{n+\frac{1}{2}}}{2\sqrt{1+(\frac{p_x^+ + p_x^-}{2})^2+(\frac{p_y^+ + p_y^-}{2})^2+(\frac{p_z^+ + p_z^-}{2})^2}} \tag{6.39}$$

and inserting equations (6.35)-(6.39) in equations (6.28)-(6.30) and simplifying we have

$$\begin{pmatrix} p_x^+ \\ p_y^+ \\ p_z^+ \end{pmatrix} = \chi \begin{pmatrix} p_x^- \\ p_y^- \\ p_z^- \end{pmatrix}, \tag{6.40}$$

where $\chi = A^{-1}B$ with

$$A = \begin{pmatrix} (1-\lambda_1) & -(\sigma_1+\tau_z) & \tau_y - \sigma_2 \\ \tau_z - \sigma_1 & (1-\lambda_2) & -(\tau_x+\sigma_3) \\ -(\tau_y+\sigma_2) & (\tau_x-\sigma_3) & (1-\lambda_3) \end{pmatrix}$$

and

$$B = \begin{pmatrix} (1+\lambda_1) & (\sigma_1+\tau_z) & -(\tau_y-\sigma_2) \\ -(\tau_z-\sigma_1) & (1+\lambda_2) & (\tau_x+\sigma_3) \\ (\tau_y+\sigma_2) & -(\tau_x-\sigma_3) & (1+\lambda_3) \end{pmatrix},$$

where

$$\lambda_1 = \frac{\eta'\Delta t\Big((B_x^2-\beta+E_x^2)^{n+\frac{1}{2}} - \Upsilon^n\Big)}{2\sqrt{1+(\frac{p_x^+ + p_x^-}{2})^2+(\frac{p_y^+ + p_y^-}{2})^2+(\frac{p_z^+ + p_z^-}{2})^2}}, \tag{6.41}$$

$$\lambda_3 = \frac{\eta'\Delta t\Big((B_y^2-\beta+E_y^2)^{n+\frac{1}{2}} - \Upsilon^n\Big)}{2\sqrt{1+(\frac{p_x^+ + p_x^-}{2})^2+(\frac{p_y^+ + p_y^-}{2})^2+(\frac{p_z^+ + p_z^-}{2})^2}}, \tag{6.42}$$

$$\lambda_3 = \frac{\eta'\Delta t\Big((B_z^2-\beta+E_z^2)^{n+\frac{1}{2}} - \Upsilon^n\Big)}{2\sqrt{1+(\frac{p_x^+ + p_x^-}{2})^2+(\frac{p_y^+ + p_y^-}{2})^2+(\frac{p_z^+ + p_z^-}{2})^2}}. \tag{6.43}$$

In the limit $\tau_o \to 0$, which is a radiation free case, the matrix χ becomes

$$\chi_{rf} = \frac{1}{1+\vec{\tau}^2} \begin{pmatrix} 1+\tau_x^2-\tau_y^2-\tau_z^2 & 2\tau_x\tau_y+2\tau_z & 2\tau_x\tau_z-2\tau_y \\ 2\tau_x\tau_y-2\tau_z & 1-\tau_x^2+\tau_y^2-\tau_z^2 & 2\tau_y\tau_z+2\tau_x \\ 2\tau_x\tau_z+2\tau_y & 2\tau_y\tau_z-2\tau_x & 1-\tau_x^2-\tau_y^2+\tau_z^2 \end{pmatrix} \tag{6.44}$$

where $\vec{\tau}^2 = \tau_x^2 + \tau_y^2 + \tau_z^2$. The matrix χ_{rf} represents a rotation. It can be shown up to first order of accuracy that

$$\left(\frac{p_x^+ + p_x^-}{2}\right)^2 + \left(\frac{P_y^+ + p_y^-}{2}\right)^2 + \left(\frac{p_z^+ + p_z^-}{2}\right)^2 = p_x^{-2} + p_y^{-2} + p_z^{-2}. \tag{6.45}$$

This relation also holds if we include the radiation reaction, however, the algebra is much more cumbersome for the matrix χ, which is very lengthy but we can simplify it for a particular case. Let us consider a circularly polarized plane wave propagating to the $\hat{z}$-direction. For such a wave the matrix χ is

$$\chi_{cp} = \frac{1}{\Omega_1}\begin{pmatrix} \Omega_2 & 2(\sigma_1(1-\lambda_3)+\tau_x\tau_y) & 2(\sigma_1\tau_x+(\lambda_2-1))\tau_y \\ 2(\sigma_1(1-\lambda_3)+\tau_x\tau_y) & \Omega_3 & 2((1-\lambda_1)\tau_x-\sigma_1\tau_y) \\ 2((1-\lambda_2)\tau_y-\sigma_1\tau_x) & 2((\lambda_1-1)\tau_x+\sigma_1\tau_y) & \Omega_4 \end{pmatrix}, \tag{6.46}$$

where

$$\begin{aligned}
\Omega_1 &= 1+\tau_x^2+\tau_y^2-\sigma_1^2-\lambda_1\tau_x^2-\lambda_2\tau_y^2+\lambda_3\sigma_1^2-\lambda_1-\lambda_2-\lambda_3 \\
&\quad +\lambda_1\lambda_2+\lambda_1\lambda_3+\lambda_2\lambda_3-\lambda_1\lambda_2\lambda_3-2\tau_x\tau_y\sigma_1, && (6.47)\\
\Omega_2 &= (1+\lambda_1)\big((\lambda_2-1)(\lambda_3-1)+\tau_x^2\big)+2\sigma_1\tau_x\tau_y+(\lambda_2-1)\tau_y^2-\sigma_1^2(\lambda_3-1), && (6.48)\\
\Omega_3 &= (1+\lambda_2)\big((\lambda_1-1)(\lambda_3-1)+\tau_y^2\big)+2\sigma_1\tau_x\tau_y+(\lambda_1-1)\tau_x^2-\sigma_1^2(\lambda_3-1), && (6.49)\\
\Omega_4 &= (1+\lambda_3)\big((\lambda_1-1)(\lambda_2-1)-\sigma_1^2\big)+2\sigma_1\tau_x\tau_y+(\lambda_2-1)\tau_y^2-(\lambda_1-1)\tau_x^2. && (6.50)
\end{aligned}$$

Equation (6.40) together with equation (6.46) updates the momentum of the particle for a circularly polarized plane wave. We will discuss some numerical examples in the next section.

One complete time step can be summarized as follows

$$\left.\begin{array}{rcl}
\vec{E}^{n} & \xrightarrow{\vec{B}^{n},\vec{j}^{n}} & \vec{E}^{n+\frac{1}{2}} \\
\vec{B}^{n} & \xrightarrow{\vec{E}^{n+\frac{1}{2}}} & \vec{B}^{n+\frac{1}{2}} \\
\vec{p}^{n} & \xrightarrow{\vec{E}^{n+\frac{1}{2}},\vec{B}^{n+\frac{1}{2}}} & \vec{p}^{n+\frac{1}{2}} \\
\vec{x}^{n+\frac{1}{2}} & \xrightarrow{\vec{p}^{n+1}} \vec{x}^{n+\frac{3}{2}} & \rightarrow \rho^{n+\frac{3}{2}} \\
\vec{j}^{n} & \xrightarrow{\rho^{n+\frac{1}{2}},\rho^{n+\frac{3}{2}}} & \vec{j}^{n+1} \\
\vec{B}^{n+\frac{1}{2}} & \xrightarrow{\vec{E}^{n+\frac{1}{2}}} & \vec{B}^{n+1} \\
\vec{E}^{n+\frac{1}{2}} & \xrightarrow{\vec{B}^{n+1},\vec{j}^{n+1}} & \vec{E}^{n+1}
\end{array}\right\} \tag{6.51}$$

6.2.3. Numerical scheme for the Caldirola equation

The motion of a radiating charged sphere is described by the Caldirola equation as we have discussed in chapter 1 and it is given by

$$m_e \dot{u^{\alpha}} = -eF^{\alpha\beta}u_{\beta} + \frac{m_{ed}}{2a}\big(u^{\alpha}(\tau - 2a/c) + \frac{1}{c^2}u^{\alpha}(\tau)u^{\beta}(\tau)u_{\beta}(\tau - 2a/c)\big), \tag{6.52}$$

where $m_{ed} = e^2/(6\pi\epsilon_o ac)$, a is the radius of the charged sphere and $2a/c$ is the time required by the light to transverse the charged sphere. In three vector notation equation (6.52) can be written as

$$\begin{aligned}
\dot{\vec{p}} \;=\; & e\Big(\vec{E} + (\vec{v}\times\vec{B})\Big) + \frac{m_{ed}}{2a}\Big[\vec{v}(\tau-\tau_1) - \vec{v}(\tau)\big(\gamma(\tau)\gamma(\tau-\tau_1) \\
& -\frac{\vec{v}(\tau)\cdot\vec{v}(\tau-\tau_1)}{c^2}\big)\Big],
\end{aligned} \tag{6.53}$$

where $\tau_1 = 2a/c$. It reduces to the LAD equation in the limit $a \to 0$, which corresponds to a point particle [74]. Equation (6.53) in normalized unit is given by

$$\begin{aligned}
\dot{\vec{p}} \;=\; & \eta\Big(\vec{E} + (\vec{v}\times\vec{B})\Big) + \eta_1\Big[\vec{v}(\tau-\tau_1) - \vec{v}(\tau)\big(\gamma(\tau)\gamma(\tau-\tau_1) \\
& -\vec{v}(\tau)\cdot\vec{v}(\tau-\tau_1)\big)\Big],
\end{aligned} \tag{6.54}$$

where $\eta = eE_o/(m_e c\omega_L)$ and $\eta_1 = m_{ed}/(2a\omega_L m_e)$. We have used the following normalized quantities $\vec{p}' = \vec{p}/(m_e c)$, $\vec{v}' = \vec{v}/c$, $t' = \omega_L t$, $\vec{E}' = \vec{E}/E_L$, and

$\vec{B}' = \vec{B}/B_o$ with $B_o = E_L/c$. We have dropped the prime in equation (6.54) for simplicity.

To solve it numerically we proceed as follows. The delay time $\tau_1 = 2a/c$ has a constant value so we introduce a positive integer $m \geq 1$ and set the time step such that $\Delta t = \tau_1/m$. With this information we can write

$$t = n\Delta t \quad \text{and} \quad \tau_1 = m\Delta t, \tag{6.55}$$

$$v(t) = v^n \quad \text{and} \quad v(t-\tau_1) = v^{n-m}. \tag{6.56}$$

In other words, the delay terms will be obtained from the history of the motion of the particles. Obviously this scheme cannot be used for large scale simulations. Using the Euler method and assuming that n is the starting time step the normalized Caldirola equation (6.54) can be written as

$$\begin{aligned} p^{n+1}_{x,y,z} &= p^n_{x,y,z} + \eta\Delta t\Big[E^{n+\frac{1}{2}}_{x,y,z} + \left(\vec{v}^{\,n+\frac{1}{2}} \times \vec{B}^{n+\frac{1}{2}}\right)_{x,y,z}\Big] + \eta_1\Delta t\Big[v^{(n-m)}_{x,y,z} \\ &\quad - v^{n+\frac{1}{2}}_{x,y,z}\Big(\gamma^{n+\frac{1}{2}}\gamma^{(n-m)+\frac{1}{2}} - \vec{v}^{\,n}\cdot\vec{v}^{\,(n-m)}\Big)\Big]. \end{aligned} \tag{6.57}$$

We introduce new variables of the kind

$$p^{n+1}_x = p^+_x + \frac{1}{2}\eta\ \Delta t\ E^{n+\frac{1}{2}}_x + \frac{1}{2}\eta_1\ \Delta t\ v^{(n-m)}_x, \tag{6.58}$$

$$p^{n+1}_y = p^+_y + \frac{1}{2}\eta\ \Delta t\ E^{n+\frac{1}{2}}_y + \frac{1}{2}\eta_1\ \Delta t\ v^{(n-m)}_y, \tag{6.59}$$

$$p^{n+1}_z = p^+_z + \frac{1}{2}\eta\ \Delta t\ E^{n+\frac{1}{2}}_z + \frac{1}{2}\eta_1\ \Delta t\ v^{(n-m)}_z, \tag{6.60}$$

$$p^n_x = p^-_x - \frac{1}{2}\eta\ \Delta t\ E^{n+\frac{1}{2}}_x - \frac{1}{2}\eta_1\ \Delta t\ v^{(n-m)}_x, \tag{6.61}$$

$$p^n_y = p^-_y - \frac{1}{2}\eta\ \Delta t\ E^{n+\frac{1}{2}}_y - \frac{1}{2}\eta_1\ \Delta t\ v^{(n-m)}_y, \tag{6.62}$$

$$p^n_z = p^-_z - \frac{1}{2}\eta\ \Delta t\ E^{n+\frac{1}{2}}_z - \frac{1}{2}\eta_1\ \Delta t\ v^{(n-m)}_z. \tag{6.63}$$

Since $\vec{v}^{(n-m)}$ is the velocity of the particle at pervious times. We can treat the previous velocities as known quantities. Inserting equations (6.58)-(6.63) in equation

(6.57), we get

$$p_x^+ - p_x^- = \eta\Delta t\big(v_y^{n+\frac{1}{2}} B_z^{n+\frac{1}{2}} - v_z^{n+\frac{1}{2}} B_y^{n+\frac{1}{2}}\big) - \eta_1\ \Delta t\ v_x^{n+\frac{1}{2}}\ \Upsilon_o^n, \tag{6.64}$$

$$p_x^+ - p_x^- = \eta\Delta t\big(v_z^{n+\frac{1}{2}} B_x^{n+\frac{1}{2}} - v_x^{n+\frac{1}{2}} B_z^{n+\frac{1}{2}}\big) - \eta_1\ \Delta t\ v_y^{n+\frac{1}{2}}\ \Upsilon_o^n, \tag{6.65}$$

$$p_x^+ - p_x^- = \eta\Delta t\big(v_x^{n+\frac{1}{2}} B_y^{n+\frac{1}{2}} - v_y^{n+\frac{1}{2}} B_x^{n+\frac{1}{2}}\big) - \eta_1\ \Delta t\ v_z^{n+\frac{1}{2}}\ \Upsilon_o^n, \tag{6.66}$$

where

$$\Upsilon_o \ = \ \Big(\gamma^{n+\frac{1}{2}}\gamma^{(n-m)} - \vec{v}^n \cdot \vec{v}^{(n-m)}\Big). \tag{6.67}$$

Using equations (6.35) and (6.36) in equations (6.64)-(6.66) and simplifying we have

$$\begin{pmatrix} p_x^+ \\ p_y^+ \\ p_z^+ \end{pmatrix} = \chi_o \ \begin{pmatrix} p_x^- \\ p_y^- \\ p_z^- \end{pmatrix},$$

where $\chi_o = C^{-1}D$ with

$$C = \begin{pmatrix} 1+\Theta & -\tau_z & \tau_y \\ \tau_z & 1+\Theta & -\tau_x \\ -\tau_y & \tau_x & 1+\Theta \end{pmatrix}, D = \begin{pmatrix} 1-\Theta & \tau_z & -\tau_y \\ -\tau_z & 1-\Theta & \tau_x \\ \tau_y & -\tau_x & 1-\Theta \end{pmatrix}$$

and

$$\Theta \ = \ \frac{\eta_1\Delta t\Upsilon_o}{2\sqrt{1+(\frac{p_x^+ + p_x^-}{2})^2 + (\frac{p_y^+ + p_y^-}{2})^2 + (\frac{p_z^+ + p_z^-}{2})^2}}. \tag{6.68}$$

After some cumbersome algebra we get the matrix χ_o as follows

$$\chi_o = \frac{1}{\Lambda_2} \ \begin{pmatrix} 1+\tau_x^2-\tau_y^2-\tau_z+\Lambda_1 & 2\tau_x\tau_y + 2\tau_z(1+\Theta) & 2\tau_x\tau_z - 2\tau_y(1+\Theta) \\ 2\tau_x\tau_y - 2\tau_z(1+\Theta) & 1-\tau_x^2+\tau_y^2-\tau_z^2+\Lambda_1 & 2\tau_y\tau_z + 2\tau_x(1+\Theta) \\ 2\tau_x\tau_z + 2\tau_y(1+\Theta) & 2\tau_y\tau_z - 2\tau_x & 1-\tau_x^2-\tau_y^2+\tau_z^2+\Lambda_1 \end{pmatrix},$$

where $\Lambda_1 = \Theta(1 - \vec{\tau}^2 - \Theta - \Theta^2)$ and $\Lambda_2 = 1 + \vec{\tau}^2 + \Theta(3 + \vec{\tau}^2 + 3\Theta + \Theta^2)$. For the radiation free case, which corresponds to $\Theta \to 0$, the above matrix clearly reduces to the one we have seen for the Lorentz force case in the last section and is given in [97]. The complete time step will remain the same as what we mentioned earlier for the case of the LL equation.

6.2.4. Numerical scheme for the LAD equation

We rewrite the LAD equation, which we discussed in chapter 1

$$m_e \dot{u^\alpha} = F_L^\alpha + m_e \tau_o (\ddot{u}^\alpha - \dot{u}^\beta \dot{u}_\beta u^\alpha / c^2). \tag{6.69}$$

The normalized LAD equation (6.69) in three vector notation can be written as

$$\dot{\vec{p}} \;=\; \eta(\vec{E} + \vec{v} \times \vec{B}) + \tau_r \gamma \Big(\dot{\vec{u}} - \big(\vec{u}^2 - \frac{(\vec{u} \cdot \dot{\vec{u}})^2}{\gamma^2} \big) \vec{u} \Big), \tag{6.70}$$

where $\eta = eE_L/(m_e c \omega_L)$ and $\tau_r = \tau_o \omega_L$. We have normalized p by mc, v by c, t with ω_L, and E by E_o.

To solve it numerically we first update the velocity using the Lorentz force part

$$\begin{aligned}
p_x^{n+1} &= p_x^n + \eta \Delta t \Big[E_x^{n+\frac{1}{2}} + \Big(\vec{v}_y^{\,n+\frac{1}{2}} \vec{B}_z^{n+\frac{1}{2}} - \vec{v}_z^{\,n+\frac{1}{2}} \vec{B}_y^{n+\frac{1}{2}} \Big) \Big], \\
p_y^{n+1} &= p_y^n + \eta \Delta t \Big[E_y^{n+\frac{1}{2}} + \Big(\vec{v}_z^{\,n+\frac{1}{2}} \vec{B}_x^{n+\frac{1}{2}} - \vec{v}_x^{\,n+\frac{1}{2}} \vec{B}_z^{n+\frac{1}{2}} \Big) \Big], \\
p_z^{n+1} &= p_z^n + \eta \Delta t \Big[E_z^{n+\frac{1}{2}} + \Big(\vec{v}_x^{\,n+\frac{1}{2}} \vec{B}_y^{n+\frac{1}{2}} - \vec{v}_y^{\,n+\frac{1}{2}} \vec{B}_x^{n+\frac{1}{2}} \Big) \Big].
\end{aligned} \tag{6.71}$$

The detailed description has been already given. In the next step we calculate the acceleration and the derivative of acceleration by using the central difference method

$$\frac{d\vec{v}^n}{dt} = \frac{\vec{v}^{n+1} - \vec{v}^{n-1}}{2\Delta t} + O(\Delta t^2), \tag{6.72}$$

$$\frac{d^2\vec{v}^n}{dt^2} = \frac{\vec{v}^{n+1} - 2\vec{v}^n - \vec{v}^{n-1}}{\Delta t^2} + O(\Delta t^2), \tag{6.73}$$

to maintain second order accuracy. The momentum is again updated using the radiation part of the LAD equation and hence there are some extra steps in the calculation. In large scale simulations, where we deal with millions of particles one extra step costs much. Therefore, this scheme does not seem practical for large scale simulations. Moreover, this numerical scheme, which is used to solved the LAD equation is perturbative to some extent. The Caldirola equation also demands much memory to save the entire history of the particle motion to integrate the delay term. We can say that the numerical solutions of the three self-force equations show that the LL equation is the best compromise for large scale simulation.

6.3. Numerical Examples

In this section we will show numerical results for the LL, the LAD and the Caldirola equations. A comparison of an analytical solution of the LL equations with the numerical solutions of the LL equation and the Caldirola equation will be given as well. The analytical solution of the LL equation is given in Chapter 3. As stated earlier we have studied the motion of an electron counter-propagating to a laser pulse of different polarization. In all examples, which are given in this section, the numerical values of the different quantities are as follows, $a_o = 100$ is the normalized laser intensity and $\gamma_o = 1000$ is the electron initial energy. The laser pulse propagates along the $\hat{z}$-direction and the electron is initially moving along the $(-\hat{z})$-direction. The laser wavelength is $\omega_L = 2.0 \times 10^{15} s^{-1}$, electron mass $m_e = 9.109 \times 10^{-31} kg$, and the electronic charge is taken to be $1.6022 \times 10^{-19} C$.

Figure 6.1 (a) shows the momenta and energy versus τ of a counter-propagating electron in a linearly polarized laser pulse. The solid blue line represents the analytical solution and red dashed line represents the numerical solution of the LL equation. The analytical solution is in good agreement with the numerical solution.

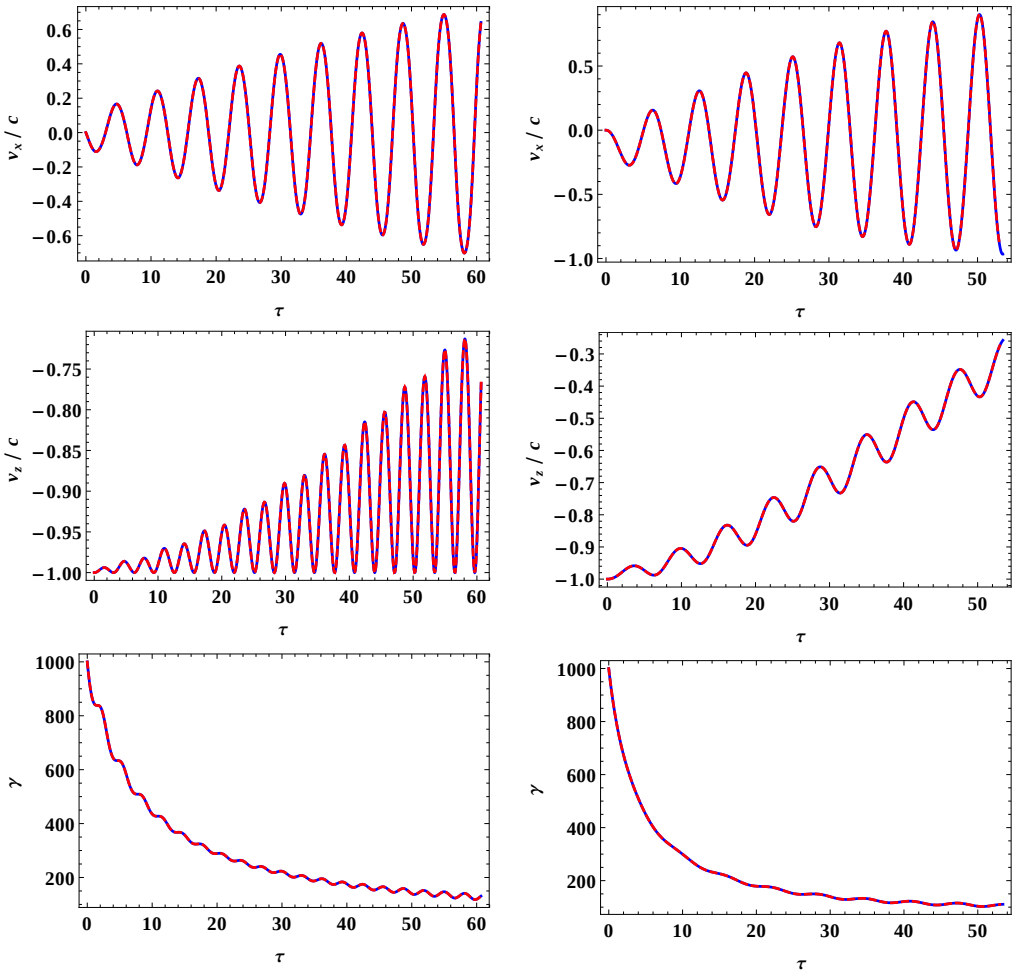

(a) (b)

Figure 6.1.: Counter-propagating electron motion in a laser pulse. Normalized transverse velocity v_x/c, normalized longitudinal velocity v_z/c, and the Lorentz factor γ of an electron versus τ counter-propagating to a laser pulse of normalized intensity $a_o = 100$ and with initial energy $\gamma_o = 1000$. The solid blue and red dashed lines represent the analytical and numerical solutions of the LL equation respectively. (a) Linear polarization and (b) circular polarization.

Similarly Figure 6.1 (b) demonstrates the motion of a counter-propagating electron in a circularly polarized laser pulse. The color scheme is the same as mentioned before. However, here we notice a small discrepancy between the analytical and numerical solutions.

The comparison between the numerical solutions of the LL and Caldirola equations is given in Figure 6.2 (a). The solution of the Caldirola equation agrees well with the LL equation if the radius of the sphere for the Caldirola equation is taken to be as small as 2.3 $\times 10^{-15}$ m. It is less than the radius of the classical electron.

We have also studied the effect of the radius of the sphere on its self-force fields. The self radiation effects are reduced with increasing radius. A sphere with three different radii (3, 2.3, 2)$\times 10^{-15}$ is shown in Figure 6.2 (b). The dotted black, red dashed, and solid blue lines represent the radii (3, 2.3, 2)$\times 10^{-15}$ respectively. It can be seen that the large sphere has less momentum oscillations and the radiation rate is also much less. It should be remember that the Caldirola equation is not a valid equation if the radius of the sphere is less than $\frac{2}{3}r_e$, where r_e is the radius of the classical electron.

6.4. Summary of the chapter

In this chapter we have numerically solved different equations of motion of a radiating electron, for example, the Landau-Lifshitz (LL) equation, the Lorentz-Abraham-Dirac (LAD) equation, and the Caldirola equation. Our main objective is to incorporate the best radiation reaction scheme into the large-scale Plasma-Simulation-Code (PSC).

The numerical solutions have been compared with the analytical solution of the LL equation. We have found good agreement between numerical and analytical solutions. Moreover, we have solved the delay differential equation (the Caldirola equation) of a radiating charged sphere. The solution of the Caldirola

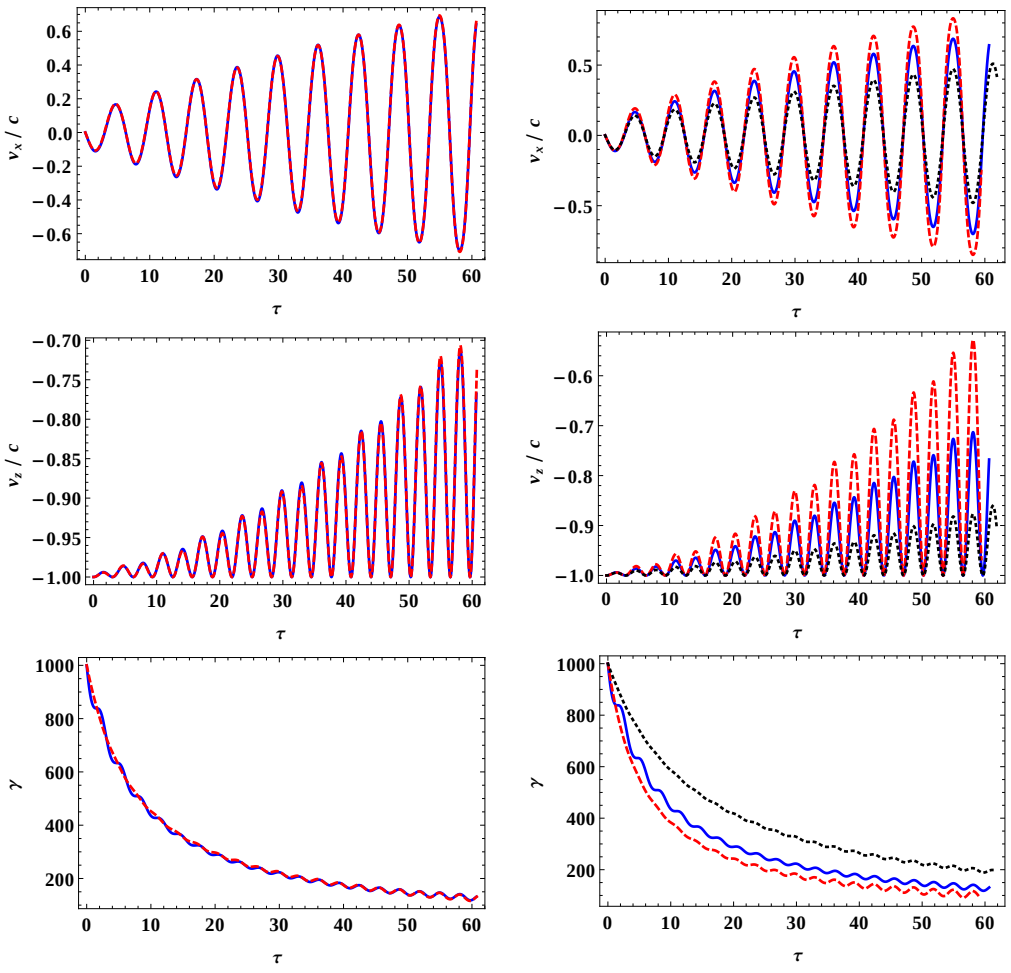

Figure 6.2.: The normalized transverse velocity v_x/c, normalized longitudinal velocity v_z/c, and the Lorentz factor γ of an electron versus τ counter-propagating to a linearly polarized laser pulse of normalized intensity $a_o = 100$ and with initial electron energy $\gamma_o = 1000$. (a) The solid blue and red dashed lines represent the numerical solutions of the LL and Caldirola equations respectively. The radius of the charged sphere is 2.3 $\times 10^{-15}$ m for the Caldirola equation. (b) The dotted black, solid blue and red dashed lines represent the radius of charged spheres with (3, 2.3, 2) $\times 10^{-15}$ m respectively.

equation gives the same radiation effects as the one obtained by the LL equation if we take the radius of the charged sphere to be equal to 2.3 $\times 10^{-15}$. The effects of radiation decrease with increasing radius of the charged sphere as one would expect.

We have compared numerical schemes of different equations. The numerical scheme, which is used to solved the LAD equation is weakly perturbative and it makes the LAD equation a numerical version of the LL equation to some extent. Moreover, it requires extra steps to incorporate the radiation reaction, which makes it costly. The Caldirola equation is a delay differential equation and its numerical technique demands extra memory to save the entire history of the particle motion to integrate the delay term. On the other hand the LL equation is highly nonlinear in external fields and velocity and it is difficult to maintain second order accuracy in its numerical solution. However, there is good agreement with its analytical solution. Over all, we can say that the numerical solutions of three self-force equations show that with the numerical techniques presented here the LL equation is a good choice to use for large scale simulation.

CHAPTER 7

Radiation reaction in a tightly focused laser beam

7.1. Introduction

The configuration of direct electron acceleration by a tightly focused laser beam is shown in Figure 7.1. It is the same set up as considered in [63, 62, 64]. Most theoretical studies of electron acceleration use low-order Hermit-Gaussian modes [98]. We consider a x-polarized laser beam, which propagates along the $\hat{z}$-direction. The transverse electric field component is given by

$$E_x(x,y,z,t) \;=\; E_L \frac{w_o}{w(z)} \exp\Big(-\frac{r^2}{w^2(z)}\Big) \exp\Big[-i(\omega t - kz - \psi_G - \psi_R - \psi_o)\Big], \quad (7.1)$$

where E_L is the amplitude of the laser field, w_o is the beam radius at focus, $w(z) = w_o\sqrt{1+(z/z_r)^2}$, $Z_r = kw_o^2/2$ is the Rayleigh length with $k = 2\pi/\lambda_L$, $r^2 = x^2 + y^2$, ψ_o is the initial phase, $\psi_R = kr^2/2R$ is the phase associated with the curvature of the wave fronts and $\psi_G = \tan^{-1}(z/z_r)$ is the Guoy phase associated with the fact that a Gaussian beam undergoes a total phase change of π as z changes from $-\infty$ to $+\infty$, and λ_L is the laser wavelength [64].

The remaining electric and magnetic field components are given by the rela-

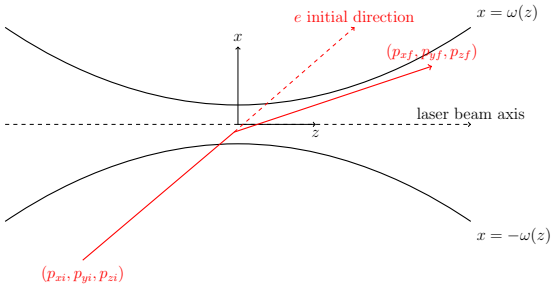

Figure 7.1.: Schematic diagram of the setup and the electron motion in the laser beam

tions

$$E_z = \frac{i}{k}\frac{\partial E_x}{\partial x}, \tag{7.2}$$

$$\vec{B} = -\frac{i}{\omega}\vec{\nabla}\times\vec{E}, \tag{7.3}$$

7.2. Governing equations

The dynamics of the electron will be described by the LL equation (i.e equation 3.12). Leading order terms of the LL equation for the field components given by equations (7.1)-(7.3) can be written as

$$\frac{du_x}{dt} = -a_o(E_x - u_z E_x/\gamma) + \tau_r a_o^2\Big(- E_x E_z + u_z E_x E_z/\gamma - u_x/\gamma\Big\{(\gamma^2+u_z^2)E_x^2 + (\gamma^2-u_z^2)E_z^2 - 2\gamma u_z E_x^2 + 2(\gamma^2-u_z)v_x E_x E_z\Big\}\Big), \tag{7.4}$$

$$\frac{du_z}{dt} = -a_o(E_z + u_x E_x/\gamma) + \tau_r a_o^2\Big(E_x^2 + u_x E_x E_z/\gamma - u_z/\gamma\Big\{\gamma^2(\gamma^2+u_z^2)E_x^2 + (\gamma^2-u_z^2)E_z^2 - 2\gamma u_z E_x^2 + 2(\gamma-u_z)u_x E_x E_z\Big\}\Big), \tag{7.5}$$

$$\frac{d\gamma}{dt} = -a_o(u_x E_x - u_z E_z)/\gamma + \tau_r a_o^2\Big((\gamma^2+u_z^2)E_x^2 + (\gamma^2-u_z^2)E_z^2 - 2\gamma u_z E_x^2 + 2(\gamma-u_z)u_x E_x E_z\Big), \tag{7.6}$$

where $a_o = eE_L/(m_e c\omega_L)$ is the normalized laser intensity, where ω_L is the laser frequency, $\tau_r = \tau_o\omega_L$, and $\vec{u} = \gamma\vec{v}$ is three vector momentum of electron. The magnetic field component is only along the $\hat{y}$-direction and has the value $B_y \simeq E_x/c$. All quantities in equations (7.4) - (7.6) are normalized and have their usual definitions, v is normalized by c, t by laser frequency ω_L, and the length r by the laser wavelength λ_L.

The analytical solution of the coupled equations (7.4) to (7.6) is almost impossible, therefore, we solve them numerically for a single particle. The trajectories of the electron are given by the relation

$$\vec{r} \;=\; \int \frac{\vec{u}}{\gamma}. \tag{7.7}$$

An electron, which is initially located at some distance from the focus of the beam, is fired towards the beam axis near the focus, where it is captured by the transverse electric field component and accelerated by the axial electric field. However, it can also be reflected by the strong ponderomotive potential of the laser or it can be transmitted depending on its initial parameters (initial energy, incident angel and incident distance from the focus of the beam).

In our all examples that will be considered here, the electron starts from a point $(x_o, 0, z_o)$, which lies outside the boundaries of the beam and travels towards a point located at a distance s from the focus on the axis of the beam. The boundaries of the beam in the xz-plane are represented by $x = \pm w(z)$. These are not the actual boundaries of the beam, however, it provides a good approximation of the beam boundaries to understand the reflection, capture and transmission of an electron by the laser beam. Strictly speaking the field intensity on the curves $x = \pm w(z)$ falls off to $1/e^2$ of its maximum value on axis. Thus, an electron beyond these boundaries will be weakly affected by the fields of the beam [64]. An electron will be considered as reflected if it crosses the lower boundary $x = -w(z)$ twice and if it crosses the boundary $x = w(z)$ it will be considered as transmitted, otherwise it is captured by the laser beam.

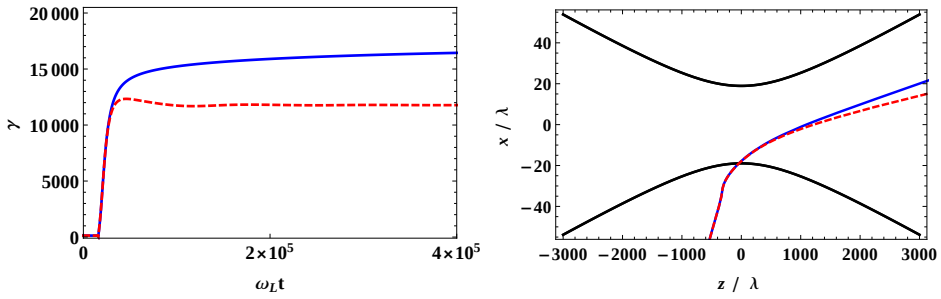

(a) (b)

Figure 7.2.: The motion of an electron in a focused laser pulse. (a) The energy γ versus laboratory time $\omega_L t$ and (b) the trajectory in xz-plane. The electron travels with initial energy $\gamma_o = 130$ from the initial coordinates $(x_o = -(s - z_o)\tan\theta, 0, z_o = -3)$mm, and $\theta = 6^o$ towards s = 0 from the focus of the beam. The normalized laser intensity is $a_o = 100$. The solid blue and red dashed lines stand for the Lorentz and LL equations respectively and black lines in (b) represent the boundaries of the laser beam.

An electron gains maximum energy in a focused laser beam if it is captured by the beam. Since we want to study the radiation effects, which are the signature of relatively high energy, we will mainly discuss the capture case.

Let us consider the example of an electron, which is fired towards a point located at the axis of the laser beam at a distance (s=0) from the focus of the beam with initial coordinates, $(x_o = -(s - z_o)\tan\theta, y_o = 0, z_o = -3)$mm. The incident angle of the electron with the laser beam axis is $\theta = 6^o$. The normalized laser intensity is $a_o = 100$ and the initial energy of the electron is 66.5 MeV. The electron is captured by the laser field and accelerated to a final energy of 8.44 GeV after traveling a total distance of about 67.22 mm as shown in Figure 7.2 (a). We have chosen a relatively long total time to study the effects of emitted radiation. It

should be noted that the electron get most of its energy in a very short fraction of time, which implies a high acceleration rate.

As stated earlier we have used the LL equation to study the self-radiation effects. The final energy predicted by the LL equation is about 6.5 GeV (red dashed line in Figure 7.2 a), which is almost 2 GeV less than the energy gain shown by the Lorentz equation (solid blue line in Figure 7.2 a). Remember that the LL equation is derived by a perturbative expansion of the LAD equation assuming that the radiation part is smaller than the applied Lorentz part i.e. $F_{rad} < F_L$. The coefficients of the Lorentz force and leading order terms of the LL equation give the condition (3.35), which is the validity limit of the LL equation. For a normalized laser intensity $a_o = 100$ and $\gamma = 1000$ the electron lies at the edge of the radiation dominant regime predicted by the LL equation. For higher intensities the validity of the LL equation shifts to even lower values of the electron energy. On the other hand the energy gain and the acceleration of the electron is expected to increase with increasing laser intensity.

In the last example, at the beginning, when the electron has small energy the radiation force is smaller than the Lorentz force, however, as the energy of the electron increases beyond $\gamma = 1000$ the radiation force becomes greater than the Lorentz force and hence the LL equation no longer valid. On the other hand, both, high energy and violent acceleration of electrons demands the study of radiation reaction.

To resolve this issue, let us return to the basic equation of a radiating electron, the LAD equation, to estimate the radiation dominant regime and its effects. The equation (1.36) can be written as

$$m_e\vec{\dot{u}} \;=\; \vec{F}_L + m_e\tau_o\gamma\Big(\vec{\ddot{u}} - \frac{1}{c^2}\big(\vec{\dot{u}}^2 - \frac{(\vec{u}\cdot\vec{\dot{u}})^2}{\gamma^2c^2}\big)\vec{u}\Big), \tag{7.8}$$

where all the quantities have their usual definition and the dot is the derivative

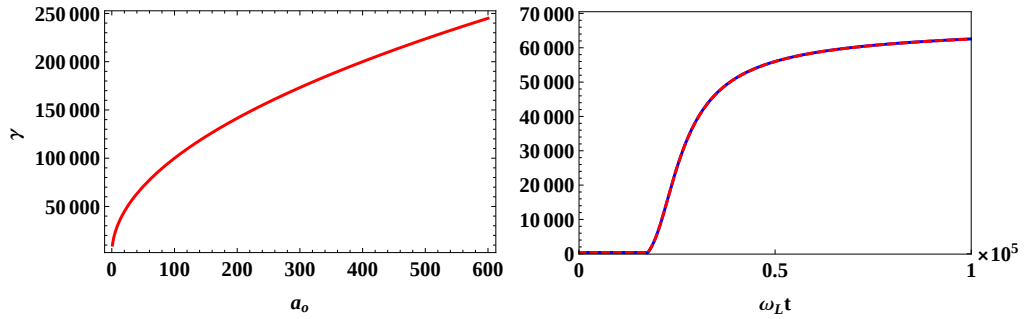

(a) (b)

Figure 7.3.: (a) The radiation dominant regime predicted by the LAD equation, energy γ versus normalized laser intensity a_o. (b) The energy γ versus normalized laboratory time $\omega_L t$. The electron travels with initial energy $\gamma_o = 370$ from initial coordinates $(x_o = -(s - z_o)\tan\theta, 0, z_o = -3)$mm and $\theta = 6^o$ towards the point at distance $s = 0.0003$ m from the focus of the beam. The normalized laser intensity $a_o = 500$. The solid blue and red dashed lines stand for the Lorentz and the LAD equations.

with respect to the time t. In normalized units equation (7.8) can be written as

$$\dot{\vec{u}} = -a_o(\vec{E} + \vec{v} \times \vec{B}) + \tau_r \gamma \Big(\ddot{\vec{u}} - \big(\dot{\vec{u}}^2 - \frac{(\vec{u} \cdot \dot{\vec{u}})^2}{\gamma^2} \big) \vec{u} \Big), \tag{7.9}$$

where $a_o = eE_L/(m_e c \omega_L)$ and $\tau_r = \tau_o \omega_L$. We have normalized $\vec{u}$ by c, $\vec{v}$ by c, t with ω_L, and E by E_L. We can write equation (7.9) in component form as follows

$$\dot{u}_x = -a_o(E_x - u_z B_y/\gamma) + \tau_r \gamma \Big(\ddot{u}_x - \big(\dot{u}^2 - \frac{(\vec{u} \cdot \dot{\vec{u}})^2}{\gamma^2} \big) u_x \Big), \tag{7.10}$$

$$\dot{u}_z = -a_o(E_z + u_x B_y/\gamma) + \tau_r \gamma \Big(\ddot{u}_z - \big(\dot{u}^2 - \frac{(\vec{u} \cdot \dot{\vec{u}}^2}{\gamma^2} \big) u_z \Big), \tag{7.11}$$

where we have considered only v_x and v_z as a simple case.

For convenience we represent the radiation terms in equation (7.10) and (7.11)

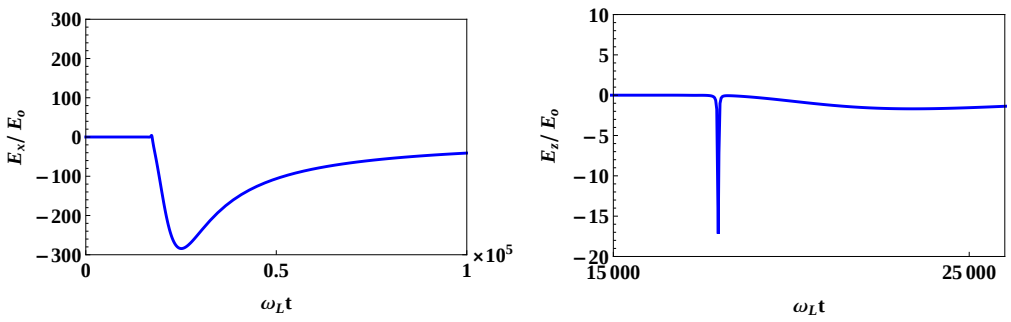

(a) (b)

Figure 7.4.: Electron motion with the LAD equation. (a) Normalized transverse E_x/E_o and (b) longitudinal fields E_z/E_o of laser beam felt by the electron versus time $\omega_L t$. The initial parameters are the same as in Figure 7.3 (b).

as the radiation fields in their respective directions, which means

$$\dot{u}_x = -a_o(E_x - u_z B_y/\gamma) + \gamma\Big(E_x^{rad} - E^{rad}u_x\Big), \tag{7.12}$$

$$\dot{u}_z = -a_o(E_z + u_x B_y/\gamma) + \gamma\Big(E_z^{rad} - E^{rad}u_z\Big) \tag{7.13}$$

with

$$E_x^{rad} = \tau_r \ddot{u}_x,\ E_z^{rad} = \tau_r \ddot{u}_z, \tag{7.14}$$

$$E^{rad} = \tau_r\Big(\dot{u}^2 - \frac{(\vec{u}\cdot\vec{\ddot{u}})^2}{\gamma^2}\Big). \tag{7.15}$$

For the fields given by equation (7.1) - (7.3) equations (7.12) and (7.13) are solved numerically. The numerical scheme is as follows: We will first numerically solve the Lorentz equation for given external fields using Mathematica and hence estimate the acceleration and the derivative of the acceleration of the electron. With the help of the acceleration and the derivate of acceleration of an electron we will calculate the radiation fields given by equations (7.14) and (7.15). Now we have radiation fields along with external fields.

In the next step we will insert these fields in the LAD equation and solve it. This is also a perturbative approach, however, it does not have the restrictions as the ones with the LL equation. It is a kind of self-consistent perturbative approach. If the acceleration provided by the Lorentz equation and by the LAD differs more than one order of magnitude then this numerical solution can differ from the analytical solution of the LL equation. We will discuss this later.

We can estimate the radiation dominant regime by equation (7.9). The acceleration $du/dt \sim 1$ for laser intensities in the range of a_o =100-500, therefore, the leading order terms of radiation damping and the Lorentz force give

$$a_o \simeq \tau_r \gamma^2, \tag{7.16}$$

$$\gamma \simeq 10^4 \sqrt{a_o}, \tag{7.17}$$

where we have assumed that for the highly relativistic electron $\gamma \simeq u_z$ and $\ddot{u}$ is much less as compared to the other terms of the radiation part of equation (7.9). The LL equation predicts that for normalized laser intensity $a_o = 100$ the radiation damping becomes comparable to the acceleration provided by the Lorentz force for $\gamma = 1000$. However, condition 7.17 gives a higher value of $\gamma = 10^5$ for radiation damping to be comparable to the Lorentz force term. The maximum energy gain of an electron in the laser beam of intensity $a_o = 100$ is $\gamma = 16\ 500$ by using the Lorentz force as can be seen in Figure 7.2 (a), which is far less than the radiation reaction dominant regime. If we increase the laser intensity the corresponding minimum energy of the electron required to include radiation effects also grows up as shown in Figure 7.3 (a).

Figure 7.3 (b) shows the energy gain of the electron with the normalized laser intensity $a_o = 500$. The electron is injected with initial energy $\gamma_o = 370$ from initial coordinates ($x_o = -(s - z_o)\tan\theta, 0, z_o = -3$)mm, and $\theta = 6^o$ towards the point, which is at distance $s = 0.0003$ m from the focus of the beam. The electron is captured by the laser beam and we obtain a final energy of $\gamma = 62000$. We have not noticed any difference in the energy gain with and without radiation reaction. The

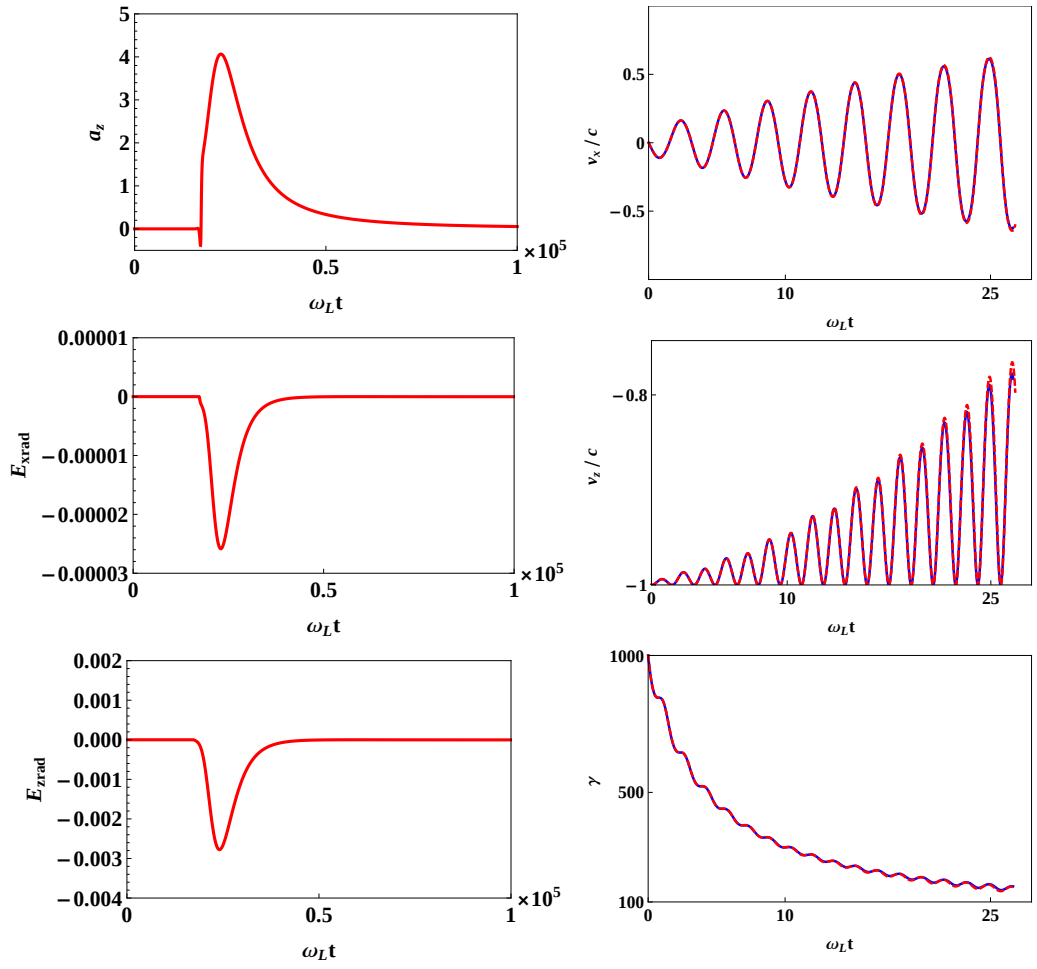

(a) (b)

Figure 7.5.: Electron motion with the LAD equation. (a) The acceleration a_z, normalized transverse radiation field E_{xrad} and normalized longitudinal radiation field E_{zrad} felt by the electron versus normalized laboratory time $\omega_L t$. The initial parameters of the electrons are the same as given in Figure 7.3(b) and (b) The normalized transverse velocity v_x, the longitudinal velocity v_z/c and energy γ versus normalized laboratory time $\omega_L t$. The electron is counter-propagating in the laser with initial energy $\gamma_o = 1000$ and $a_o = 100$. The solid blue and red dashed lines represent the analytical solution of LL equation and numerical solution of LAD equation respectively.

value of γ is almost 2.24$\times 10^5$ for the radiation damping to be effective whereas the electron gains energy up to $\gamma = 6.2 \times 10^4$ in this case. The external laser fields felt by an electron inside a focused laser beam of normalized laser intensity $a_o = 500$ are shown in Figure 7.4 while acceleration of the electron and radiation fields felt by the electron are shown in Figure 7.5 (a). Although the radiation fields are stronger, however, they are still much smaller than the electric fields of the laser.

To test the authenticity of our approach used to solve the LAD equation we have studied the case of a counter-propagating electron with initial $\gamma_o = 1000$ in a linearly polarized laser pulse with normalized intensity $a_o = 100$. The numerical solution shows a good agreement with the analytical solution of the LL equation, which clearly approves our approach. The results have been shown in Figure 7.5 (b). The solid blue line stands for the analytical solution of the LL equation and the red dashed line represents the numerical solution of the coupled equations 7.12 and (7.13) respectively.

7.3. Summary of the chapter

In this chapter we have studied the radiation effects on the motion of an electron in a focused laser beam. The dynamics of the electron is described by the LL and the LAD equations. It is found that the LL equation is not suitable to study the motion of an electron in a laser beam of high intensity because of its lower validity limit. Using the LAD equation, it is found that the self-radiation effects are usually unimportant for acceleration with the laser intensities up to $a_o = 500$. It is due to the fact that the energy gained by the electron for a given laser intensity is far less than the corresponding energy of the electron required for the radiation effects to be important. Therefore, the Lorentz force is a suitable candidate to study the electron dynamics in the focused laser beam up to the normalized laser intensity $a_o = 500$. Moreover the critical energy (minimum electron energy required for the

radiation effects to be important) of the electron increases as $\sqrt{a_o}$ with increasing laser intensity.

We have also verified our numerical approach of the LAD equation by comparing the motion of a counter-propagating electron in a linearly polarized laser pulse, which shows good agreement with the analytical solution of the LL equation.

CHAPTER 8

Conclusions

This work is mainly devoted to the theoretical and numerical investigation of radiation effects on the motion of electrons in laser wakefield accelerators. The experiments concerning electron acceleration are being conducted in many laboratories around the world. GeV energy electron beams have been produced using laser wakefield accelerators and efforts are being made to obtain TeV energy electron beams. Different applications require electron beams with different properties, however, there are some basic effects, which need to be studied before making them available for medical or scientific purposes. High energy charged particle beams radiate a large amount of energy, in particular in a laser wakefield due to transverse betatron oscillations. This radiation affects the energy dependent properties of the charged particle beams, for example, mean energy, energy spread and transverse emittance. Before conducting costly experiments one needs to first optimized the laser wakefield parameters to obtain good quality beams. This is our main emphasis in this thesis: Design a high energy linear laser wakefield accelerator and study the radiation effects of high energy electron beams in laser wakefields.

8.1. 1 TeV energy linear wakefield electron accelerator

As discussed in Chapter 4 the dephasing length and energy gain per stage increases in low density plasma and, therefore, a relatively high energy electron beam can be obtained without going into the trouble of coupling and the complexity of many stages in laser wakefield accelerator. Different parameters have been optimized to generate a linear wakefield for different background plasma densities. It is found that relatively high laser peak power is required to create a linear laser wakefield for a plasma density $n_o = 10^{15}$ cm^{-3}. However, the accelerated beam charge and beam energy per stage are much higher than in the high density plasma case. Therefore, both less number of stages and high bunch charge make the plasma density of 10^{15} cm^{-3} suitable for experiments and practical applications where high charge electron bunches are required along with high energy and small emittance. The comparison of different parameters corresponding to different background plasma densities is given in Table 8.1

8.2. Retardation and radiation effects in strong external fields

High energy charged particles radiate when they are accelerated. An electron can be affected by two kinds of radiation, the first one is self-radiation and second one is the radiation fields of other electrons called retarded fields. Self-radiation of a relativistic electron counter-propagating to an intense laser pulse transfers its energy from the longitudinal direction to the transverse direction. On the other hand, retardation fields always have their polarization opposite to the polarization of the applied laser pulse, therefore, they reduce the effect of the applied laser pulse and hence the electron is less affected by its self-force.

In laser wakefields the electrons exhibit betatron oscillations due to the transverse focusing force and this gives rise to betatron radiation. It is found that for

Table 8.1.: Parameters for TeV scale linear laser plasma accelerator

Beam final energy E_b (TeV)	1	1	1	1	1
Injection beam energy E_i (GeV)	1	1	1	1	1
Plasma density n_o (cm^{-3})	10^{15}	10^{16}	2.3×10^{16}	10^{17}	10^{18}
Plasma wavelength $\lambda_p(\mu)$m	1056	334	220	106	33
Acceleration field E_z (GV/m)	1.5	4.7	7.2	15	47
Energy gain per stage W_{stage} (GeV)	500	45	19	4.5	0.47
Number of stages N_{stage}	2	22	50	222	2125
Stage length L_{stage} (m)	333	9.7	2.8	0.3	0.01
Total linac length L_{total} (L_{coupl})m	1000 (167)	321 (4.9)	210 (1.4)	100 (0.15)	32 (0.005)
Total linac length L_{total} (L_{coupl})m	686 (10)	433 (10)	640 (10)	2287 (10)	21271 (10)
Total linac length L_{total} (L_{coupl})m	668 (1)	235 (1)	190 (1)	289 (1)	2146 (1)
Particles per bunch N_b (10^9)	7.5	2.4	1.6	0.75	0.24
Initial emittance ε_{no} rad(μm)	2068	646	432	209	54
Initial beam radius σ_{xo} (μm)	168	53	35	17	5.3
Bunch length σ_{bz} (μm)	4.1	1.3	0.9	0.4	0.13
Normalized laser intensity a_o	1.4	1.4	1.4	1.4	1.4
Laser wavelength λ_o (μm)	1	1	1	1	1
Laser pulse duration τ_L (fs)	950	300	200	100	30
Laser spot radius r_o (μm)	504	160	105	51	16
Channel depth at $r_o\Delta n_c/n_o$	0.44	0.44	0.44	0.44	0.44
Laser peak power P_L (TW)	10913	1091	474	109	11
Laser energy per stage U_L (J)	10367	327	95	11	0.33

weak self radiation effects the transverse emittance of the beam can decrease, however, it increases for strong self-radiation effects. Moreover, we also studied retardation effects (effects of radiation of one electron on other electrons in the system) of an electron beam. It is found that for an electron bunch with a total charge in the range of pC and with bunch length smaller than a μm the retardation effects become essential. Retardation effects can increase the transverse emittance of an electron beam. The retardation effects decrease with decreasing bunch charge and transverse size and vice versa as discussed in Chapter 5. Thus it is concluded

that in order to obtain a high energy electron beam with small transverse emittance one must inject an electron bunch with smaller size as both, self radiation and retardation effects are low for an electron beam with smaller initial transverse size.

8.3. Numerical simulation of self force equations

In Chapter 6 the numerical recipes for the Lorentz-Abraham-Dirac (LAD) equation, the Landau-Lifshitz (LL) equation, and the Caldirola equation are discussed. A numerical solver for the self force equation has to be implemented in the large scale computing code (e.g., the Plasma Simulation Code) to study the radiation effects in laser plasma interaction and also to study the motion of high energy electron beams in laser based plasma wakefield accelerators. We have discussed numerical solutions of these three equations, but the LL equation appears to be most appropriate candidate to use for large scale simulations because the results of the numerical simulation of the LL equation are in good agreement with its analytical solution. The Caldirola equation is not suitable because one needs to calculate the delay term from the history of the electron motion, which requires a lot of memory storage. The numerical solver of the LAD equation needs some extra steps to integrate the radiation terms, which makes it costly.

APPENDIX A

Linearly polarized plane wave

Trajectories of P_2 for a linearly polarized plane wave

$$
\begin{aligned}
z^{(2)}(\tau) = \frac{10^{-3}}{54432k_o^2}\Big(&210(259200k_o^2 z_o + 207360a_o^2\tau^5\eta^4\Lambda^2 + 259200a_o^2\tau^4\eta^3\Lambda(1+2\Lambda) + a_o^2\eta^3\Lambda(2235617 + 12234456\Lambda)\\
&-194400a_o(1+\Lambda)^2\zeta + 24a_o\eta^2\Lambda(163056 + 168311\Lambda)\zeta - 7200\tau^2\eta(-36 + a_o^2(-18 + \Lambda(-54 + 169\eta^2 + 6(-6 + 55\eta^2)\Lambda))\\
&+6a_o\eta\Lambda(16 + 41\Lambda)\zeta + 18\Lambda(1+\Lambda)\zeta^2) + 1800\eta(72 - 9a_o^2(1+\Lambda)(11 + 40\Lambda) + 581\Lambda(1+\Lambda)\eta^2) - 9600\tau^3\eta^2(a_o^2(-9\\
&+\Lambda(-54 - 54\Lambda + 37\eta^2\Lambda)) - 21a_o\eta\Lambda^2\zeta - 9(2 + 3\Lambda^2\zeta^2)) + 4\tau(a_o^2(2300867\eta^4\Lambda^2 + 16200(1+\Lambda)^2 + 2700\eta^2(35\\
&+2\Lambda(29 + 73\Lambda))) + 150a_o\eta(900 + \Lambda(2304 + (1404 + 14363\eta^2)\Lambda))\zeta + 900(36 - 36k_o^2 + 54(1+\Lambda)^2\zeta^2 + \eta^2(18 + 563\Lambda^2\zeta^2))))\\
&-3.0\times10^6(4a_o^2\eta(-6(1+2\tau\eta) - 4(6 + 12\tau\eta - 25\eta^2)\Lambda + (-18 + \eta(357\eta + 2\tau(-30 + \eta(-311\eta + 12\tau(-1 + 2\tau\eta)))))\Lambda^2)\\
&+3a_o(-6(1+2\tau\eta) - 4(3 + 6\tau\eta - 37\eta^2)\Lambda + (-6 + \eta(191\eta + 2\tau(-6 + \eta(-383\eta + 12\tau(1 + 2\tau\eta)))))\Lambda^2)\zeta + 108\eta\Lambda(1+\Lambda\\
&-3\tau\eta\Lambda)\zeta^2)\cos(\tau) - 75600(20a_o^2\tau(-2167 + 432\tau^2)\eta^4\Lambda^2 + 180a_o(1+\Lambda)^2\zeta + 2a_o\eta^3\Lambda(a_o(-5221 - 12115\Lambda + 240\tau^2(13 + 27\Lambda))\\
&+5\tau(-1955 + 144\tau^2)\Lambda\zeta) + 120\eta(3 + (1+\Lambda)(a_o^2(4 + 9\Lambda) + 3a_o\tau(1 + 3\Lambda)\zeta - 13\Lambda\zeta^2)) + 5\eta^2(144a_o\tau^2\Lambda(2 + 3\Lambda)\zeta\\
&-a_o\Lambda(1502 + 2531\Lambda)\zeta + 48\tau(3 + a_o^2(4 + \Lambda(26 + 27\Lambda)) - 7\Lambda^2\zeta^2)))\cos(2\tau) - 168000\eta\Lambda(4a_o^2\eta^2(60 + (147 + 158\tau\eta)\Lambda)\\
&+3a_o\eta(92 + (161 + 190\tau\eta)\Lambda)\zeta + 72(1 + \Lambda + \tau\eta\Lambda)\zeta^2)\cos(3\tau) + 37800(a_o^2\eta(30(1+\Lambda) + \eta(60\tau + (-257\eta + 120\tau(1+\tau\eta))\Lambda\\
&+434\eta(1 + 2\tau\eta)\Lambda^2)) + 2a_o\eta\Lambda(-16 + 119(1 + 2\tau\eta)\Lambda)\zeta + 30\Lambda(1 + \Lambda + 2\tau\eta\Lambda)\zeta^2)\cos(4\tau)\\
&+60480a_o\eta^2\Lambda(4a_o\eta(4 + (-3 + 2\tau\eta)\Lambda) + 3(4 + (-1 + 2\tau\eta)\Lambda)\zeta)\cos(5\tau) + 8400a_o\eta^2\Lambda(2a_o\eta(-13 + 21(1 + 2\tau\eta)\Lambda)\\
&+3(-2 + (3 + 6\tau\eta)\Lambda)\zeta)\cos(6\tau) - 9450a_o^2\eta^3\Lambda\cos(8\tau) + 252000(4a_o^2\eta^2(-252 - 288(4 + \tau\eta)\Lambda + (-1548 + \eta(-7907\eta + 144\tau\\
&(-11 + 21\tau\eta)))\Lambda^2) + 3a_o\eta(-348 - 24(43 + 12\tau\eta)\Lambda + (-684 + \eta(-9907\eta + 48\tau(7 + 71\tau\eta)))\Lambda^2)\zeta + 36(-6 + \Lambda(-12 + (-6\\
&+(-125 + 24\tau^2)\eta^2)\Lambda))\zeta^2)\sin(\tau) - 18900(-1440\eta^2 + a_o^2(30(12 + \eta(-85\eta + 48\tau(1+\tau\eta))) + 20(1 + 2\tau\eta)(6 + (-35 + 12\tau)\eta)\\
&(6 + (35 + 12\tau)\eta])\Lambda + (360 + 2880\tau\eta + 20(-1345 + 432\tau^2)\eta^2 + 80\tau(-1345 + 144\tau^2)\eta^3 + (133061 + 80\tau^2(-1345 + 72\tau^2))\eta^4)\\
&\Lambda^2) - 12a_o\eta(140 + 880(1 + 2\tau\eta)\Lambda + (740 + \eta(-6889\eta + 2960\tau(1+\tau\eta)))\Lambda^2)\zeta - 90(4 + 8(1 + 2\tau\eta)\Lambda + (4 + \eta(-151\eta + 16\tau(1\\
&+\tau\eta)))\Lambda^2)\zeta^2)\sin(2\tau) - 5600\eta(4a_o^2\eta(-180 + 1440\tau\eta\Lambda + (540 + \eta(-7961\eta + 2160\tau(1+\tau\eta)))\Lambda^2) + 3a_o(-180 + 360(1 + 4\tau\eta)\\
&\Lambda + (540 + \eta(-12241\eta + 2160\tau(1+\tau\eta)))\Lambda^2)\zeta - 9630\eta\Lambda^2\zeta^2)\sin(3\tau) + 12600\eta(2\eta(-135 + a_o^2(-90 - 102(1 + 2\tau\eta)\Lambda + (123\\
&+\eta(-2021\eta + 492\tau(1+\tau\eta)))\Lambda^2)) + 15a_o(-6 + (6 + \eta(-233\eta + 24\tau(1+\tau\eta)))\Lambda^2)\zeta - 810\eta\Lambda^2\zeta^2)\sin(4\tau) + 2016\eta^2\Lambda^2(4a_o\eta\\
&+3\zeta)(413a_o\eta + 150\zeta)\sin(5\tau) + 350\eta^2(a_o^2(180 + 216(1 + 2\tau\eta)\Lambda + (216 + \eta(-4337\eta + 864\tau(1+\tau\eta)))\Lambda^2) - 2280a_o\eta\Lambda^2\zeta\\
&-180\Lambda^2\zeta^2)\sin(6\tau) + 1600a_o\eta^3\Lambda^2(4a_o\eta + 3\zeta)\sin(7\tau) - 1575a_o\eta^3\Lambda^2(17a_o\eta + 6\zeta)\sin(8\tau) - 378a_o^2\eta^4\Lambda^2\sin(10\tau)\Big),
\end{aligned}
\tag{A.1}
$$

$$x^{(2)}(\tau) = \frac{1}{(2700k_o)}\Big(900a_o(-3+4\tau\eta) + 4a_o(-675+2\eta(9223\eta - 450\tau(-3+\tau\eta)))\Lambda$$
$$+150(18k_o x_o + (127\eta\Lambda - 18\tau^2\eta\Lambda + 18\tau(1+\Lambda))\zeta) + 450(a_o(6(1+\Lambda)$$
$$+\eta(-167\eta\Lambda + 24\tau^2\eta\Lambda + 12\tau(1+2\Lambda))) - 45\eta\Lambda\zeta)\cos(\tau) + 450\eta\Lambda(4a_o\eta + 3\zeta)\cos(2\tau)$$
$$-25\eta\Lambda(17a_o\eta + 6\zeta)\cos(3\tau) - 9a_o\eta^2\Lambda\cos(5\tau) - 1350(a_o\eta(7+16(1+2\tau\eta)\Lambda)$$
$$+2(1+\Lambda+2\tau\eta\Lambda)\zeta)\sin(\tau) + 150a_o\eta\sin(3\tau)\Big). \tag{A.2}$$

$$t = \tau + z^{(2)} \tag{A.3}$$

APPENDIX B

Circularly polarized plane wave

Trajectories of P_2 for a circularly polarized plane wave

$$z^{(2)} = \frac{1}{(60k_o^2)}\Big(6a_o^2\tau^5\eta_o^4\Lambda^2 + 15a_o^2\tau^4\eta_o^3\Lambda(1+2\Lambda) + 30\tau^2\eta_o(1+a_o^2(1+\Lambda(2+2\eta_o^2(-1 +\Lambda)+\Lambda))) + 60(k_o^2 z_o + a_o^2\eta_o(1+\Lambda(2+\Lambda+2\eta_o^2(-1+8\Lambda)))) + 10\tau^3\eta_o^2(1+a_o^2(1 +\Lambda(6+7\Lambda+2\eta_o^2\Lambda)) + 4a_o\eta_o\Lambda^2\zeta + 2\Lambda^2\zeta^2) + 30\tau(1-k_o^2+2a_o^2(\eta_o^2(-1+\Lambda)^2+16\eta_o^4\Lambda^2 +(1+\Lambda)^2) + 4a_o\eta_o(1+\Lambda(2+\Lambda+8\eta_o^2\Lambda))\zeta + 2(1+\Lambda(2+\Lambda+4\eta_o^2\Lambda))\zeta^2) - 60\eta_o(a_o^2(1 -\tau\eta_o+2\Lambda-2\eta_o(\tau+\eta_o)\Lambda+(1+\eta_o(16\eta_o+\tau(-7-7\tau\eta_o+(-36+\tau^2)\eta_o^2)))\Lambda^2) +a_o\tau(-1+\Lambda(-2+(-1+(-34+\tau^2)\eta_o^2)\Lambda))\zeta - 6\tau\eta_o\Lambda^2\zeta^2)\cos(\tau) + 60(a_o^2(-1 -\eta_o(\tau+2\eta_o)-2\Lambda+2\tau\eta_o(-1+\eta_o^2)\Lambda+(-1-\tau\eta_o+(-8+\tau^2)\eta_o^2+\tau(-16+\tau^2)\eta_o^3 +2(-26+5\tau^2)\eta_o^4)\Lambda^2) + a_o\eta_o(-3+\Lambda(-6+(-3+(-50+9\tau^2) \eta_o^2)\Lambda))\zeta + (-1+\Lambda(-2+(-1+(-10+\tau^2)\eta_o^2)\Lambda))\zeta^2)\sin(\tau)\Big), \tag{B.1}$$

$$y^{(2)} = \frac{1}{(2ko)}\Big(2k_o y_o + a_o(-2(1+\Lambda)+\eta_o(18\eta_o\Lambda-\tau^2\eta_o\Lambda+\tau(2+6\Lambda))) + (6\eta_o\Lambda-\tau^2\eta_o\Lambda +2\tau(1+\Lambda))\zeta + 2(a_o(1+\Lambda+\eta_o(\tau+2\tau\Lambda-9\eta_o\Lambda+\tau^2\eta_o\Lambda)) -3\eta_o\Lambda\zeta)\cos(\tau) - 2(a_o\eta_o(2+5\Lambda+5\tau\eta_o\Lambda)+(1+\Lambda+\tau\eta_o\Lambda)\zeta)\sin(\tau), \tag{B.2}$$

$$
\begin{aligned}
x^{(2)} &= \frac{1}{(2ko)}(2k_o x_o - 2a_o(\tau + 2\eta_o) + a_o(-10\eta_o + \tau(-2 + \eta_o(\tau + 8\eta_o)))\Lambda - 2\zeta \\
&\quad +2(-1 + 2\tau\eta_o)\Lambda\zeta + 2(a_o\eta_o(2 + 5\Lambda + 5\tau\eta_o\Lambda) + (1 + \Lambda + \tau\eta_o\Lambda)\zeta)\cos(\tau) \\
&\quad +2(a_o(1 + \Lambda + \eta_o(\tau + 2\tau\Lambda - 9\eta_o\Lambda + \tau^2\eta_o\Lambda)) - 3\eta_o\Lambda\zeta)\sin(\tau)\Big). \qquad \text{(B.3)} \\
t &= \tau + z^{(2)} \qquad \text{(B.4)}
\end{aligned}
$$

Bibliography

[1] S. W. Bahk, P. Rousseau, T. A. Planchon, V. Chvykov, G. Kalintchenko, A. Maksimchuk, G. A. Mourou, and V. Yanovsky, "Generation and characterization of the highest laser intensities," *Opt. Lett.*, vol. 29, pp. 2837–2839, 2004.

[2] V. V. Lozhkarev and G. I. Friedman, "200 tw 45 fs laser based on optical parameteric chirped pulse amplification," *Opt. Express*, vol. 14, pp. 446–454, 2006.

[3] D. Strickland and G. Mourou, "Compression of amplified chirped optical pulses," *Optics Communication*, vol. 56, pp. 219–221, 1985.

[4] T. Tajima and J. M. Dawson, "Laser electron accelerator," *Phys. Rev. Lett.*, vol. 43, pp. 267–270, 1979.

[5] Landau and Lifshitz, *The Classical Theory of Fields 2nd Edition*. Paragoman press: Paragoman press, 1975.

[6] E. S. Sarachik and G. T. Schappert, "Classical theory of the scattering of intense laser radiation by free electrons," *Phys. Rev. D*, vol. 1, pp. 2738–2753, 1970.

[7] P. Sprangle, E. E. andA. Ting, and G. Joyce, "Laser wakefield acceleration and relativistic optical guiding," *Appl. Phys. Lett.*, vol. 53, no. 53, p. 2146, 1988.

[8] P. Sprangle, E. Esarey, A. Ting, and G. Joyce, "Propagation and guiding of intense laser pulses in plasmas," *Phys. Rev. Lett*, vol. 69, no. 69, p. 2200, 1992.

[9] L. M. Gorbunov, P. Mora, and A. A. Solodov, "Dynamics of a plasma channel created by the wakefield of a short laser pulse," *Phys. Plasmas*, vol. 10, no. 10, p. 1124, 2003.

[10] N. E. Andreev, L. M. Gorbunov, V. I. Kirsanov, and A. A. Pogosova *JETP Lett.*, vol. 60, no. 60, p. 713, 1994.

[11] P. Jha, P. Kumar, A. Upadhyaya, and G. Raj, "Electric and magnetic wakefields in a plasma channel," *Phys. Rev. ST. Accel. Beams*, vol. 8, no. 8, p. 071301, 2005.

[12] D. Umstadter, J. K. Kim, and E. Dodd, "Laser injection of ultrashort electron pulses into wakefield plasma waves," *Phys. Rev. Lett.*, vol. 76, no. 76, p. 2073, 1996.

[13] W. P. Leemans, B. Nagler, A. J. Gonsalves, C. Toth, K. Nakamura, C. G. R. Geddes, E. Esarey, C. B. Schroeder, and S. M. Hooker, "Gev electron beams from a centimetre accelerator," *Nature.Phys.*, vol. 2, p. 696, 2006.

[14] N. A. M. Hafz, T. M. Jeong, W. Choi, S. K. Lee, K. H. Pae, V. V. Kulagin, J. H. Sung, T. J. Yu, K.-H. Hong, T. Hosokai, J. R. Cary, D.-K. Ko, and J. Lee, "Stable generation of gev-class electron beams from self-guided laser-plasma channels," *Nature Photonics*, vol. 2, p. 571, 2008.

[15] E. Esarey, P. Sprangle, J. Krall, and A. Tang, "Overview of plasma-based accelerator concepts," *IEEE Trans. Plasma Sci*, vol. 24, no. 2, p. 252, 1996.

[16] E. Esarey, C. B. Schroeder, and W. P. Leemans, "Physics of laser-driven plasma-based electron accelerators," *Review of Modern Physics*, vol. 81, no. 123, p. 1229, 2009.

[17] B. Brozek-Pluskab, D. Gliger, A. Hallou, V. Malka, and Y. A. Gauduel, "Direct observation of elementary radical events: low and high energy radiation femtochemistry in solutions," *Radiat. Phys. Chem.*, vol. 72, p. 149, 2005.

[18] R. Crowell, D. J. Gosztola, I. A. Shkrob, D. A. Oulianov, C. D. Jonah, and T. Rajh, "Ultrafast processes in radiation chemistry," *Radiat. Phys. Chem*, vol. 70, p. 501, 2004.

[19] K. Nakajima, A. Deng, X. Zhang, B. Shen, J. Liu, R. Li, Z. Xu, T. Ostermayr, S. Petrovics, C. Klier, K. Iqbal, H. Ruhl, and T. Tajima, "Operating plasma density issues at low density," *Phys. Rev. ST Accel. Beams*, vol. 14, no. 14, p. 091301, 2011.

[20] E. Esarey, C. B. Schreoder, and W. P. Leemans, "Physics of laser-driven plasma-based electron accelerators," *Rev. of Modern Physics*, vol. 81, no. 3, p. 1229, 2009.

[21] J. Faure, Y. Glinec, A. Pukhov, S. Kiselev, S. Gordienko, E. Lefebvre, J. P. Rousseau, F. Burgy, and V. Malka, "A laser-plasma accelerator producing monoenergetic electron beams," *Nature*, vol. 431, no. 123, p. 541, 2004.

[22] C. R. Geddes, C. Toth, J. van Tilborg, E. Esarey, C. B. Schrodder, D. Bruhwiler, C. Nieter, J. Cary, and W. P. Leemans, "High-quality electron beams from a laser wakefield accelerator using plasma channel guiding," *Nature*, vol. 431, no. 123, p. 538, 2004.

[23] S. P. D. Mangles, C. D. Murphy, Z. Najmudin, A. G. R. Thomas, J. L. Collier, A. E. Dangor, E. J. Divall, P. S. Foster, J. G. Gallacher, C. J. Hooker, D. A. Jaroszynski, A. J. Langley, W. B. Mori, P. A. Norreys, F. S. Tsung, R. Viskup,

B. R. Walton, and K. Krushelnick, "Monoenergetic beams of relativistic electrons from intense laser-plasma interactions," *Nature*, vol. 431, no. 123, p. 535, 2004.

[24] W. P. Leemans, B. Nagler, A. J. Gonsalves, C. Toth, K. Nakamura, C. G. R. Geddes, E. Esarey, C. B. Schroeder, and S. M. Hooker, "Gev electron beams from a centimetre-scale accelerator," *Nat. Phys.*, vol. 2, no. 2, p. 696, 2006.

[25] J. M. Dawson *Phys. Rev.*, vol. 113, no. 123, p. 383, 1959.

[26] X. L. Chen and R. N. Sudan, "Two dimensional self focusing of short intense laser pulse in under-dense plasma," *Phys. Fluids B*, vol. 5, no. 4, p. 1336, 1992.

[27] E. Esarey, P. Sprangle, J. Krall, A. Tang, and G. Joyce, "Optically guided laser wake field acceleration," *Phys. Fluids B*, vol. 5, no. 7, p. 2690, 1993.

[28] P. Sprangle and E. Esarey, "Interaction of ultrahigh laser fields with beams and plasmas," *Phys. Fluids B*, vol. 4, no. 7, p. 2241, 1992.

[29] E. Esarey, A. Ting, P. Sprangle, and G. Joyce *Plasma Phys. Controlled Fusion*, vol. 12, no. 123, p. 191, 1989.

[30] W. K. H. Panofsky and W. A. Wenzel, "Some considerations concerning the transverse deflection of charged particles in radio-frequency fields," *Rev. Sci. Instrum*, vol. 27, no. 11, p. 967, 1956.

[31] P. Sprangle, E. Esarey, and A. Ting, "Nonlinear interaction of intense laser pulses in plasmas," *Phys. Rev. A*, vol. 41, no. 8, p. 4463, 1990.

[32] P. Sprangle, E. Esarey, and A. Ting, "Nonlinear theory of intense laser-plasma interactions," *Phys. Rev. Lett*, vol. 64, no. 17, p. 2011, 1990.

[33] S. V. Bulanov, V. I. Kirsanov, and A. S. Sakharov *JETP Lett*, vol. 50, no. 123, p. 198, 1989.

[34] P. Mora and T. M. Antonsen, "Electron cavitation and acceleration in the wake of an ultra-intense, self-focused laser pulse," *Phys. Rev. E*, vol. 53, no. 3, p. 2068, 1996.

[35] A. Pukhov and J. M. T. Vehn, "Laser wake field acceleration the highly non-linear broken-wave regime," *Appl. Phys. B*, vol. 74, no. 74, pp. 355–361, 2002.

[36] W. Lu, C. Huang, M. Zhou, M. Tzoufras, F. S. Tsung, W. B. Mori, and T. Katsouleas, "A nonlinear theory for multidimensional relativistic plasma wave wakefields," *Phys. Plasma*, vol. 13, no. 5, p. 056709, 2006.

[37] A. Pukhov, "Strong field interaction of laser radiation," *Reports on Progress in Physics*, vol. 66, pp. 47–101, 2003.

[38] J. B. Rosenzweig, B. Breizman, T. Katsouleas, and J. J. Su, "Acceleration and focusing of electrons in two-dimensional nonlinear plasma wake fields," *Phys. Rev. A*, vol. 44, p. 6189, 1991.

[39] A. Caldwell, K. Lotov, A. Puhkov, and F. Simon, "Proton driven plasma-wakefield acceleration," *Nature Physics*, vol. 5, no. 123, p. 363, 2009.

[40] M. J. Hogan, R. Assmann, F. J. Decker, R. Iverson, P. Raimondi, S. Rokni, R. H. Siemann, D. Walz, D. Whittum, B. Blue, C. E. Clayton, E. Dodd, R. Hemker, C. Joshi, K. A. Marsh, W. B. Mori, S. Wang, T. Katsouleas, S. Lee, P. Muggli, P. Catravas, S. Chattopadhyay, E. Esarey, , and W. P. Leeman, "A 1.4-m-long plasma wake field acceleration experiment using a 30 gev electron beam from the stanford linear accelerator center linac," *Phys. Plasmas*, vol. 7, no. 123, p. 2241, 2000.

[41] M. J. Hogan, C. D. Barnes, C. E. Clayton, F. J. Decker, S. Deng, P. Emma, C. Huang, R. H. Iverson, D. K. Johnson, C. Joshi, T. Katsouleas, P. Krejcik, W. Lu, K. A. Marsh, W. B. Mori, P. Muggli, C. L. OÕConnell, E. Oz, R. H.

Siemann, , and D. Wal, "Multi-gev energy gain in a plasma-wakefield accelerator," *Phys. Rev. Lett.*, vol. 95, no. 123, p. 054802, 2005.

[42] I. Blumenfeld, C. E. Clayton, F. J. Decker, M. J. Hogan, C. Huang, R. Ischebeck, R. Iverson, T. K. C. Joshi, N. Kirby, W. Lu, K. A. Marsh, W. B. Mori, P. Muggli, E. Oz, R. H. Siemann, D. Walz, and M. Zhou, "Energy doubling of 42 gev electrons in a metre-scale plasma wakefield accelerator," *Nature(London)*, vol. 445, no. 123, p. 741, 2007.

[43] E. Esarey, B. A. Shadwich, P. Catravas, and W. P. Leemans, "Synchrotron radiation from electron beams in plasma-focusing channels," *Phys. Rev. E*, vol. 65, no. 123, p. 056505, 2002.

[44] I. Kostyukov, A. Pukhov, and S. Kiselev, "Phenomenological theory of laser-plasma interaction in bubble regime," *Phys. Plasmas*, vol. 11, no. 123, p. 5256, 2004.

[45] G. Z. Sun, E. Ott, Y. C. Lee, and P. Guzdar, "Self?focusing of short intense pulses in plasmas," *Phys. Fluids*, vol. 30, no. 123, p. 526, 1987.

[46] T. Kurki-Suonio, P. J. Morrison, and T. Tajima, "Stable solitary propagation of optical beams," *Phys. Rev. A*, vol. 40, no. 123, p. 3230, 1989.

[47] P. Sprangle, E. Esarey, J. Krall, and G. Joyce, "Propagation and guiding of intense laser pulses in plasmas," *Phys. Rev. Lett.*, vol. 69, no. 123, p. 2200, 1992.

[48] S. Gordienko and A. Pukhov, "Scalings for ultrarelativistic laser plasmas and quasimonoenergetic electrons," *Phys. Plasmas*, vol. 12, no. 123, p. 043109, 2005.

[49] W. Lu, C. Huang, M. Zhou, W. B. Mori, and T. Katsoulleas, "Nonlinear theory for relativistic plasma wakefields in the blowout regime," *Phys. Rev. Lett.*, vol. 96, no. 16, p. 165002, 2006.

[50] W. Lu, C. Huang, M. Zhou, M. Tzoufras, F. S. Tsung, W. B. Mori, and T. Katsouleas, "A nonlinear theory for multidimensional relativistic plasma wave wakefields," *Phys. Plasmas*, vol. 13, no. 5, p. 056709, 2006.

[51] T. T. G. A. Mourou and S. V. Bulanov, "Optics in the relativistic regime," *Reviews of Modern Physics*, vol. 78, no. 2, p. 309, 2006.

[52] D. Umstadter, "Relativistic laser plasma interaction," *Journal of Physics D*, vol. 36, no. 8, pp. R151–R165, 2003.

[53] U. Teubner and P. Gibbon, "High order harmonics from laser irradiated plasma surfaces," *Reviews of Modern Physics*, vol. 81, no. 2, p. 445, 2009.

[54] W. Horton and T. Tajima, "Pump depletion in the plasma-beat-wave accelerator," *Phys. Rev. A*, vol. 34, no. 123, p. 4110, 1986.

[55] A. Ting, E. Esarey, and P. Sprangle, "Nonlinear wake-field generation and relativistic focusing of intense laser pulses in plasmas," *Phys. Pluids B*, vol. 2, no. 123, p. 1390, 1990.

[56] S. V. Bulanov, I. N. Inovenkov, V. I. Kirsanov, N. M. Naumova, and A. S. Sakharov, "Nonlinear depletion of ultrashort and relativistically strong laser pulses in an underdense plasma," *Phys. Fluids B*, vol. 4, p. 1935, 1992.

[57] D. Teychenne, G. Bonnaud, and J. L. Bobin, "Electrostatic and kinetic energy in the wake wave of a short laser pulse," *Phys. Plasmas*, vol. 1, no. 123, p. 1771, 1994.

[58] C. Joshi, W. B. Mori, T. Katsouleas, J. M. Dawson, J. M. Kindel, and D. W. Forslund, "Ultrahigh gradient particle acceleration by intense laser-driven plasma density waves," *Nature (London)*, vol. 311, no. 123, p. 525, 1984.

[59] E. Esarey, B. A. Shadwick, C. B. Schroeder, and W. P. L. P. Sprangle, "*Pro-*

ceedings of the Advanced Accelerator Concepts Workshop," *AIP, New York*, vol. 737, no. 123, p. 578, 1990.

[60] B. A. Shadwick, C. B. Schroeder, and E. Esarey, "Nonlinear laser energy depletion in laser-plasma accelerator," *Phys. Plasmas*, vol. 16, no. 5, p. 056704, 2009.

[61] G. Malka, E. Lefebvre, and J. L. Miquel, "Experimental observation of electrons accelerated in vacuum to relativistic energies by a high-intensity laser," *Phys. Rev. Lett.*, vol. 78, no. 17, p. 3314, 1997.

[62] J. X. Wang, Y. K. HO, Q. Kong, L. J. Zhu, L. Feng, S. Scheid, and H. Hora, "Electron capture and violent acceleration by an extra-intense laser beam," *Phys. Rev. E*, vol. 58, no. 5, p. 6575, 1998.

[63] J. X. Wang, W. Scheid, M. Hoelss, and Y. K. HO, "Mechanism of electron violent acceleration by extra-intense lasers in vacuum," *Phys. Lett. A*, vol. 280, no. 1, p. 121, 2001.

[64] Y. I. Salamin and C. H. Keitel, "Electron acceleration by a tightly focused laser beam," *Phys. Rev. Lett.*, vol. 88, no. 9, p. 095005, 2002.

[65] P. Schmuser, M. Dohlus, and J. Rossbach, *Ultraviolet and Soft X-Ray Free-Electron Laser*. Springer: Springer, 2008.

[66] P. Michel, C. B. Schreoder, B. A. Shadwick, E. Esarey, and W. P. Leemans, "Radiative damping and electron beam dynamics in plasma-based accelerators," *Phys. Rev. E*, vol. 74, no. 74, p. 026501, 2006.

[67] T. Ostermayr, S. Petrovics, K. Iqbal, C. Klier, T. Tajima, H. Ruhl, K. Nakajima, A. Deng, X. Zhang, B. Shen, J. Liu, R. Li, and Z. Xu, "Laser plasma accelerator driven by a super-gaussian pulse," *submitted to J. Plasma Phys.*, vol. 123, no. 123, p. 123, 2012.

[68] K. Iqbal and H. Ruhl, "Betatron radiation effects on the motion of electron beam in a laser wakefield." preprint (2012).

[69] Y. Hadad, L. Labun, J. Rafelski, N. Elkina, C. Klier, and H. Ruhl, "Effects of radiation-reaction in relativistic laser acceleration," *Phys. Rev. D*, vol. 82, no. 123, p. 096012, (2010).

[70] A. D. Piazza, "Exact solution of the landau-lifshitz equation in a plane wave," *Lett. Math. Phys.*, vol. 83, no. 3, p. 305, 2008.

[71] J. Koga, T. Z. Esirkepov, and S. Bulanov, "Nonlinear thomson scattering in the strong radiation damping regime," *Phys. Plasmas*, vol. 12, no. 123, p. 093106, 2005.

[72] R. Giovanelli, "Relativistic electron motion in fel-like fields taking retarded interaction into account," *IL Nuovo Cimento D*, vol. 15, no. 123, p. 23, 1993.

[73] A. R. Rossi, A. Bacci, L. Serafini, C. Maroli, and V. Petrillo, "Numerical treatment of retarded radiation effects from high brightness electron beams," *Phys. Rev. ST Accel. Beams*, vol. 12, no. 123, p. 104202, 2009.

[74] F. Rohrlich, "The dynamics of a charged sphere and the electron," *Am. J. Phys.*, vol. 65, no. 123, p. 1051, 1997.

[75] M. Abraham, *Theorie der elekrizitat, Vol II: Elektromagnetische Theorie der Strahlung*. Teubner, Leipzig: Teubner, Leipzig, 1905.

[76] H. A. Lorentz, *The theory of Electrons*. Teubner, Leipzig 1909, 1916: Teubner, Leipzig, 1905.

[77] A. Einstein, "On the electrodynamics of moving bodies," *Annalen der Physik*, vol. 17, pp. 891–921, 1905.

[78] A. Einstein, "Does the inertia of a body depend upon its energy content?," *Annalen der Physik*, vol. 18, pp. 639–641, 1905.

[79] A. D. Yaghjian, *Relativistic Dynamics of a Charged Sphere, Lect. Notes Phys. 686.* Springer-Verlag, Berlin 2008: Springer-Verlag, Berlin 2008, 2008.

[80] C. Eliezer, "On the classical theory of particles," *Proc. Roy. Soc. A.*, vol. 194, no. 123, p. 543, 1948.

[81] M. T. Chin and C. H. Papas, "New equation of motion for classical charged particles," *Phys. Rev. D*, vol. 4, no. 123, p. 3566, 1971.

[82] P. Caldirola, "A new model of classical electron," *Nuovo Cim.*, vol. 3, no. 2, p. 297, 1956.

[83] I. V. Sokolov, "Renormalization of the lorentz-abraham-dirac equation for radiation reaction force in classical electrodynamics," *JETP*, vol. 109, no. 2, p. 207, 2009.

[84] I. V. Sokolov, N. M. Naumova, J. A. Nees, G. A. Mourou, and V. P. Yanovsky, "Dynamics of emitting electrons in strong laser fields," *Phys. Plasmas*, vol. 16, no. 9, p. 093115, 2009.

[85] A. Sommerfeld, "Simplified deduction of the field and the forces of an electron, moving in any given way," *Akad. VAn Wetensch. Amsterdam*, vol. 13, no. 123, p. 377, 1904.

[86] B. Altschul, "Bounding isotropic lorentz violation using synchrotron losses at lep," *Phys. Rev. D*, vol. 80, no. 123, p. 091901, 2009.

[87] C. Chiu, S. Ceshkov, and T. Tajima, "High energy laser-wakefield collider with synchronous acceleration," *Phys. Rev. ST. Accel. Beams*, vol. 3, no. 3, p. 101301, 2000.

[88] T. Tajima, M. Kando, and M. Teshima, "Feeling the texture of vacuum," *prog. theor. phys.*, vol. 125, no. 125, p. 617, 2011.

[89] M. Xie, T. Tajima, K. Yokoya, and S. Chattopadhyay, *In Advanced Accelerator Concepts: Seventh Workshop, Lake Tahoe*. AIP, New York: AIP New York, 1997.

[90] S. Cheshkov, T. Tajima, W. Horton, and K. Yokoya, "Particle dynamics in multistage wakefield collider," *Phys. Rev. ST. Accel. Beams*, vol. 3, no. 3, p. 071301, 2000.

[91] E. Esarey, "Laser cooling of electron beams via thomson scattering," *Nucl. Instrum. Methods Phys. Res. A*, vol. 7, no. 7, p. 455, 2000.

[92] A. W. Chao and M. Tigner, *Handbook of Accelerator Physics and Engineering*. World Scientific, Singapore: World Scientific, Singapore, 1999.

[93] Z. Haung, P. Chen, and R. D. Ruth, "Radiation reaction in a continuous focusing channel," *Phys. Rev. Lett.*, vol. 74, no. 10, p. 1759, 1995.

[94] S. F. Martins, R. A. Fonseca, W. Lu, W. B. Mori, and L. O. Silva, "Exploring laser-wakefield-accelerator regimes for near-term lasers using particle-in-cell in lorentz-boosted frames," *Nature Phys.*, vol. 6, no. 123, p. 311, 2010.

[95] C. E. C. et al., "Transverse envelope dynamics of a 28.5-gev electron beam in a long plasma," *Phys. Rev. Lett.*, vol. 88, p. 154801, 2002.

[96] C. Birdsall, A. Langdon, and H. Ruhl, *Plasma Physics via Computer Simulation*. Rinton Press: Rinton Press, 2006.

[97] K. Thust, "Numerical simulation of a micro discharge," 2008.

[98] O. Svelto and D. C. Hannal, *Principles of Lasers, 3rd Edition*. Plenum, New York: Plenum, New York, 1989.

Acknowledgement

At the end of my thesis I would like to thank all those people who made this work possible and an unforgettable experience for me. I have worked with a great number of people whose contribution in assorted ways to the research and the making of the thesis deserved special mention. It is a pleasure to convey my gratitude to them all in my humble acknowledgment.

First of all , All praise to almighty Allah and many blessing to his Prophets (P.B.U.H).

It cannot be argued with that the most influential person in my graduate career is my supervisor Prof. Hartmut Ruhl whose keen guidance and discipline have been indispensable to grow my scientific thought over these past four and a half years. I am especially grateful for his devotion to his student's education and success. It is a great honour to work with him.

Special thanks goes to Prof. Toshiki Tajima for his valuable discussions that helped me a lot. It is always great to interact with somebody who has discovered the field you are working in.

I am also thankful to Prof. Armin Scrinzi for useful comments and discussion.

In my research work I have been blessed with a friendly and cheerful group of fellow students. I gratefully acknowledge all my colleagues in particular, Nina Elkina, Constantin Klier, Karl-Ulrich Bamberg and Sergey Rykovanov for their help and support whenever I was in need. The name of Neil Moschuering needs special mention for his valuable discussion and for his help to pull me out when ever I stuck with the code.

It is a pleasure to express my gratitude to Kay Thust for all the supports and exercises to learn the basic of the Plasma-Simulation-Code.

I am thankful to Tobias Ostermayr and Stefan Petrovics for their fruitful discussions.

I am thankful to Dr. Ben King for his encouragement and also for his flawless grammatical editing of my thesis.

Frau Ute Tobiasch is always very helpful and cooperative. I want to thanks her for her valuable support in administrative matters.

I gratefully acknowledge the funding of this work provided by the DAAD/HEC of Pakistan, by the DFG through Grant No. DFG RU 633/1-1, and the Cluster-of-Excellence "Munich-Centre for Advanced Photonics" (MAP).

Sincere thanks to all my friends especially Ahsan, Shahid, Ammara, Ashish, Aslam, Haseeb, Wahab, Maria, and Honia to provide me the home-like atmosphere and for their moral support during my study. Thanks for the friendship and memories.

Finally, I take this opportunity to express the profound gratitude from my deep heart to my beloved parents, brothers, and sisters for their love and continuous support both spiritually and materially. I also would like to thank my nephews and nieces for the laughter gifted to me with their cute and tender voice on the phone.

I want to pay deepest regard to my uncle Rasheed Ahmad who motivated me for higher studies.

To those who indirectly contributed in this research, your kindness means a lot to me. Thank you very much.

This part of the thesis appeared to be very tough to write. I was trying not to forget anybody but most likely I did that. Unintentionally, of course.

Curriculum Vitae

Personal Data:

FAMILY NAME, FIRST NAME:	Iqbal, Khalid
PLACE AND DATE OF BIRTH:	Sargodha, Pakistan. 02-01-1980
POSTAL ADDRESS:	Willi-Graf-Str. 9, Zi. 344 haus 5c, 80805 München
CELL NO.:	0176-3491-5947
EMAIL:	kk_t3@yahoo.com

Academic Career:

Ludwig-Maximilians-Universität München, Germany, Ph.D. student, "Radiation effects on relativistic electrons in strong external fields".
Govt. College University Lahore, Pakistan, Master of Philosophy in Physics, 2006.
Govt. College University Lahore, Pakistan, Master of Science, 2003.

Research Profile:

2008 Onward: Working in the group of Prof. Hartmut Ruhl. We study the motion of radiating electrons in laser and laser-plasma based accelerators by theoretical and numerical modeling. The accelerated electrons emit radiation and radiation reaction affects the energy gain and other energy dependent properties of the electrons.
2004-2006: M. Phil Dissertation Title; "To Study the Drift Alfven Waves using (r,q) Distribution Function in Electromagnetic Hot Plasma".
2002-2003: M. Sc Dissertation Title; "A Comprehensive Survey of Natural Radio nuclides Pollutants in the Outdoor Environment of Tehsil Sillanwali and Sargodha District".